Development of a Three-Dimensional Multibody Model of the Human Leg and Foot for Application to Movement Analysis

Tiago de Melo Lopes Martinho Malaquias

Thesis to obtain the Master of Science Degree in

Biomedical Engineering

Examination Committee

Chairperson: Profª. Patrícia Margarida Piedade Figueiredo

Supervisors: Prof. Miguel Tavares da Silva

Prof. João Eurico da Fonseca

Members of the Committee: Profª. Helena Cristina Matos Canhão

Prof. João Manuel Pereira Dias

December 2013

I

Para os meus pais

III

Agradecimentos

Ao Professor Miguel Tavares da Silva pela disponibilidade que apresentou desde cedo na minha integração no *Biomechanics of Movement Research Group* e pelo empenho e motivação que demonstrou no leccionamento da cadeira de Biomecânica do Movimento, fatores que me levaram a desenvolver a tese de mestrado na área. E um forte agradecimento por todas as horas despendidas como orientador científico no desenvolvimento deste trabalho.

Ao Professor João Eurico da Fonseca, orientador científico da Faculdade de Medicina de Lisboa pelo apoio prestado.

Ao Sérgio Gonçalves por ter facilitado o contacto antecipado com o grupo, bem como por toda a ajuda e tempo disponibilizado durante o desenvolvimento desta tese.

A todo o restante *Biomechanics of Movement Research Group*, por toda a ajuda, companhia e boa disposição que demonstraram, em especial ao João Veiga, Paulo Melo e Daniel Simões por toda a disponibilidade que demonstraram e pelas valiosas contribuições apresentadas. À Salomé Azevedo e ao Miguel Castro por todo o tempo despendido em trocas de ideias, aquisições laboratoriais e acima de tudo pelos momentos de descontração proporcionados ao longo do desenvolvimento da tese*.*

A todos os colegas e amigos que direta ou indiretamente permitiram a realização deste trabalho e deste curso. Sem o companheirismo, amizade e interajuda que experienciei nos últimos cinco anos não teria sido possível chegar até este ponto da mesma forma. Um especial agradecimento, à Rita Levy, Miguel Almeida, Martina Fonseca, Joana Lourenço, João Guilherme, João Silva, Pedro Chagas, Pedro Pinheiro e Rafael Gonçalves.

A todos os amigos que se mantiveram ao meu lado e me motivaram durante a realização deste trabalho, foram preciosos os momentos de descontração que me proporcionaram. Ao Diogo, Filipa, Leitão, Lopes, Marta, Mafalda, Tatiana, Luísa, Gonçalo, Nuno, João, André, Francisca, Daniel, Miguel, Tiago e Diana.

À Catarina por todo o apoio, compreensão e amizade que foram essenciais durante o período de realização da tese e durante o curso.

À minha família por ter sempre apoiado, compreendido e respeitado as minhas opções. Em especial aos meus pais que sempre estiveram ao meu lado, sem eles este percurso não teria sido possível.

Resumo

O movimento humano tem sido sempre um assunto de grande interesse para a ciência. Nas últimas décadas métodos centrados em sistemas Multicorpo têm sido aplicados com sucesso no desenvolvimento desta área. Dentro de um largo espectro de aplicações destas metodologias pode destacar-se o desenvolvimento de novos dispositivos médicos (i.e. Ortóteses e Próteses) e a simulação das consequências de algumas intervenções médicas. Assim, uma boa modelação da perna e do pé é crucial para a compreensão cinemática e dinâmica do movimento humano, e eventualmente para analisar disfunções a este nível.

Neste trabalho, apresenta-se um novo modelo dinâmico tridimensional da perna e do pé, com quatro segmentos (Perna, Retro-pé, Médio-pé e Ante-pé, e Dedos), seis corpos rígidos e treze graus de liberdade. O principal objetivo do modelo é a sua aplicação num software integrado de multicorpo dinâmico com coordenadas naturais – Apollo. O modelo é testado usando simulações de dinâmica inversa, aplicando um novo protocolo de marcadores reflectores para adquirir a informação necessária para a análise.

Os resultados são obtidos com ensaios realizados com dois participantes, proporcionando no geral, resultados cinemáticos e cinéticos consistentes e realistas. Entre eles destacam-se alguns padrões conhecidos como os momentos e a variação angular gerados nas articulações subastragalina, tibioperoneoastragálica e metatarsofalângica que sustentam a robustez do modelo. E alguns resultados inovadores como o momento e variação angular na articulação médiotársica que proporciona uma nova compreensão sobre os graus de liberdade do pé, abrindo portas para uma possível análise de diferentes disfunções na marcha.

Palavras-chave

Pé Multissegmentado, Modelos de pé, Multicorpo, Cinética, Cinemática, Análise de Marcha

Abstract

The human movement has always been a subject of great interest to science. In the last decades Multibody systems-based methodologies have been successfully applied in development of this field. Among the broad range of application of these methodologies one can highlight the development of new medical devices (e.g. Orthosis and Prosthesis) and the simulation of the outcome of some medical procedures. Therefore, a proper leg and foot modulation is crucial to understand the kinematics and dynamics of the human movement, and eventually to analyze dysfunctions at this level.

In the present work, a novel three dimensional leg and foot dynamic model with four segments (Leg, Rear-foot, Mid-foot and Fore-foot, and Toes), six rigid bodies and thirteen degrees-of-freedom, is presented. The main objective of the model is its application in a built-in multibody dynamics software with natural coordinates – Apollo. The model is tested using inverse dynamic simulations, applying a new marker set protocol to acquire the necessary data to perform the analysis.

The results were based on a set of trials performed onto two subjects, providing overall consistent and realistic kinematic and kinetic results. Among them, some well know patterns like the torques and angle variations generated at the talocrural, talocalcaneal and metatarsophalangeal joints support the robustness of the model. And some innovative results like the angle variation and torque generated at the midtarsal joint provides a new insight over foot analysis, opening doors to the possible evaluation of different gait disorders.

Keywords

Multi-segment foot, Foot models, Multibody, Kinetics, Kinematics, Gait analysis

Contents

List of Figures

List of Tables

List of Symbols

H_{bP} - Mean body heights reported by Parham *et al.* (1989)

L_{fP} - Mean foot lengths reported by Parham *et al.* (1989)

L_h - Mean rear-foot height adapted from Parham *et al.* (1989)

L_{RF} - Mean rear-foot length adapted from Parham *et al.* (1989)

L_{Mf} - Mean mid-foot and fore-foot length adapted from Parham *et al.* (1989)

L_T - Mean toes length adapted from Parham *et al.* (1989)

v_{APi} - Center of mass vectors reported by Anderson & Pandy (1999)

m_L - Leg mass reported by Anderson & Pandy (1999)

m_H - Hind-foot mass reported by Anderson & Pandy (1999)

m_T - Toes mass reported by Anderson & Pandy (1999)

H_{bAP} - Body heights reported by Anderson & Pandy (1999)

L_{fAP} - Foot length reported by Anderson & Pandy (1999)

m_b - Body mass reported by Anderson & Pandy (1999)

$x_{v_{APi}}, y_{v_{APi}}, z_{v_{APi}}$ - Coordinates of the v_{APi} vectors

L_n - Segment n length

h_{III} - Height of segment III

m_n - Segment n mass

L_f - General Foot Length

H_b - General Body Height

M_b - General Body Mass

x_i, y_i, z_i - Points or Vectors coordinates

J n - Joints

CM n - Segment n Center of Mass

r n - Anthropometric vectors

I_n - Segment inertia of body n.

ξ - Correction factor used to calculate I_{III}

I_{0x}, I_{0y}, I_{0z} - Inertias of segment 0 in the three main directions

$I_{IIIx}, I_{IIIy}, I_{IIIz}$ - Inertias of segment III in the three main directions

$I_{IIx}, I_{IIy}, I_{IIz}$ - Inertias of segment II in the three main directions

$r_{IIIx}, r_{IIIy}, r_{IIIz}$ - Distances between the parallel axis that pass through the center of mass of segment II

$r_{IIx}, r_{IIy}, r_{IIz}$ - Distances between the parallel axis that pass through the center of mass of segment II

$m_n\%$ - Segment n mass percentage

$r_n\%$ - Mean relative radius of gyration of the segment n about the considered axis

$\boldsymbol{q}$ - Vector of generalized coordinates

$\dot{\boldsymbol{q}}$ - Vector of generalized velocities

$\ddot{\boldsymbol{q}}$ - Vector of generalized accelerations

Φ - Kinematic constraints expressions

$\mathbf{\Phi}_q$ - Jacobian matrix of the kinematic constraints

$\mathbf{\nu}$ - Right-Hand-Side of the velocity equation

$\mathbf{\gamma}$ - Right-Hand-Side of the acceleration equation

P^* - Virtual Power produced by the external forces

$\mathbf{f}$ - Vector of all forces that produce virtual power (external and inertial forces)

$\mathbf{g}$ - Vector of generalized forces

$\mathbf{g}^*$ - Vector of generalized forces that contains the internal constraint forces

$\mathbf{\lambda}$ - Vector of Lagrange Multipliers

$\mathbf{M}$ - Global Mass matrix

α, β - Parameters of the Baumgarte stabilization method

ρ - Rigid body density

Ω - Rigid body volume

$\mathbf{r}$ - Global coordinates of a generic point P

$\dot{\mathbf{r}}$ - Virtual velocities of a generic point P

$\ddot{\mathbf{r}}$ - Virtual accelerations of point P

$\mathbf{u}, \mathbf{v}, \mathbf{w}$ - Non coplanar unit vectors

$\mathbf{c}$ - Coefficients vector

$\mathbf{C}$ - Coordinates transformation matrix

$\mathbf{X}'$ - Matrix containing the local coordinates of segment $\mathbf{r}_{ij}$

$\mathbf{I}$ - Identity matrix

$\mathbf{\Gamma}$ - Actuator

P n - Model points

$\mathbf{s}\,n$ - Model local vectors

$\mathbf{v}\,n$ - Model theoretical joint vectors

M n - Reflective markers location

$\mathbf{v}_{Knee}$ - Knee joint vector

$\mathbf{v}_{Talocrural}$ - Talocrural joint vector

$\mathbf{v}_{Talocalcaneal}$ - Talocalcaneal joint vector

$\mathbf{v}_{Midtarsal}$ - Midtarsal joint vector

$\mathbf{v}_{Metatarsophalangeal}$ - Metatarsophalangeal joint vector

$\mathbf{v}_{RFT}$ - Rear foot top vector

$\mathbf{v}_{Massless}$ - Massless link vector

$\mathbf{x}_{Leg}, \mathbf{y}_{Leg}, \mathbf{z}_{Leg}$ - Local Leg referential (Body 4)

$\mathbf{x}_{RF}, \mathbf{y}_{RF}, \mathbf{z}_{RF}$ - Local Rear-foot referential (Body 3)

$\mathbf{x}_{MFFF1}, \mathbf{y}_{MFFF1}, \mathbf{z}_{MFFF1}$ - Local Mid-foot and Fore-foot referential (Body 2)

$\mathbf{x}_{MFFF2}, \mathbf{y}_{MFFF2}, \mathbf{z}_{MFFF2}$ - Local Mid-foot and Fore-foot referential (Body 3)

$\mathbf{x}_{Toes}, \mathbf{y}_{Toes}, \mathbf{z}_{Toes}$ - Local Toes referential (Body 1)

ϕ_i - Kinematic angles

v_i - Model Vectors

Glossary

2D – Two-Dimensional

3D – Three-Dimensional

3DMFMs – Three-Dimensional Multisegment Foot Models

AFO – Ankle Foot Orthosis

AIM – Automatic Identification of Markers

CM – Center of Mass

COP – Center Of Pressure

DOF's – Degrees Of Freedom

FF – Foot Flat

GRF's – Ground Reaction Forces

HS – Heel Strike

IC – Initial Contact

IS – Initial Swing

LBL – Lisbon Biomechanics Laboratory

LR – Loading Responce

MFM – Milwaukee Foot Model

MiS – Midswing

MS – Midstance

ODE's – Ordinary Differential Equantions

OFM – Oxford Foot Model

PS – Pre Swing

QTM – Qualysis Track Manager

RHS – Right Hand Side

TO – Toe Off

TS – Terminal Stance

TSw – Terminal Swing

US – United States of America

Chapter I

Introduction

This introductory chapter is intended to expose the motivation and the objectives for this Thesis and to briefly describe the state of the art of the scientific field that it belongs.

1.1. Motivation

The human body has been studied for centuries; one can say that the first human studies were performed by the Egyptian culture thousands of years before Christ. The interest in the human body was also present in the ancient Greece (600 B.C. – 200 A.C.), were the society lived by the motto *Mens sana in corpore sano* (a healthy mind in a healthy body). The quest for knowledge about our specie was kept active for periods in human history like *The Renaissance* (1450 – 1600 A.C.) and *The scientific Revolution* (1600 – 1730 A.C.). The nineteenth century it's known among the Biomechanics community as the *Gate Century*, in part because the first's quantitative locomotion studies were performed by Etienne Marey in the first biomechanics laboratory. It was also in this period that the first's electromyographies were performed. The twentieth century brought the definition of the word Biomechanics, the study of the mechanical principles of living organisms (Hall, 2011). This century provided a fast development in the biomechanics area, especially due to the world wars that lead to an investment in the medical investigation. A. V. Hill received a Nobel Prize in the medical area due to his study over the function and structure of the muscles (Martin, 1999).

In the present century human locomotion continues to be of great interest to science, namely, the analysis of athlete's action in order to improve their performance and reduce their injury probability (Bahr & Krosshaug, 2005; Lees *et al.*, 2010), the optimization of sports equipment (Dabnichki, 1998), the evaluation of surgical procedures (Abuzzahab *et al.*, 1993; Delp, 1990), the improvement of performance and comfort of prostheses and orthoses (Vasconcelos, 2010), the creation of databases

that can compare pathological and non-pathological gait patterns (Gonçalves, 2010), gait analysis and ergonomic studies (Abuzzahab *et al.*, 1993; Kidder *et al.*, 1996; Leardini *et al.*, 1999; Meglan, 1991; Silva, 2003), the implementation of human gate patterns in robots (Hyon & Cheng, 2007), among others.

This broad range of applications is possible in part due to the fact that computer modeling and simulation has reach unprecedented levels in recent years, mainly because of the growing belief that this approach can provide more quantitative explanations of how the neuromuscular and musculoskeletal systems interact to produce movement. The use of these computational tools, namely multibody system-based models is powered by this continuum increase of computers capacity; with the technology available today it is already possible to simulate reliable and realistic human models that take into account many degrees of freedom, muscles and tendons (Pandy, 2001).

The present computational power, acquisition instruments and mathematical methods enables the simulation of complex structural systems like the human foot and ankle with no need to use invasive procedures. The foot can be described as a multi-joint structure which serves as an intermediate between the ground and the rest of the body. This complex structure serves to support and propel the body, transfer forces from the ground, and provide rotation for adaptations to all kinds of terrain. Dysfunctions of the foot can cause instability or disability of motions, so the kinematic modeling of the leg and foot complex is therefore a major goal in biomedical investigations (Leardini *et al.*, 1999; Myers *et al.*, 2001). Despite being a high focus area of research, the majority of the existing kinetic foot models lack some resemblance to the human motion. They do not take into account some movements that are easily detected by the human eye. The experience arising from gait evaluation points towards the development of more reliable and robust models. The present thesis tries to fulfill this gap, presenting a new and realistic tridimensional multibody model of the leg and foot complex that can improve the reliability of a human locomotion simulation.

1.2. Objectives

The main purpose of the present work is the development of a new tridimensional multibody model, using Natural coordinates, of the leg and foot that enables a realistic and reliable representation of its kinematic and dynamic behavior both in analysis and simulation, and that allows in the future for an efficient and accurate representation of the foot-ground interaction. There are a great number of models that represent the entire foot as a single rigid body (Pandy & Berme, 1988; Silva, 2003; P. C. Silva *et al.*, 2010), despite being efficient for 2D modeling and for simple human movements they are inadequate to depicture real 3D human gait motion. In this field there are also some detailed studies that consider the foot as two (hind-foot and toes) (Anderson & Pandy, 1999; Moreira, 2009; Vilà, 2012) or three rigid bodies (calcaneus, talus and toes), in order to improve the resemblance to real human motion (Delp, 1990). In this study an alternative approach to a three rigid body's foot is proposed: (1) rear-foot (calcaneus), (2) mid-foot (cuboid, navicular and cuneiforms) and fore-foot (metatarsals), and (3) toes (phalanges). This division emerged from the laboratory experience on gait evaluation, were the foot main segments can be noticed as the ones referred before. The separation is supported by arthrology studies such as the one provided by Isman & Inman

(1969), Hicks (1952) and Gray (1989). The model will also comprehend the leg (tibia and fibula), represented by a fourth segment.

In a first stage an anthropometric study of the foot will be necessary. The basis of this anthropometric study will be the work made by Anderson & Pandy (1999), where the foot is represented by a two segment structure (hind-foot and toes) and the report performed by and Parham *et al.* about the foot lengths. An anthropometric table will be developed, in which all of its inputs should be parameterized; the mass of each segment will be represented as a percentage of the total body mass, the length of each segment will be represented as a percentage of the foot length, except for the leg, which will be represent as a percentage of the height. This table should also present parameterized positions of the center of mass and inertias of each segment. The final table should be able to generate all the anthropometric measures needed for the next step, knowing only three input parameters: weight, height and foot size.

The following stage is centered on the creation of the multibody model using Natural coordinates, where the academic software Apollo (Silva, 2003) will have a central role. The model should be developed in order to be tested by this software, additional Fortran routines should be added to the program in case of need. A fully functional dynamic model is supposed to be developed by the end of this phase; the formulation must respect the necessary constraints that are imposed by the software.

The final stage comprehends the application of the model to a gait cycle, in order to study the foot-ground interaction, using an inverse dynamics analysis. This will require the formulation of a markers set protocol that incorporates the necessary information to represent the model proposed and that enables data processing to generate the remaining files to be used by Apollo (Silva, 2003). Having the necessary files to run the software, results as the angles between the bodies, joint moments and internal reaction forces will be generated and analyzed.

1.3.   Literature Review

In order to develop a computational model that represents realistically and reliably the human foot, many aspects have to be taken into account. Anthropometry is the basis of any model, it is crucial that the models' parameters are based on realistic human measures. The model is then formulated in order to be implemented in adequate software. To prove the correct performance of the model, kinematic, inverse and forward dynamic tests are to be performed. The following sections report the state of the art of the aspects mention above.

1.3.1. Anthropometry

Recent anthropometric studies are scarce; the majority of the available studies were performed during the twentieth century. Even rarer are the anthropometric studies that consider the foot as more than a simple segment. This imposes an increased degree of difficulty in the construction of human models, which is amplified in the present case due to the complex anthropometry and subtle movements of the foot. Within these studies an informal division can be applied: the studies that comprise only the lengths or volumes of the segments (Parham *et al.*, 1989);

the studies that report masses, inertias and centers of mass of the segments (McConville *et al.*, 1980) and last but not least the studies that evaluate the joints motion and mobility (Isman & Inman, 1969).

1.3.1.1. Segments Lengths and Volumes

Regarding anthropometric studies that comprises segments lengths or volumes it is important to make a brief historical introduction. The interest in the human body proportions as a subject of study started by calculating relations between body segments. The oldest study in this field remounts to the ancient Egypt (3000 B.C.), it uses the distance between the ground (sole) and the ankle as a unit of measurement and defines the height of the human body equal to 21.25 units. Another unit of measurement that was also introduced by the Egyptians, was the length of the middle finger; in this case the body height was set equal to 19 units. The pursuit of a standard measurement continued during the ancient Greece and a new unit of measurement was introduced in 500 B.C. The width of the palm at the base of the fingers; in this case the height of the body was considered to be 20 units. Vitruvius, an ancient Roman architect (100 B.C.) established that the body height was equal to the arm spread, this created a square limited by two horizontal lines (the sole and the top of the head) and two vertical lines (at the finger tips). Leonardo da Vinci adopted this square for his studies, and he later modified it by a circle around the human figure (Drillis *et al.*, 1964).

A jump in the temporal line brings the human segments lengths studies to the eighteenth century, when the firsts controlled studies were performed. In Germany Harless used the immersion method (determination of how much water is displaced by a submerged segment) to determine the absolute length of the segments (in centimeters) and the relative length using the hand as a standard unit. In 1858 he publishes his results in a text book on *Plastic Anatomy*, and in 1860 a treatise, *The Static Moments of the Human Body Limbs*. Although extremely complete and innovator for the time, this study considered the foot as a single segment. In 1884 Meeh using the same method as Harless, investigated the body segment volumes and for the first time the foot is studied as three different segments, base of the foot, middle foot and toes. Many other studies were performed using the immersion method during the eighteenth and nineteenth centuries (Drillis *et al.*, 1964).

The interest in human anthropometric studies continued for many years, having a considerable growth during and post wars and stagnating in the present century. Two different types of studies can be considered, the ones that use direct measurements and the ones that use computational models to calculate segments parameters. Regarding the first type, Contini (1972), De Leva (1996) and Anderson & Pandy (1999) present complete academic studies with different types of subjects. As mentioned previously anthropometry has high focus during war periods, due to this fact military data is of high importance in this field (Chandler *et al.*, 1975; Clauser *et al.*, 1969; Mcconville & Churchill, 1981; Parham *et al.*, 1989). Computational methods to estimate body parameters were introduced by Harless (Drillis *et al.*, 1964) and are still used today. Jensen (1975), Hatze (1980) built a model based on direct measurements from different subjects, Anderson & Pandy (1999) used this tool to compute the parameters regarding the foot segment only and Vilà (2012) used motion capture software to calculate average segment lengths.

4

Paying special attention to the information regarding the foot, one comes across an immediate finding; this body part is in the majority of times considered as a unique segment, being reported with only the foot size. Despite this fact, the US Army Natick Research, Development and Engineering Center produced a complete report about the anthropometry of the foot lower leg, presenting important measures about different aspects of the foot (Parham *et al.*,1989). Anderson & Pandy (1999) and Vilà (2012) also took a different approach, considering the foot as a two segment structure. The first ones representing the volume of each segment as a set of interconnected vertices.

1.3.1.2. Masses, Inertias and Centers of Mass

Knowing the mass, inertia and centers of mass of the segments that form the human body is extremely important in many fields of science. While the specific information may vary from author to author, the objective is common to all, to fully comprehend the biomechanics of the human body (Clauser *et al.*, 1969). Like in the previous section, a division can be made regarding this topic, the studies that comprise direct measurements from subjects and the ones that use computational methods. In the first category Clauser *et al.* (1969) used thirteen male cadavers and dissected them into fourteen segments, Contini (1972) performed different measurements in living American individuals, Chandler et al (1975) in a military study used six cadavers and dissected them into fourteen segments, Mcconville & Churchill (1981) in a different military study used thirty one living subjects, De Leva (1996) proposed a correction to Zatsiorsky-Seluyanov's parameters on Caucasian living subjects and Anderson & Pandy (1999) used five male living subjects to obtain the masses, inertias and centers of mass of each segment. For the computational type: Hanavan (1964) represented the human body by a set of simple geometric shapes and uniform densities; Jensen (1975) estimated the inertial properties of each segment based on the assumption that the body is composed of elliptical zones and that the segment densities are known; Hatze (1980) built a computational model that calculates the inertial properties of each segment based on direct measurements taken from different individuals; Anderson & Pandy (1999) complemented their data of living human subjects with a computational model for the feet and Vilà (2012) also used computational based methods to calculate these parameters for the studied model.

In the majority of the works described above the foot is once again treated as a single segment, only Anderson & Pandy (1999) and Vilà (2012) made an effort to specify this information for two different foot segments (Hind-foot and Toes).

1.3.1.3. Foot Joints Motion

The foot is an extremely complex system due to its large number of bones, ligaments, tendons, muscles and joints. The motion study of the foot takes great interest in evaluating the allowed degrees of freedom in each joint. Manter (1941) studied in great detail the movements in the subtalar and midtarsal joints. He arrived to the conclusion that the subtalar joint can be represented by one axis that allows screw like movements. The midtarsal joint can be represented by two axes, one that allows the fore part of the foot to rotate around a longitudinal axis with a screw like movement with opposite direction to that of the subtalar joint. The second axis lies obliquely in the foot and the

movement around this axis causes a marked change in the shape of the longitudinal arch. Manter also concluded that the pronation at the subtalar joint is accompanied by eversion in the midtarsal joint. Hicks (1953) proved that all the movements in the foot are described by rotations. His experiments demonstrated that in natural conditions and excluding the toes, these rotations occur at the ankle (two axes), at the midtarsal joint (two axes) and at tarsometatarsal joint (five ray joints described in the document). The movements were described as: the whole foot undergoes flexion extension upon the fixed leg (the flexion is accompanied by slight supination and the extension by slight pronation); the part distal to the talus in addition undergoes pronation-abduction-extension and supination- adduction-flexion; the part distal to the midtarsal joint in addition undergoes (approximate) pronation-supination; the forepart of the foot in addition undergoes a pronation-supination twist.

Special attention has been dedicated to the study of the ankle joint. Barnett & Napier (1952) studied the axis of rotation of the ankle joint in man and its influence upon the form of the talus and the mobility of the fibula. The authors arrived to the conclusion that the axis of rotation of this joint changes according to the foot movements. The axis is inclined downwards and laterally during dorsiflexion, and downwards and medially during plantar-flexion. Isman & Inman (1969) performed an exhaustive study, based on cadavers, about the talocalcaneal and talocrural joint. The measurements obtained from the experiments indicate that these joints can be considered as non-intersecting single-axis joints for purposes of bracing but that the variation in the positions of the different axes is such that they require individual determination. Figure 1.1 represents one of the measurements considered in this study, the perpendicular distance between these two axes.
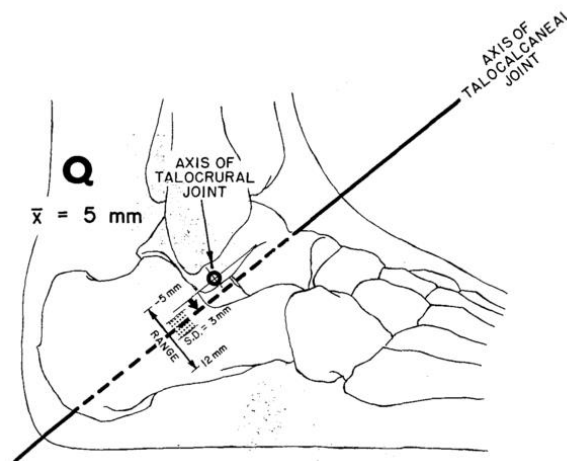
Figure 1.1 - Perpendicular distance between the axis of the talocrural and talocalcaneal joints (Isman & Inman, 1969).

A muscle force model was used by Procter & Paul (1982) to describe the action of the talocrural and midtarsal joint. Dul & Johnson (1985) developed a mathematical model that studied the motion of the foot with respect to the leg. This model had two input variables, namely: plantar-flexion/dorsiflexion angle and inversion/eversion angles. The authors modeled a three rigid body system: leg, talus and foot where the segments were connected by hinge joints, represented in Figure 1.2. An important consideration made in this work was the position of the talus segment, limited above by the line between the two malleolus and bellow by the line between a navicular point and the calcaneous point.

6

In the model used by Anderson & Pandy (1999), the authors intersected the talocrural and talocalcaneal joint in order to decrease integration time, and described the motion between the mid-foot and toes through the metatarsophalangeal joint.
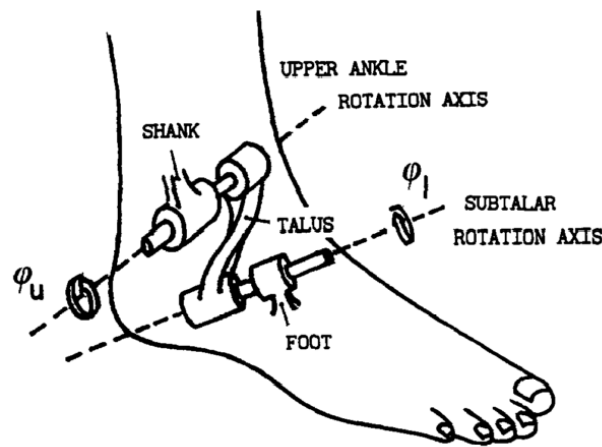
Figure 1.2 - Kinematic model of the human ankle (Dul & Johnson, 1985).

1.3.2. 3D Multisegment Lower Extremity Models

Lower extremity models are of great importance in the study of human movement, especially in locomotion analysis. These models allow, among other aspects, the comparison between normal and pathological gait, the development of improved prostheses and orthoses, and the improvement of sports performance.

1.3.2.1. Kinematic Models – Markers Protocol

The mechanical analysis of the foot while performing an activity, such as gait has been a challenge for many years. Problems as the inability to measure in vivo foot kinematics, the moderate scientific results arousing from qualitative measurements, and invasive approaches used during measurements were the main barriers in the progress of human motion analysis. Presently 3D stereophotogrammetric analysis (method for the study of joint kinematics in humans) is based on a procedure using skin-mounted markers, arrays of markers or a combination of both is the standard approach used by gait laboratories (Deschamps *et al.*, 2011).

In the last two decades many researchers have used this method to develop foot models using smaller segments, instead of considering the foot as a whole, the so called 3D multisegment foot models (3DMFMs) (Deschamps *et al.*, 2011). The number of 3DMFMs existent is currently too broad; however there are two models that stand out due to the number of clinical studies that applied them. The first, developed by Kidder *et al.* (1996) describes a system designed to track 3D motion of the leg (tibia and fibula), hind-foot (calcaneus, talus and navicular), fore-foot (cuneiforms, cuboid and metatarsals), and toes (phalanges and hallux) segments during both stance and swing phases of the gait cycle. A total of twelve markers (9 markers and a triad) were used in this protocol to represent the model, depicted in Figure 1.3. This model is known as the *Milwaukee Foot Model* (MFM) (Deschamps *et al.*, 2011). The same model and protocol was used by Myers *et al.* (2001) to describe the

7

kinematics of pediatric gait during both stance and swing. The MFM is widely used in kinematic clinical studies such as: ankle arthrosis (Khazzam *et al.* 2006), systemic rheumatoid arthritis (Khazzam *et al.*, 2007), hallux rigidus (Canseco *et al.*, 2008, 2009), and posterior tibial tendon dysfunction (Marks *et al.*, 2009; Ness *et al.*, 2008). Long *et al.* (2010) studied the repeatability and sources of variability associated with the assessment of segmental foot kinematics using MFM during multiple testing sessions at two different test sites.
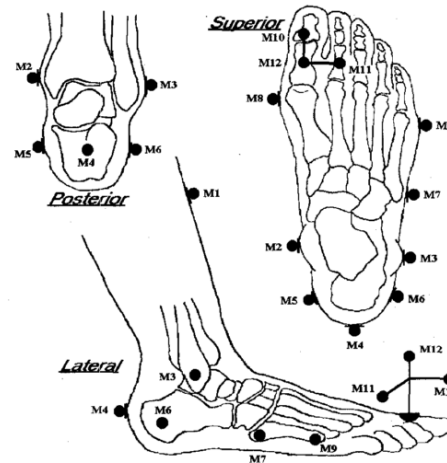
Figure 1.3 – Markers protocol of the *Milwaukee Foot Model* (MFM) (Kidder *et al.*, 1996).

The second, the *Oxford Foot Model* (OFM), named after the city where it was developed, was thought by Carson *et al.* (2001). The authors used a four segment foot model: leg (tibia and fibula), hind-foot (calcaneus and talus), fore-foot (five metatarsals) and hallux. The acquisition is performed through seventeen markers (fifteen normal markers and two stick markers). This model is commonly used in clinical analysis; some examples of that are: children treated for congenital talipes equinovarus (Theologis *et al.*, 2003) and rheumatoid arthritis (Turner *et al.*, 2006; Turner & Woodburn, 2008; Woodburn *et al.*, 2004).

Other important studies are worth to mention due to their relevance in the area. Leardini *et al.* (1999) designed a technique to describe the ankle and other foot joints rotation, using a five segment leg-foot model: leg (tibia and fibula), calcaneus, mid foot (navicular, cuneiforms and cuboid), first metatarsal and hallux. The kinematics was accessed using five clusters, attached to each segment, with four markers each. MacWilliams *et al.* (2003) established a nine-segment foot model, in order to present results of a kinematic and kinetic normal database of adolescent population. The segments described in this study are: hallux, medial toes, lateral toes, medial fore-foot, lateral fore-foot, calcaneus, cuboid, talus/navicular/cuneiforms and tibia/fibula. The data was obtained through a nineteen marker set protocol. Simon *et al.* (2006) developed and evaluated a kinematic measurement method for the foot that could be applied clinically to measure foot function including all typical foot deformities. The process is referred as *Heidelberg* method and does not model rigid foot segments; instead it describes the angular orientation of anatomical landmarks. Leardini *et al.* (2007) proposed a new protocol designed to track a large number of foot segments during the stance phase of gait using the smallest possible number of markers, oriented to foot pathological patients. The study segmented the foot into leg (tibia and fibula), calcaneus, mid-foot (navicular, cuboid and cuneiforms) and

metatarsus. This protocol is established based on fourteen reflective markers. Recently a study using pediatric participants used a markers protocol designed to divide the leg and the foot into four segments: leg (tibia and fibula), hind-foot (calcaneus and talus), fore-foot (navicular, cuboid, cuneiforms, and metatarsals) and hallux (proximal and distal phalanges). The protocol applied in that study used sixteen reflective markers (Bruening *et al.*, 2012a).

A different approach was used by Lundgren *et al.* (2008), in order to describe the kinematics of the tibia, fibula, talus, calcaneus, navicular, cuboid, medial cuneiform, first and fifth metatarsals during gait, the author used invasive bone anchored external markers. The protocol was defined through nine intracortical pins, inserted in the bones mentioned before; each pin was attached with a triad of reflective markers. The proposed procedure was developed to avoid some problems that arise from reflective markers protocols/ kinematic models such as: skin movement artifacts, assumptions that state that individual bones of the foot do not move relatively to each other and descriptions of foot and ankle kinematics may be incomplete because not all foot bones are included in the measurements.

1.3.2.2. Kinetic Computational Models

As seen before, there are a great number of kinematic studies of the foot, however complete and realistic foot models for dynamic simulations are limited. With the computational increasing power came the interest of developing *in silico* models of the human motion that can quantitatively evaluate velocities, accelerations, forces, moments and joint rotations. Pandy & Berme (1988) developed a mathematical model to study the single support phase of normal, level, human walking. Their lower extremity model was composed by three segments: foot, leg and thigh. Delp *et al.* (1990) formulated a model of the human lower extremity to study how surgical changes in musculoskeletal geometry and musculotendon parameters would affect muscle force and joint moments. The group modeled the lower extremity as six rigid-body segments: femur, patella, tibia/fibula, talus, foot (comprising the calcaneus, navicular, cuboid, cuneiforms and metatarsals) and toes. In this work, the foot is modeled with three degrees of freedom from three revolute joints, ankle, subtalar and metatarsophalangeal. Anderson & Pandy (1999) developed a three-dimensional model of the human body to simulate a maximal vertical jump. The lower extremity of their model was composed by four segments: thigh, leg, hind-foot (comprising all the foot bones except the phalanges) and toes. The foot model used in this study had the same joints and degrees of freedom as the one described before. Neptune *et al.* (2000) developed a method to simulate single-limb ground contact events, in order to study musculoskeletal injuries associated with such movements. The lower leg model used in their simulations was represented by: rear-foot, mid-foot, toes, talus, leg, patella, thigh and pelvis. The foot considered in this study had five degrees of freedom: two rotations around the subtalar and talocrural joints; flexion/extension in the metatarsophalangeal joint; flexion/extension and internal/external rotation in the joint separating the rear-foot and mid-foot.

In the past decade the pursuit of better human body models continued. Silva (2003) in his PhD thesis presented a multibody methodology with fully Cartesian coordinates for the dynamic analysis of complex human motions. The lower extremity of the whole body model was composed by three

segments: Thigh, Leg and Foot. In this case the foot had three degrees of freedom all due to the ankle joint (Flexion/Dorsiflexion, Inversion/Eversion and abduction/Adduction). Moreira (2009) developed a three-dimensional computational multibody model to characterize the interaction between the foot and ground, simulating the human gait during the stance and swing phases. The model proposed in his work is divided in three segments: leg, hind-foot and toes. This model had two degrees of freedom, one in the metatarsophalangeal joint and the other in the ankle joint, both represented by a revolute joint. P. C. Silva *et al.* (2010) developed a 2D multibody model of an active Ankle-Foot Orthosis (AFO) and integrated it in a whole body multibody model. The human lower extremity model consisted in three segments: thigh, leg and foot; the AFO was segmented in two parts: plantar module and lateral module. Both the foot and the AFO were assigned with one degree of freedom from the ankle revolute joint. Vilà (2012) presented a kinematic and dynamic study of human motion through multibody system dynamics techniques. The lower leg models used in this work are composed by four segments: thigh, leg, hind-foot and toes. The author connected all the segments through spherical joints in the 3D model and by revolute joints in the 2D model. So the foot has six degrees of freedom in the first model (three from the ankle joint and three from the metatarsophalangeal joint). And in the second model only two, from the same joints. Bruening *et al.* (2012b) developed a kinetic model based on the kinematic model previously described (Bruening *et al.*, 2012a). This model comprehends eight degrees of freedom arising from the joints: six from the ankle and midtarsal joint and two from the metatarsophalangeal joint. In order to study the kinetics of the model, the segments were converted to simple geometric shapes; the model was then subdivided into three sub-models in order to study each joint individually. Despite the number of lower extremity kinetic models existent, few of them report the anthropometry information needed to reproduce them.

1.3.3. Inverse Dynamics

The study of human movement implies the knowledge of the forces and moments of force produced by the musculoskeletal system during motion. The measurement of these physical parameters can be performed directly, using invasive techniques, *in vivo*, in human volunteers (Henning *et al.*, 1985) or animals (Herzog *et al.*, 1996) and *in situ,* using cadavers (Livesay *et al.*, 1995). Alternatively, these measurements can be quantified indirectly, using multibody methodologies, which have become a reliable replacement to the techniques presented before. This type of analysis can be divided in two main topics, inverse and forward dynamics. In the present work, only inverse dynamics methodology was applied, therefore this review approaches only this type of analysis.

Inverse dynamics consists in the determination of the driving or motor forces and reactions at the joints of a multibody system once the movement and the external forces are known (De Jalón & Bayo, 1994). From a computational point of view, this approach is far more efficient than forward dynamics and should be adopted when the goal of the analysis are exclusively the calculation of the joint reaction forces, muscle forces or their equivalent moment of force around the joints (Anderson & Pandy, 2001; Silva, 2003). As referred previously, to perform inverse dynamic analysis it is essential to know: kinematic information, such as the location of the joints obtained through motion capture techniques and markers set protocols; and dynamic information to describe the externally applied

forces and inertial properties, generally obtained using force plates (Alkjaer *et al.*, 2001; Gonçalves, 2010; Silva & Ambrósio, 2002; Winter, 1990). The use of this type of analysis in human motion has been growing; examples of that are the works of: Koopman *et al.* (1995), Alkjaer *et al.* (2001), Pandy (2001), Silva (2003), Blajer *et al.* (2007) and Gonçalves (2010).

1.4. Main Contributions

The principal contributions of this work are:

- A parametric model of a four segments leg and foot complex. This model calculates the lengths, masses, inertias and centers of mass positions of the segments that the multibody system requires from three single inputs – weight, height and foot size;
- A new tridimensional multibody model of the leg and foot complex, using natural coordinates, that enables a more realistic and reliable representation of the foot kinematics and dynamics;
- A new markers protocol that comprehend the joints needed for this model;

1.5. Structure and Organization

The thesis is divided in six chapters:

Chapter I – Presents the motivation of the author in respect to the theme, the objective that he proposes to achieve, a literature review over the main topics approached in the work and a brief resume with the main contributions of this work;

Chapter II – Covers the anatomical and physiological aspects the lower extremity limbs, paying special attention to the leg and foot. It also presents a study about the osteology, arthrology, myology and biomechanics of the leg and foot. A brief overview over gait analysis closes this chapter;

Chapter III – Describes the anthropometric model of the foot, explaining the approaches made to the Anderson & Pandy (1999) model and to the measurements taken by Parham *et al.* (1989);

Chapter IV – Presents a brief description over Multibody Formulation using Cartesian coordinates. The leg and foot model description using the methodology described closes this chapter.

Chapter V – Describes the markers set protocol that was used to acquire the kinematic data. Approaches the methods used to develop the files that need to be introduced in the analysis software Apollo.

Chapter VI – Presents the Kinematic and Kinetic results that validate the model.

Chapter VII – Closes this work by presenting the conclusions and possible future developments.

Chapter II

Anatomy, Physiology & Biomechanics

The human locomotion is a complex synchronous effort made by the interaction between bones, muscles, tendons and joints. To study the principles underlying human locomotion, it is necessary to first understand the anatomy and physiology of the lower limbs (thigh, leg and foot). Each lower limb is composed by thirty bones (excluding the sesamoid bones) and thirty three joints (excluding hip joints). Regarding the bones, the thigh comprehends the femur, the leg comprises the patella, fibula and tibia and the foot is subdivided in three functional complexes, the tarsus that is composed by seven bones (calcaneus, talus, navicular, cuboid and three cuneiforms), the metatarsus (five bones) and the phalanges (fourteen bones). On the subject of joints, the leg comprises the knee joint and the foot comprehends the other thirty two joints: Talocrural, Talocalcaneo-navicular, Calcaneo-cuboid, Talocalcaneal, Cuneo-navicular, Cuboid-navicular, two Intercuneiforms, Cuneo-cuboid, five Tarsometatarsal, four Intermetatarsal, five Metatarsophalangeal and nine Interphalangeal (Gray, 1989; Tortora & Derrickson, 2007).

The model presented in this work is intended to simulate the foot kinematics and dynamics, to do so the inferior limbs were reduced to leg and foot. This chapter presents a brief clinical description over the leg and foot complex, paying special attention to the osteology, arthrology, myology, physiology and biomechanics of it.

2.1. Osteology

2.1.1. Tibia

The Tibia, or shin bone, is located on the medial side of the leg; it is the only weight-bearing bone of the leg and the larger one (regarding its size, it's only surpassed by the femur). It has a

prismoid shape expanded in its two extremities. At its proximal end it articulates with the femur and fibula and at its distal end with the fibula and talus (Gray, 1989; Tortora & Derrickson, 2007).

2.1.2. Fibula

The fibula is located on the lateral side of the tibia, with which it is connected above and below. It is the smaller of the two bones, and, in proportion to its length, the most slender of all the long bones (Gray, 1989).

2.1.3. Foot

Anatomically the foot can be divided in Tarsus, Metatarsus and Phalanges, depicted in Figure 2.1. The Tarsus is subdivided in two rows of seven tarsal bones, proximal and distal. The proximal row comprises the talus and the calcaneus. The talus is the only bone of the foot that articulates with the tibia. The calcaneus projects itself posteriorly to the tibia and fibula and it is the largest and strongest bone of the tarsals, it serves to transmit the weight of the body to the ground. The distal row includes the cuboid, navicular and the three cuneiform bones, called first, second and third cuneiform. The cuboid bone is found between the calcaneus (proximally) and the basis of the IV and V metatarsals (distally). The navicular bone articulates between the head of the talus (proximally) and the cuneiform bones (distally). The cuneiform bones (lateral, intermedial and medial) articulate with the navicular bone (proximally) and with the basis of the first three metatarsals. Each bone of the tarsus is arbitrarily considered as cuboid in shape with six faces (Gray, 1989; Tortora & Derrickson, 2007).

The Metatarsus comprehends five long and thin metatarsal bones, numbered from I to V, they connect the tarsus to the phalanges. These bone are characterized by their prismatic section shape and can be divided into three areas, head, body and basis. The first metatarsal is shorter and thicker than the others, its basis articulates with the medial cuneiform bone and laterally with the second metatarsal. The second metatarsal is longer than the rest, its basis has four articular surfaces: one proximal, with the intermedial cuneiform bone; one dorsomedial, with the medial cuneiform bone; two lateral, one anterior, with the third metatarsal and one posterior, with the third cuneiform and sometimes a fifth facet is present and articulates with the first metatarsal. The basis of the third metatarsal has three articular surfaces: proximally with the lateral cuneiform bone; medially with the second metatarsal and laterally with the fourth metatarsal. The fourth metatarsal is shorter than the third, and its basis articulates proximally with cuboid bone, medially with the third metatarsal and the cuneiform bone and laterally with the fifth metatarsal. Finally the basis of the fifth metatarsal has an articulated surface in its proximal side with the fourth metatarsal and the cuboid bone. It is also characterized by a tuberosity in its lateral side. The heads of the metatarsals are articulated with the respective phalanges (Gray, 1989; Tortora & Derrickson, 2007).

The Phalanges are subdivided in proximal, medial and distal except for the hallux (big toe) that only has two, proximal and distal (Gray, 1989; Tortora & Derrickson, 2007). Another common foot division used in the literature relates to the foot functionality, where the subdivisions are rear-foot (calcaneus and talus), mid-foot (cuboid, navicular and cuneiforms), fore-foot (metatarsus) and toes (phalanges) (Abboud, 2002; Leardini *et al.*, 2007).

2.2. Arthrology

2.2.1. Knee joint

The knee joint must be regarded as consisting of three types of joints in one: two condyloid joints, between each condyle of the femur and the corresponding meniscus and condyle of the tibia; and a third, a saddle joint between the patella and the femur. The bones are connected together by the following ligaments: The articular capsule; The Ligamentum Patellae; The Oblique Popliteal; The Tibial Collateral; The Fibular Collateral; The Anterior Cruciate; The Posterior Cruciate; The Medial and Lateral Menisci; The Transverse; The Coronary.

The movements which take place at the knee-joint are flexion and extension, and, in certain positions of the joint, internal and external rotation (adduction and abduction). The movements of flexion and extension at this joint are different from those in a typical hinge-joint by two main reasons: the axis around which motion takes place is not a fixed one, but shifts forward during extension and backward during flexion; the beginning of flexion and the end of extension are accompanied by rotatory movements associated with the fixation of the limb in a position of great stability (Pina, 1999; Gray, 1989).

2.2.2. Talocrural joint

The talocrural joint is a hinge joint, approximately uniaxial; its line can be estimated by the anterior margin of the distal extremity of the tibia, which is palpable when the overlying tendons are relaxed. Despite being uniaxial, the rotation angle is dynamic, changing during dorsiflexion and plantar flexion. This joint is found on the mortise for the reception of the upper convex surface of the talus, formed by the inferior extremity of the tibia, the medial malleolus and the lateral malleolus, as represented in Figure 2.1. The bones are connected by a fibrous capsule, and by the following ligaments: the medial deltoid; the anterior and posterior talofibular; calcaneo-fibular.

When the foot is perpendicular to the leg, the active movements are the dorsiflexion and plantar flexion. During plantar flexion some small gliding, rotation, adduction and abduction movements are allowed (Pina, 1999; Gray, 1989).
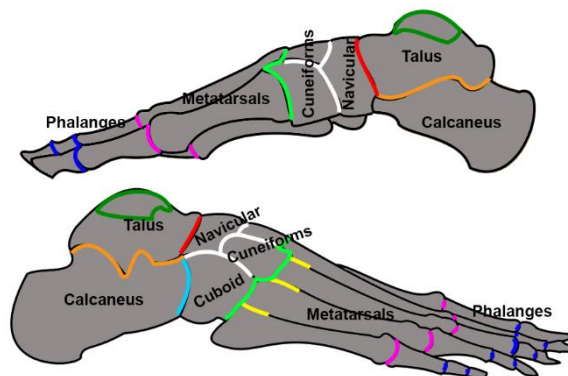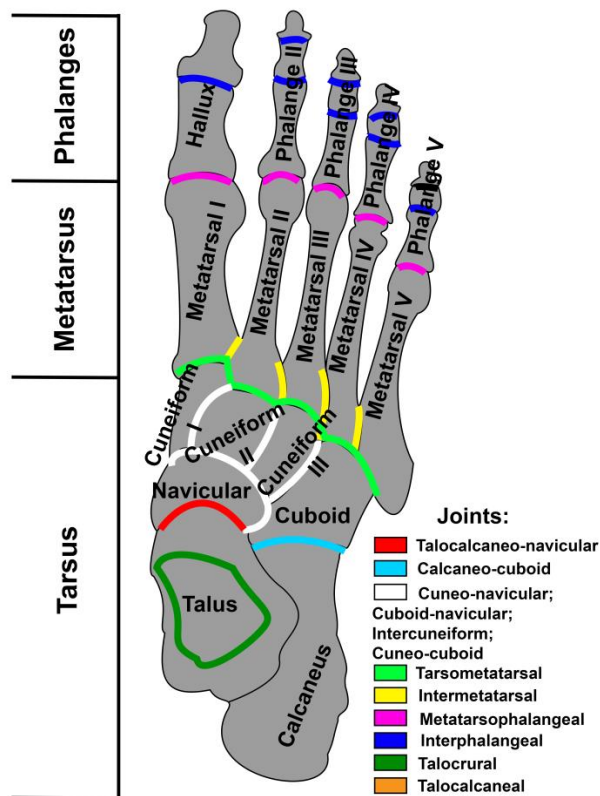
Figure 2.1 - Foot bones and joints. (Up) Top View. (Middle) Medial View. (Down) Lateral View.

2.2.3. Intertarsal joints

2.2.3.1. Talocalcaneo-navicular joint

The talocalcaneo-navicular joint is a spherical joint. It is formed by the rounded head of the talus being received into the concavity formed by the posterior surface of the navicular, the anterior articular surface of the calcaneus, and the upper surface of the planter calcaneonavicular ligament, as depicted in Figure 2.1. There are two ligaments in this joint, the articular capsule and the dorsal talonavicular.

The active movements are the inversion end eversion of the foot (Pina, 1999; Gray, 1989).

2.2.3.2. Calcaneo-cuboid joint

The calcaneo-cuboid is a biaxial saddle joint formed between the calcaneus and the cuboid, as represented in Figure 2.1. There are five intervenient ligaments in this joint: the articular capsule; the dorsal calcaneocuboid; part of the bifurcated; the long plantar; the plantar calcaneocuboid.

The movements between the calcaneus and the cuboid are slight gliding movements of the bones upon each other. There is also some rotation of one over the other during inversion and eversion of the whole foot (Pina, 1999; Gray, 1989; Tortora & Derrickson, 2007).

The Talocalcaneo-navicular joint and the Calcaneo-cuboid joint together form the Midtarsal joint or Transverse tarsal joint or Chopart's joint (Pina, 1999; Hicks, 1953).

2.2.3.3. Subtalar or Talocalcaneal joint

The subtalar joint is a rudimental condyloid joint. It is formed between the posterior calcaneal facet on the inferior surface of the talus, and the posterior facet on the superior surface of the calcaneus, as depicted in Figure 2.1. The two bones are connected by an articular capsule and by anterior, posterior, lateral, medial, and interosseous talocalcaneal ligaments.

The movements between the talus and the calcaneous follow the ones described in the talocalcaneo-navicular joint (Pina, 1999; Gray, 1989).

2.2.3.4. Cuneo-navicular, Cuboid-navicular, Intercuneiform and Cuneo-cuboid joints

These are all arthrodial joints and they are formed between the bones that they enunciate, as represented in Figure 2.1. The cuneo-navicular joint is connected by dorsal and plantar ligaments. The cuboid-navicular, intercuneiform and cuneo-cuboid are coupled by dorsal, plantar and interosseous ligaments.

The movements that these joints allow are slight gliding movements and rotation during pronation and supination (Pina, 1999; Gray, 1989; Tortora & Derrickson, 2007).

2.2.4. Tarsometatarsal joints

The tarsometatarsal joints are arthrodial joints. The first metatarsal articulates with the medial cuneiform bone; the second is deeply wedged in between the first and third cuneiforms articulating by its base with the second cuneiform; the third articulates with the third cuneiform; the fourth, with the cuboid and third cuneiform; and the fifth, with the cuboid, as depicted in Figure 2.1. The bones are connected by dorsal, plantar and interosseous ligaments.

The movements allowed in these joints are reduced to slight gliding upon each other (Pina, 1999; Gray, 1989).

The tarsometatarsal joint is also called Lisfranc joint (DiDomenico & Cross, 2012; Pina, 1999).

2.2.5. Intermetatarsal joints

The intermetatarsal joints are arthrodial joints, Figure 2.1. The bases of the metatarsals are connected by the dorsal, plantar, and interosseous ligaments, except for the first metatarsal, which is not connected by any ligaments with the second metatarsal.

The movements allowed in these joints are reduced to slight gliding upon each other (Pina, 1999; Gray, 1989).

2.2.6. Metatarsophalangeal joints

The metatarsophalangeal joints are condyloid joints. They are formed by the reception of the rounded heads of the metatarsal bones in shallow cavities on the ends of the first phalanges, as represented in Figure 2.1. The ligaments that involve these joints are plantar and two collateral.

The movements permitted in the metatarsophalangeal joints are dorsiflexion, plantar flexion, abduction, and adduction (Pina, 1999; Gray, 1989).

2.2.7. Interphalangeal joints

The interphalangeal joints are hinge joints, Figure 2.1. There are three ligaments in these joints: a plantar and two collateral.

The only movements permitted in the joints of the digits are dorsiflexion and plantar flexion (Pina, 1999; Gray, 1989).

2.3. Myology

Muscles that provide movement to the foot bones can be differentiated in extrinsic, arising from the leg, and intrinsic, originating in the foot itself. The extrinsic muscles are divided into three compartments by deep fascia: anterior compartment; lateral compartment; posterior compartment. A brief overview over these muscles is presented in Table 2.1 and Table 2.2.

Table 2.1 - Description of the extrinsic muscles intervenient in the foot movement (Pina, 1999; Gray, 1989; Tortora & Derrickson, 2007)

Muscle	Origin	Insertion	Function
Extrinsic Muscles			
Anterior Compartment			
Extensor digitorum longus	Tibia and Fibula	Middle and distal phalanges of the four outer toes	Dorsiflexes, abducts and everts foot; plantarflexes the four lateral toes
Extensor hallucis longus	Fibula	Distal Phalange of the hallux	Plantarflexes hallux, dorsiflexes and inverts foot
Tibialis anterior	Tibia	First metatarsal and first cuneiform	Dorsiflexes, adduces and inverts foot
Fibularis tertitus	Fibula	Fifth metatarsal	Dorsiflexes, abducts and everts foot
Lateral Compartment			
Fibularis brevis	Fibula	Fifth metatarsal	Everts and abducts foot
Fibularis longus	Fibula	First metatarsal	Everts, abducts and plantarflexes foot
Posterior Compartment			
Gastrocnemius	Femur	Calcaneus by means of calcaneal (Achilles) tendon	Plantarflexes foot, adduces and inverts foot
Plantaris	Femur	Calcaneus by means of calcaneal (Achilles) tendon	Assists *Gastrocnemius*
Soleus	Tibia and Fibula	Calcaneus by means of calcaneal (Achilles) tendon	Plantarflexes foot, adduces and inverts foot
Flexor digitorum longus	Tibia	Distal phalanges of the four lateral toes	Dorsiflexes four lateral toes and plantarflexes foot
Flexor hallucis longus	Fibula	Distal phalange of hallux	Dorsiflexes hallux and plantarflexes foot
Popliteus	Femur	Posterior tibia	Dorsiflexes and medially rotates leg
Tibialis posterior	Tibia and Fibula	Navicular; The three cuneiforms; Cuboid; Metatarsals (2-4)	Adduces and inverts foot

Table 2.2 - Description of the intrinsic muscles intervenient in the foot movement (Pina, 1999; Gray, 1989; Tortora & Derrickson, 2007)

Intrinsic Muscles			
Muscle	**Origin**	**Insertion**	**Function**
Abductor digiti minimi	Calcaneus	Proximal phalange of fifth toe	Abducts and dorsiflexes fifth toe
Abductor hallucis	Cuboid, Lateral Cuneiform, second and third metatarsals, three last metatarsophalageal joints	Fused with *Flexor hallucis brevis* and *Flexor hallucis longus*	Abducts and dorsiflexes hallux
Adductor hallucis	Calcaneus	Proximal phalange of hallux	Adduces and dorsiflexes hallux
Extensor digitorum brevis	Calcaneus	Proximal phalange of the hallux and three tendons fused with *Extensor digitorum longus*	Plantarflexes the proximal phalanges of the four lateral toes
Flexor digiti minimi brevis	Fifth metatarsal	Proximal phalange of fifth toe	Dorsiflexes the proximal phalange of the fifth toe
Flexor digitorum brevis	Calcaneus	Medial phalanges of second to fifth toe	Dorsilexes the lateral four toes
Flexor hallucis brevis	Cuboid and Lateral Cuneiform	Proximal phalange of the hallux and lateral sesamoid	Dorsiflexes hallux
Dorsal interossei	Metatarsals (3-5)	Proximal phalanges (3-5)	Dorsiflexes the proximal phalanges (3-5)
Plantar interossei	Metatarsals	Proximal phalanges (2-4)	Dorsiflexes the proximal phalanges (2-4)
Lumbricales	*Flexor digitorum longus*	Extensor tendons of the four lateral toes	Dorsiflexes the proximal phalanges and plantarflexes the medial and distal phalanges
Quadratus plantae	Calcaneus	Tendons of *Flexor digitorum longus*	Assists *Flexor digitorum longus*

2.4. Arches of the Foot

Usually the human foot is not a flat surface; on the contrary it has an arched aspect. This is due to a series of bony longitudinal and transverse arches, maintained by ligaments, tendons and muscles that provide the combined strength, flexibility and movement necessary for normal function, Figure 2.2. The longitudinal arch is generally described by two main arches: the medial and the lateral arch. The medial arch comprises the calcaneus, talus, navicular, the three cuneiforms and their three metatarsals. The supports of this arch are the tuberosity of the calcaneus and the heads of the three metatarsal bones. This arch is taller, more mobile and more flexible than the lateral arch. The lateral arch consists of the calcaneus, the cuboid and the lateral two metatarsal bones. Both arches are relatively rigid in standing but become more compliant during walking. The importance of the anatomic structures that support them differs; while muscles are indispensable to the maintenance of the medial arch, ligaments are a relatively more important part in the lateral arch. A series of transverse arches exist at the posterior part of the metatarsus, at the anterior part of the tarsus and in the middle of the tarsus, forming a convex curve in the direction of the dorsum when looking at the plantar surface of a non-weight bearing foot. This series of transverse arches disappear and flatten to varying degrees, during weight bearing (Abboud, 2002; Gray, 1989).
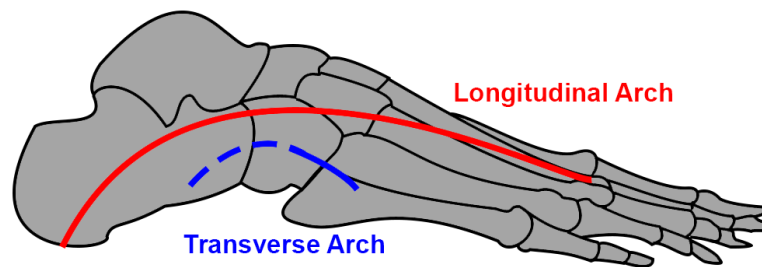
Figure 2.2 - Foot arches representation.

2.5. Physiology and Biomechanics

The foot, as seen before, is a complex multi-articular mechanical structure consisting of bones, joints and soft tissues, playing an extremely important role in the biomechanical function of the lower extremity and is controlled by both intrinsic and extrinsic muscles. It has to both support body weight whilst standing and to act as a lever to propel the body during locomotion. It must be able to conform to even and uneven surfaces, and thus be capable of making good contact with almost any supporting surface, forming a rigid platform that will not collapse under body weight.

Joints of the foot are controlled by extrinsic and intrinsic muscles of the lower limb and provide for the major motion function, angulation and support of the foot. As with all joints, motion occurs by rotation about an axis in a plane of motion. The three planes of motion in the foot are defined as: sagittal plane, frontal plane and transverse plane. The basic foot movements are described as follows:

Adduction occurs when the distal aspect of the foot is angulated towards the midline of the body in the transverse plane and deviated from the sagittal plane. **Abduction** occurs when the distal aspect of the foot is angulated away from the midline. These movements are depicted in Figure 2.3.

Plantar flexion is verified when the distal aspect is angulated downwards in the sagittal plane away from the tibia. **Dorsiflexion** is verified when the distal aspect is angulated towards the leg in the sagittal plane. These movements are represented in Figure 2.3.
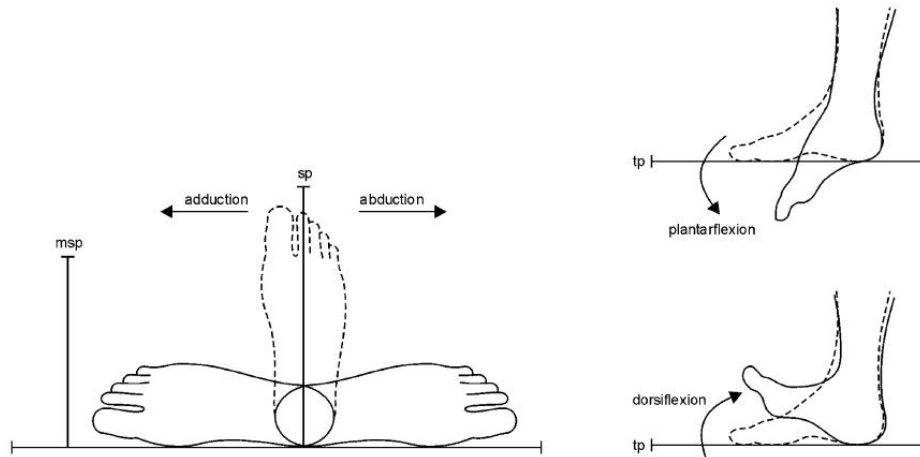
Figure 2.3 - Basic foot movements. (Left) Adduction/Abduction. (Right) Plantarflexion/Dorsiflexion (Abboud, 2002).

Inversion occurs when it is tilted in the frontal plane, such that its plantar surface faces towards the midline of the body and away from the transverse plane. **Eversion** occurs when its plantar surface faces away from the midline of the body and away from the transverse plane. These movements are depicted in Figure 2.4.

Supination is verified when it is simultaneously adducted, inverted and plantar flexed. **Pronation** is verified when it is abducted, everted and dorsiflexed (Abboud, 2002). These movements are represented in Figure 2.4.
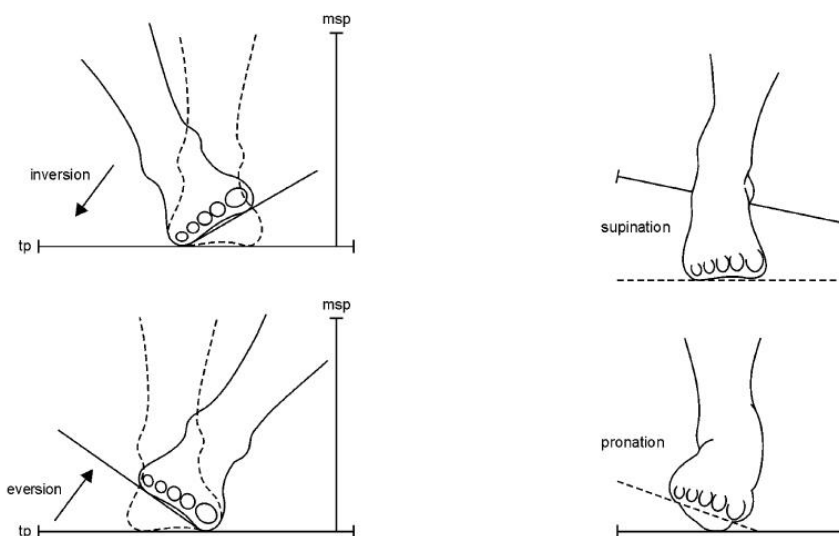
Figure 2.4 - Basic foot movements. (Left) Inversion/Eversion. (Right) Supination/Pronation (Abboud, 2002).

22

2.6. Human Gait Analysis

A succinct overview over normal human gait analysis is intended in this section in order to introduce the application case discussed on Chapter 5. Walking is the natural set of movements for human locomotion in a horizontal distance. Normally we learned it around the first year of age and it becomes part of our daily life, without even thinking about it. To define this set of movements it's trickier than to perform them. Lakany (2008) describes normal walking as a method of locomotion involving the use of two legs, alternately, to provide both support and propulsion. Whittle (2001) makes the distinction between walking, a periodic process, and gait, the manner or style of walking rather than the walking itself. The gait cycle can be defined as the time interval between two successive occurrences of one of the repetitive events of walking. Gait can be divided into two main temporal periods, Stance phase and Swing phase.

Stance phase is the time period in which a determined foot is in contact with ground and it can be described as five sub-phases as depicted in Figure 2.5:

1. **Initial Contact (IC) or Heel Strike (HS)** refers to the instant in which the foot of the leading lower limb touches the ground. Normally this initial contact is made by the heel;

2. **Loading Response (LR) or Foot Flat (FF)** occurs immediately after initial contact. During loading response, the foot comes in full contact with the floor, and body weight is fully transferred onto the stance limb. It represents 10% of gait cycle. The term foot flat is the point in time when the foot becomes approximately planar;

3. **Midstance (MS)** represents the beginning of single support. It begins when the contralateral foot leaves the ground and continues as the time at which the swing–period foot passes the stance-period foot. Midstance occurs from the 10 to 30 % of gait cycle;

4. **Terminal Stance (TS)** begins when the heel lifts the ground (heel off) and ends when the contralateral foot contacts the ground, supporting the body weight. This phase occurs between 30 and 50% of the gait cycle;

5. **Preswing (PS) or Toe Off (TO)** begins when the contralateral foot contacts the ground and ends when terminal contact is made with the toe of stance limb (toe off).

Swing phase represents the period of time, in which the foot is not in contact with the ground and can be divided in three sub-phases as depicted in Figure 2.5:

1. **Initial Swing (IS)**, from 60 to 75% of gait cycle, begins at the moment the foot leaves the ground and continues until maximum knee flexion occurs;

2. **Midswing (MiS)** begins following maximum knee flexion and ends when the leg is in a vertical position, from 75 to 85%. Midswing corresponds to midstance of contra lateral foot, being the time at which the two feet are side by side;

3. **Terminal Swing (TSw)** is the final phase of terminal swing. It is the deceleration phase, were the leg passes beyond perpendicular, and the knee fully extends in preparation for heel contact (Lakany, 2008; Moreira, 2009; Winter, 1991).
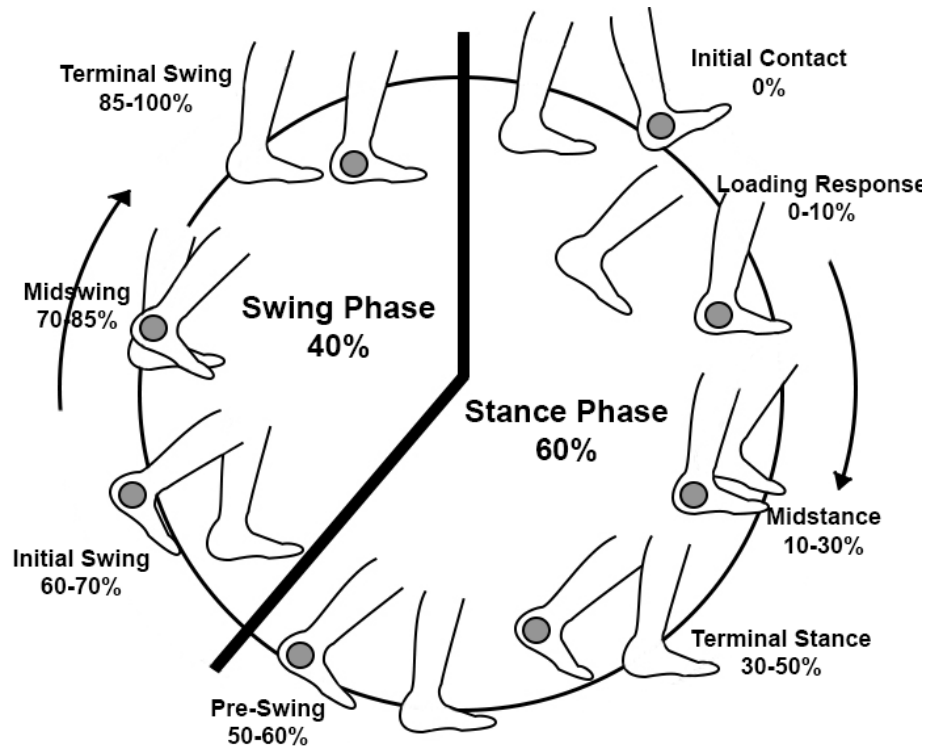
Figure 2.5 - Gait Cycle.

Chapter III

Model Anthropometry

Anthropometry is the science that studies the measurements of the human body. During history anthropometry was used to study the evolution of the human being, what differentiate us from our ancestors, what were the differences between genders, ages, races, and so on. With the evolution of technology, anthropometry regained attention; it became extremely important that the equipment and facilities that we use every day are adjustable to the individual (Winter, 1990).

3.1. Model Description

The main objective of this work was the development of a leg and foot model, which presents simultaneously robustness and efficiency, enabling the study of the main kinematic and dynamic patterns during human motion, in particular human gait. Since one of the objectives of the model is its application in academic and clinical studies, the developed model should consider several of the aspects previously addressed. The model should be detailed to study the major kinematic and kinetic parameters during the motion, enabling also the perception of possible deviations that happen at the ankle-foot level, taking in account the complexity of the required acquisition protocol.

In order to maximize the resemblance of the model to real human motion, the proposed model divides the leg in four segments, composed osteologically by:

1. Leg: Tibia and fibula;
2. Rear-foot: Calcaneus;
3. Mid/fore-foot: Navicular, cuboid, the three cuneiform bones and metatarsus;
4. Toes: Phalanges.

The segments are brought together by a set of joints; in total the model has four:

1. Talocrural joint;
2. Talocalcaneal or subtalar joint;
3. Midtarsal or Chopart's joint;
4. Metatarsophalangeal joint;

The choice of the four segments emerged from literature review (Hicks, 1953) and from the experience obtained from the laboratory practice. The intrinsic foot motions were acquired for different daily movements such as walking, jumping, climbing stairs and pure movements (plantar flexion and dorsiflexion, eversion and inversion), using an optical motion capture system. This set of trials enabled to conclude that the insertion of a third rigid body between the toes segment and the rear foot would increase the reliability of the model, since its inclusion would enable the study of movements that happen at the midtarsal and tarsometatarsal joint. This data indicates that the motion of the metatarsals due to movements at both of these joints should not be neglected, being visually detected if a force is applied in the metatarsal region. It is important to note that the midtarsal and tarsometatarsal joints are responsible for different movements. However, in order to avoid the increase of computational effort during the simulations and the time spent during the preparation of the required acquisition protocol, the model will consider that the different DOF's of each joint are concentrated at the midtarsal joint. A universal joint will be used to study sagittal and horizontal movements, and a coincident second rigid body to study the rotation of the mid/fore-foot segment around itself. This approach, of using a coincident rigid body, is also used to study the internal rotation of the leg. This consideration is further explained in Section 4.5.

Another important aspect of the model is the non-intersecting axes of the Talocrural and the Talocalcaneal joint, referred by Isman & Inman (1969). This is achieved by considering the talus as a massless link, avoiding the problem pointed out by Anderson & Pandy (1999) that the addition of the talus, due to its small mass, would increase the integration time for the model considerably, this consideration is depicted in Figure 3.1. This solution solves the kinematic problem without the introduction of a dynamic problem. This consideration is further explained in Section 4.5.
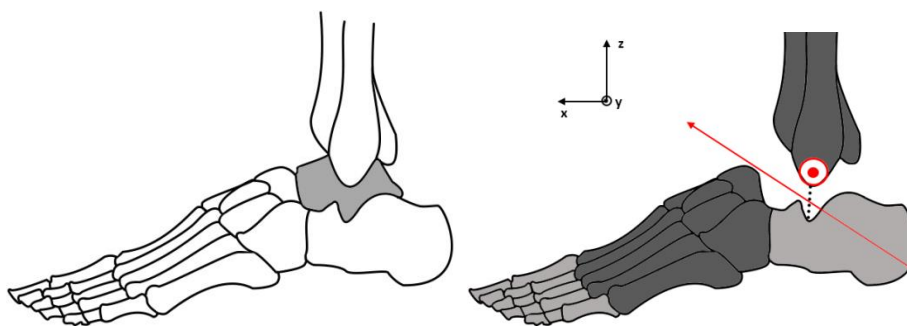
Figure 3.1 - (Left) Foot bones with the Talus highlighted. (Right) Massless Link representation with the Talocrural and Talocalcaneal axis depicted.

In total the model has thirteen degrees of freedom (DOF), they arise from:
- 1 DOF – Flexion (plantar/dorsiflexion) at the Metatarsophalangeal joint;
- 2 DOF – Flexion (plantar/dorsiflexion) and Abduction/Adduction at the Midtarsal joint;
- 1 DOF – Internal mid-foot and fore-foot rotation;

- 1 DOF – Flexion (plantar/dorsiflexion) at the talocrural joint;
- 1 DOF – Inversion/Eversion at the talocalcaneal joint;
- 1 DOF – Internal leg rotation;
- 6 DOF – Rotations and Translations over the three axes of the model as a whole.

The model DOF's are depicted in Figure 3.2.
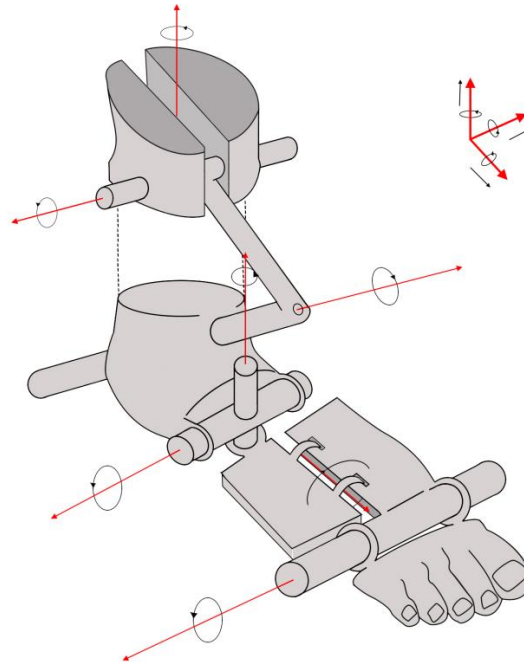
Figure 3.2 - Representation of the system Degrees of Freedom. (Red) Rotation and Translation Axis.

3.2. Leg and Foot Anthropometry

The study of human locomotion requires the use of kinetic and kinematic analysis, which in turn involve the use of anthropometric measures such as: segments dimensions, masses, moments of inertia, the location of the centers of mass, joints centers of rotation, the origin and insertion of muscles, the angle of pull of tendons, and the length and cross-sectional of muscles. (Winter, 1990)

In order to build a foot model to study the foot-ground interaction it is fundamental to study the anthropometry of this body segments.

3.2.1. Segment dimensions

In Section 1.3 it was seen that the majority of the anthropometric studies consider the foot as a unique segment. However, an extensive study was performed by the US Army Natick Research, Development and Engineering Center in 1985 in Fort Jackson, South Carolina, in order to access various aspects of fit of a new boot (i.e. the MIL-5) (Parham *et al.*, 1989). This study had the particularity to involve 293 males and 574 females, providing a good statistical distribution. The measurements taken are described in Table 3.1 and Figure 3.3.

Table 3.1 - Description of the measurements taken by Parham *et al.* (1989).

	Measurements taken by Parham *et al.* (1989)				
1	Stature	10	Maximum Toe Height	22	Ankle Length
2	Calf Height	11	Outside Ball of Foot Height	23	Instep Length
3	Ankle Height	12	Calf Circumference	24	Ball of Foot Length, Right
4	Medial Malleolus Height	13	Ankle Circumference	25	Foot Length, Right
5	Lateral Malleolus Height	14	Heel-Ankle Circumference	26	Ball of Foot Breadth, Right
6	Dorsal Arch Height	15	Instep Circumference	27	Outside Ball of Foot Length
7	Plantar Arch Height	16	Ball of Foot Circumference	28	5th Toe Length
8	Ball of Foot Height	17	Heel Breadth, Right	32	Bimalleolar Breadth
9	First Toe Height	18	Ball of Foot Breadth, Diagonal	33	1st-3rd Toe Breadth
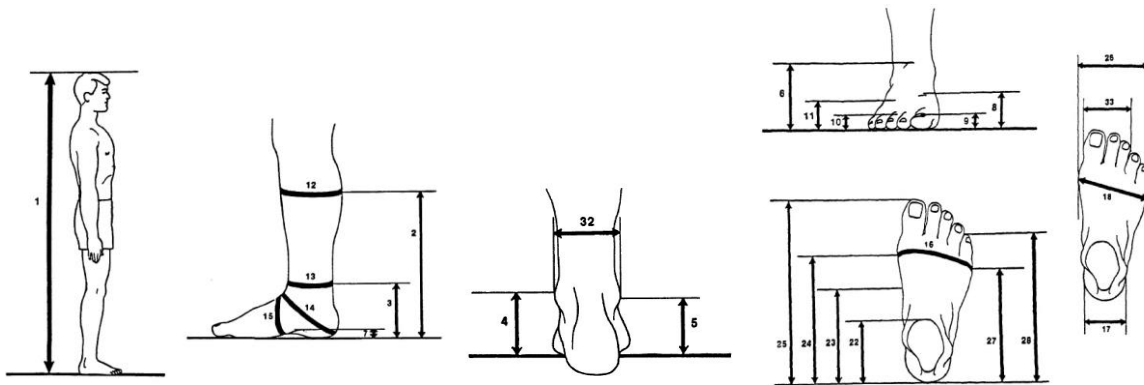
Figure 3.3 - Representation of the measurements taken by Parham *et al.* (1989).

For the present model, the important measurements presented in this document are the mean of the: Stature (1), Medial Malleolus Height (4), Lateral Malleolus Height (5), Ankle Length (22), Ball of Foot Length (24) and Foot Length (25). They are summarized in Table 3.2.

Table 3.2 - Measurements taken into consideration in the present work (Parham *et al.*, 1989).

	Mean Male (cm)	Mean Female (cm)
Stature (1) (H_{bP})	175.71	161.85
Medial Malleolus Height (4)	8.12	7.17
Lateral Malleolus Height (5)	7.26	6.59
Ankle Length (22)	10.84	9.65
Ball of Foot Length (24)	19.67	17.75
Foot Length (25) (L_{fP})	26.96	24.38

It is necessary to adapt this information to the anthropometric measurements of the model. This is done considering that:

- Rear-foot height – Average between the Medial Malleolus height (4) and the Lateral Malleolus height (5);

- Rear-foot length – Equal to Ankle length (22);
- Mid-foot and Fore-foot length – Subtraction of Ankle length (22) to Ball of Foot length (24);
- Toes – Subtraction of Ball of Foot length (24) to Foot length (25);

The previous calculations are summarized in Table 3.3.

Table 3.3 - Adaptation of the measurements taken by Parham *et al.* (1989) to the present work.

	Mean Male (cm)	Mean Female (cm)
Rear-foot height (L_h)	7.69	6.88
Rear-foot length (L_{RF})	10.84	9.65
Mid-foot and Fore-foot length (L_{Mf})	8.83	8.1
Toes (L_T)	7.29	6.63

Drillis & Contini (1966) were pioneers by presenting the segments' length as a percentage of body height; this procedure serve as a good approximation in the absence of individual direct measures (Winter, 1990). In the present work a similar idea will be applied, the segments' length will be presented as a percentage of the foot length (L_{fP} , Male 26.96 cm, Female 24.38 cm) (Parham *et al.*, 1989). This approach instead of the one applied by Drillis & Contini (1966) is related with the fact that the size of the foot does not have a direct relation with the body height. Table 3.4 is the application of this approach to the data in Table 3.3.

Table 3.4 - Summary of the measurements presented in Table 3.3 as a percentage of the foot length.

	Formula	Mean Male	Mean Female
Rear-foot height	$L_h \ / \ L_{fP} \ \times 100$	28.52	28.22
Rear-foot length	$L_{Rf} \ / \ L_{fP} \ \times 100$	40.21	39.58
Mid-foot and Fore-foot length	$L_{Mf} \ / \ L_{fP} \ \times 100$	32.75	33.22
Toes length	$L_T \ / \ L_{fP} \ \times 100$	27.04	27.20

3.2.2. Segments Mass and Center of Mass

Information regarding a three segment foot model is sparse or non-existent, so in order to construct one, the two segment foot described by Anderson & Pandy (1999) served as the basis for this work. A summary of the information taken from this document is presented in: Table 3.5 regarding the centers of mass positions, Table 3.6 concerning the masses, and Figure 3.4 depicts the model used by these authors.

Table 3.5 – Summary of the relevant information (Right Leg and Foot) for the model, regarding the centers of mass presented by Anderson & Pandy (1999). Each body articulates with an Inboard Body by a joint of a particular type. The position of a joint relative to the center of mass of the body is defined by the Body-To-Joint vector. The position of the joint relative to the Inboard Body's center of mass is given by the Inboard-To-Joint vector.

	Vector	Body	Inboard Body	CM x (m)	CM y (m)	CM z (m)
Inboard-To-Joint	v_{AP1}	Hind-foot	Leg	0.0000	-0.2438	0.0000
	v_{AP2}	Toes	Foot	0.0980	-0.0380	0.0180
Body-To-Joint	v_{AP3}	Hind-foot	Leg	-0.0359	0.0513	-0.0055
	v_{AP4}	Toes	Foot	-0.0269	-0.0185	-0.0051
	v_{AP5}	Leg	Thigh	0.0000	0.1862	0.0000

Table 3.6 - Summary of the relevant information (Right Leg and Foot) for the model, regarding the masses presented by Anderson & Pandy (1999).

	Mass (kg)
Leg (m_L)	3.510
Hind-foot (m_H)	1.20
Toes (m_T)	0.2051
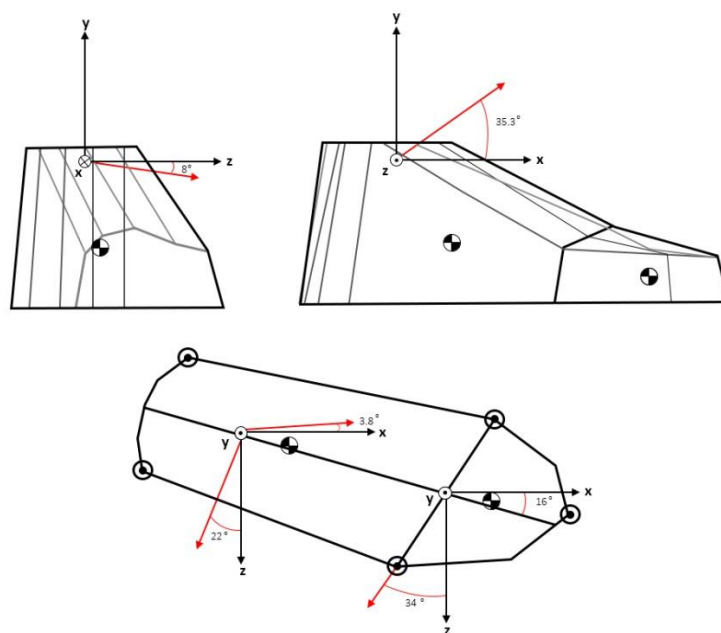
Figure 3.4 - Locations of the talocrural, talocalcaneal and metatarsophalangeal joint axes for the right foot in the model used by Anderson & Pandy (1999).

In this document, Anderson & Pandy (1999) calculated the hind-foot and toes mass, position of the centers of mass and the moments of inertia by representing the volume of each segment by a set of interconnected vertices, in which the coordinates were derived by measuring the surface of a size 10 shoe. They assumed a uniform density of 1.1gm/cm^{3} for the feet, the density was numerically integrated over the volume of each segment. The combined mass of these two segments is similar to the one reported by (Mcconville & Churchill, 1981) plus the mass of a 10 size shoe.

Following the approach presented on the previous section, the positions of the centers of mass relative to the joints and to the inboard body (body that articulates with the body being studied) were generalized, meaning that they were converted to percentages relative to the foot size (L_{fAP}), i.e. the lengths of the segments were divided by the total length of the foot (27cm, 10 size shoe); except for the hind-foot position relative to the inboard body (leg) and the leg center of mass relative to the knee joint, that were converted to a percentage relative to the body height (H_{bAP} , 177cm). The mass of each segment was also converted to percentages relative to the body total mass (m_b , 71.0052 kg). The weight of the body, its height and the foot size are described in Anderson & Pandy (1999).

Another important modification was made on the axes; representing the local reference frames of each foot segment in order to make these compatible with the experimental set up and with the multibody software adopted. The x axis was aligned with the medial foot line and the y axis became z. The novel y axis is perpendicular to the novel x and z axis, so the coordinates in y of the centers of mass become null (Table 3.4). The final alteration was made regarding the direction of the vectors *Body-To-Joint* described on Table 3.5. Anderson & Pandy (1999) presented them from the center of mass to the joint, in this work they will be presented from the joint to the center of mass, as matter of visual simplicity. The summary of this information is presented in Table 3.7, Table 3.8, Table 3.9 and Figure 3.5.

Table 3.7 - Masses of the segments described by Anderson & Pandy (1999) converted to percentages relative to the total body mass (m_b).

	Formula	Masses
Leg	$\dfrac{m_L}{m_b} \times 100$	4.943
Hind-foot	$\dfrac{m_H}{m_b} \times 100$	1.690
Toes	$\dfrac{m_T}{m_b} \times 100$	0.289
Foot (Toes + Hind-foot)	$\dfrac{m_H + m_T}{m_b} \times 100$	1.979

Table 3.8 - Position of the Centers of Mass relative to the Joints ($-x_{v_{AP_i}}$, $-y_{v_{AP_i}}$, $-z_{v_{AP_i}}$) of the segments described by Anderson & Pandy (1999) converted to percentages relative to the foot length (L_{fAP} - Hind-foot CM and Toes CM) or body height (H_{bAP} - Leg CM) and converted to the new axes.

Centers of Mass relative to the Joints					
Hind-foot CM (Relative to the Ankle Joint)		Toes CM (Relative to the Metatarsophalangeal Joint)		Leg CM (Relative to the Knee Joint)	
Formula	Value	Formula	Value	Formula	Value
$x = \dfrac{-x_{v_{AP3}}}{L_{fAP}} \times 100$	13.30	$x = \dfrac{-x_{v_{AP4}}}{L_{fAP}} \times 100$	9.96	$x = \dfrac{-x_{v_{AP5}}}{H_{bAP}} \times 100$	0
y	0	y	0	y	0
$z = \dfrac{-z_{v_{AP3}}}{L_{fAP}} \times 100$	-19.00	$z = \dfrac{-y_{v_{AP4}}}{L_{fAP}} \times 100$	6.85	$z = \dfrac{-y_{v_{AP5}}}{H_{bAP}} \times 100$	-10.52

Table 3.9 - Position of the Joints relative to the Inboard bodies Centers of Mass ($-x_{v_{AP_i}}$, $-y_{v_{AP_i}}$, $-z_{v_{AP_i}}$) of the segments described by Anderson & Pandy (1999) converted to percentages relative to the foot length length (L_{fAP} - Metatarsophalangeal Joint) or body height (H_{bAP} - Ankle Joint) and converted to the new axes.

Joints relative to the Inboard Bodies Centers of Mass			
Ankle Joint (Relative to the Leg CM)		Metatarsophalangeal Joint (Relative to the Hind-foot CM)	
Formula	Value	Formula	Value
$x = \dfrac{-x_{v_{AP1}}}{H_{bAP}} \times 100$	0	$x = \dfrac{-x_{v_{AP2}}}{L_{fAP}} \times 100$	36.30
y	0	y	0
$z = \dfrac{-y_{v_{AP1}}}{H_{bAP}} \times 100$	-13.77	$z = \dfrac{-y_{v_{AP2}}}{L_{fAP}} \times 100$	-14.074
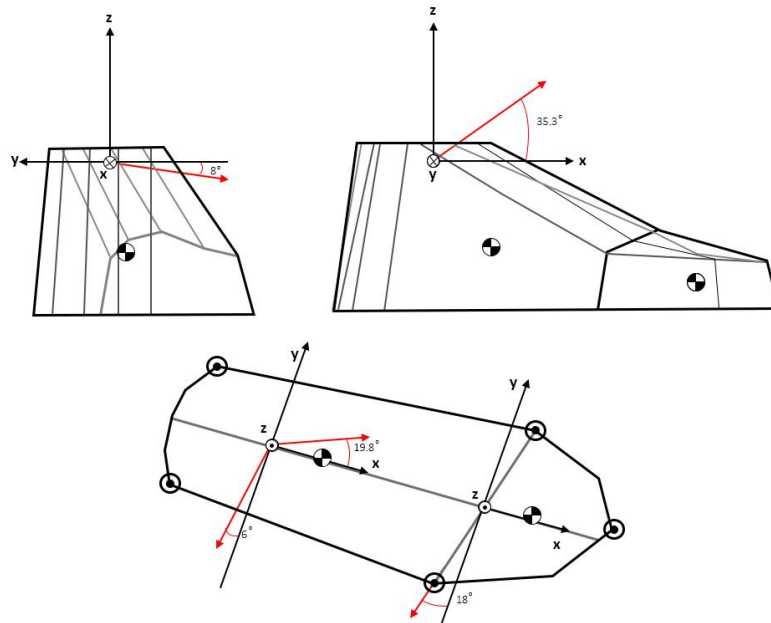
Figure 3.5 - Locations of the talocrural, talocalcaneal and metatarsophalangeal joint axes for the right foot in the modified model based on the one formulated by Anderson & Pandy (1999).

From the initial two segments foot, it was necessary to convert it into three segments; this was achieved by splitting the hind-foot (Segment 0) into rear-foot (Segment III) and mid-foot and fore-foot (Segment II). The segment corresponding to the toes (Segment I) was kept unchanged therefore equal to the one in the original model. A new joint was added between segment III and II, so this new arrangement has four joints: Knee joint (J4), Talocrural joint (J3), Midtarsal joint (J2) and Metatarsophalangeal joint (J1), as depicted in Figure 3.6. To calculate the anthropometric data for the proposed model some assumptions had to be made due to the lack of information available in articles or experimental data.

- The segment II center of mass (CM2) position relative to Joint 2 (r_2 vector - Figure 3.6 and Table 3.12). It was assumed that CM2 position correspond to the middle point between J2 and J1;
- The mass percentages of segment III and II relative to segment 0 (m_3 and m_2). It was assumed that the mass of segment II is equivalent to 40% of the mass of segment 0 and the mass of segment III is therefore 60% of the mass of segment 0;
- The Inertia of segment III. This assumption is explained in Section 3.2.3.

These assumptions were formulated so that the model presented in this work was, from the anthropometric and inertial point of view, equivalent to the one presented by Anderson & Pandy (1999) when both are in the same initial reference position. It is important to notice that these assumed data is easily modified in order to adjust the model. The final scheme is presented in Figure 3.6.
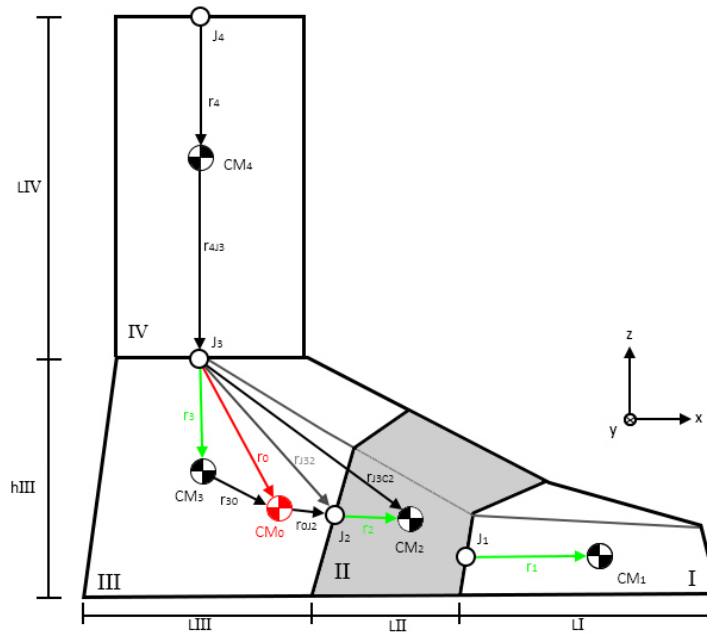
Figure 3.6 – Anthropometric final scheme with the representation of the four segments, the corresponding centers of mass and important anthropometric vectors (Table 3.12 and Table 3.13) – Right Foot

In order to complement the information presented in Section 3.2.1, the segments lengths assigned to the proposed model (L_0, L_I, L_{II}, L_{III}, L_{IV} and h_{III}) are reported in Table 3.10; based on the work of Parham *et al.* (1989) (Table 3.4), except for the length of the shank (LIV) that is the sum of the length between the knee joint (J4) and the leg center of mass (CM4) with the length between the leg center of mass (CM4) and the talocrural joint (J3), presented by Anderson & Pandy (1999) (Table 3.5).

Table 3.10 - Segments Length.

	Formula	Value
Segment 0 (L_0)	$\dfrac{L_{Mf} + L_{Rf}}{L_{fP}} \times 100$	73
Segment I (L_I)	$\dfrac{L_T}{L_{fP}} \times 100$	27
Segment II (L_{II})	$\dfrac{L_{Mf}}{L_{fP}} \times 100$	33
Segment III (L_{III})	$\dfrac{L_{Rf}}{L_{fP}} \times 100$	40
Segment IV (L_{IV})	$\dfrac{\left| y_{v_{AP1}} \right| + \left| y_{v_{AP5}} \right|}{H_{bAP}} \times 100$	24
Height segment III (h_{III})	$\dfrac{L_h}{L_{fP}} \times 100$	28

The masses designated to each segment in the proposed model ($m_0, m_I, m_{II}, m_{III}, m_{IV}$), after applying the assumptions over the information in Table 3.7, are reported in Table 3.11.

Table 3.11 – Segments Mass.

	Formula	Value
Segment 0 (m_0)	$\dfrac{m_H}{m_b} \times 100$	1.690
Segment I (m_I)	$\dfrac{m_T}{m_b} \times 100$	0.289
Segment II (m_{II})	$m_0 \times 40\%$	0.676
Segment III (m_{III})	$m_0 \times 60\%$	1.014
Segment IV (m_{IV})	$\dfrac{m_S}{m_b} \times 100$	4.943

Using the segments dimensions presented in Table 3.10 and the vectors parameters reported in Table 3.8 and Table 3.9, allows the computation of the anthropometric vectors that define the proposed model (depicted in Figure 3.6). These vectors are presented in Table 3.12 and Table 3.13, the description of the calculations is detailed following the tables.

Table 3.12 – Anthropometric foot vectors description.

	Vectors (Foot)				
	Initial Point	Final Point	$\dfrac{x_i}{L_f} \times 100$	$\dfrac{y_i}{L_f} \times 100$	$\dfrac{z_i}{L_f} \times 100$
$\mathbf{r}_0$	Joint 3	CM0	13.30	0.00	-19.00
$\mathbf{r}_3$	Joint 3	CM3	1.20	0.00	-14.31
$\mathbf{r}_{0J2}$	CM0	Joint 2	3.30	0.00	0.00
$\mathbf{r}_2$	Joint 2	CM2	14.85	0.00	-7.04
$\mathbf{r}_1$	Joint 1	CM1	9.96	0.00	6.85
$\mathbf{r}_{3J2}$	CM3	Joint 2	15.40	0.00	-4.69
$\mathbf{r}_{J32}$	Joint 3	Joint 2	16.59	0.00	-19.00
$\mathbf{r}_{J3C2}$	Joint 3	CM2	31.44	0.00	-26.04
$\mathbf{r}_{30}$	CM3	CM0	12.10	0.00	-4.69
$\mathbf{r}_{02}$	CM0	CM2	18.15	0.00	-7.04
$\mathbf{r}_{0J1}$	CM0	Joint 1	36.3	0.00	-14.07

Table 3.13 – Anthropometric leg vectors description.

		Vectors (Leg)		
	Initial Point	Final Point	$\frac{x_i}{H_b} \times 100$	$\frac{y_i}{H_b} \times 100$	$\frac{z_i}{H_b} \times 100$
$\mathbf{r}_4$	Joint 4	CM4	0	0	-10.52
$\mathbf{r}_{4J3}$	CM4	Joint 3	0	0	-13.77

Description of the calculations:

- $\mathbf{r}_0$ – Vector generalized from Anderson & Pandy (1999), CM0 relative to J3, Table 3.8;
- $\mathbf{r}_3$ – Vector obtained from the separation of CM0 into CM2 and CM3 in relation to J3, Equation (3.1);

$$r_3 = \frac{r_0 \cdot m_0 - r_{J3C2} \cdot m_2}{m_3}$$ (3.1)

- $\mathbf{r}_{0J2}$ – Vector calculated from the difference between r_{0J1} x coordinate with the length of segment II (LII);
- $\mathbf{r}_2$ – Assumption, CM2 is considered to be exactly in the middle position of segment 2, so this vector is obtain from dividing r_{0J1} by two and subtracting r_{0J2};
- $\mathbf{r}_1$ – Vector generalized from Anderson & Pandy (1999), CM1 relative to J1, Table 3.8;
- $\mathbf{r}_{3J2}$ – Vector obtained from the difference between $\mathbf{r}_{J32}$ and $\mathbf{r}_3$;
- $\mathbf{r}_{J32}$ – Vector obtained from the sum of $\mathbf{r}_0$ and $\mathbf{r}_{0J2}$;
- $\mathbf{r}_{J3C2}$ – Vector obtained from the sum of $\mathbf{r}_{J32}$ and $\mathbf{r}_2$;
- $\mathbf{r}_{30}$ – Vector obtained from the difference between $\mathbf{r}_0$ and $\mathbf{r}_3$;
- $\mathbf{r}_{02}$ – Vector obtained from the difference between $\mathbf{r}_{J3C2}$ and $\mathbf{r}_0$;
- $\mathbf{r}_{0J1}$ – Vector generalized from Anderson & Pandy (1999), J1 relative to CM0, Table 3.9;
- $\mathbf{r}_4$ – Vector generalized from Anderson & Pandy (1999), CM4 relative to J4, Table 3.8;
- $\mathbf{r}_{4J3}$ – Vector generalized from Anderson & Pandy (1999), J3 relative to CM4, Table 3.9.

3.2.3. Inertias and Radius of Gyration

For this section, once again, few information was available, so the base data is referenced again to Anderson & Pandy (1999), Table 3.14.

Table 3.14 - Summary of the relevant information (Right Leg and Foot) for the model, regarding the inertias presented by Anderson & Pandy (1999).

	Inertias		
	x (kg/m²)	y (kg/m²)	z (kg/m²)
Hind-foot (I_0)	0.0013	0.0039	0.0037
Toes (I_1)	0.0001	0.0001	0.0002

As written above, one assumption was made, the inertia of segment III (I_{III}) this inertia was assumed to be the product of an inertial scaling factor with the inertia of segment 0 (I_0). The scaling factor was formulated as:

$$\xi = \frac{m_{III}}{m_0} \cdot \left(\frac{L_{III}}{L_0}\right)^2 \times 100 = 26.67\% \tag{3.2}$$

$$I_{III} = I_0 \cdot \xi \tag{3.3}$$

The scaling factor formulation arrived from the inertia formula $I = m \cdot L^2$ .So the product of I_0 by the product of the masses ratio with the square of the lengths ratio gives I_{III}. The inertia of segment II was calculated using the Parallel Axis Theorem, Equation (3.4).

$$\begin{cases} I_{0x} = I_{IIIx} + m_{III} \cdot r_{IIIx}^2 + I_{IIx} + m_{II} \cdot r_{IIx}^2 \\ I_{0y} = I_{IIIy} + m_{III} \cdot r_{IIIy}^2 + I_{IIy} + m_{II} \cdot r_{IIy}^2 \\ I_{0z} = I_{IIIz} + m_{III} \cdot r_{IIIz}^2 + I_{IIz} + m_{II} \cdot r_{IIz}^2 \end{cases} \Leftrightarrow \begin{cases} I_{IIx} = I_{0x} - (I_{IIIx} + m_{III} \cdot r_{IIIx}^2 + m_{II} \cdot r_{IIx}^2) \\ I_{IIy} = I_{0y} - (I_{IIIy} + m_{III} \cdot r_{IIIy}^2 + m_{II} \cdot r_{IIy}^2) \\ I_{IIz} = I_{0z} - (I_{IIIz} + m_{III} \cdot r_{IIIz}^2 + m_{II} \cdot r_{IIz}^2) \end{cases} \tag{3.4}$$

Where I_{0x}, I_{0y}, I_{0z} stand for the inertias of segment 0 in the three main directions; $I_{IIIx}, I_{IIIy}, I_{IIIz}$ the same for segment III and $I_{IIx}, I_{IIy}, I_{IIz}$ for segment II. $r_{IIIx}, r_{IIIy}, r_{IIIz}$ and $r_{IIx}, r_{IIy}, r_{IIz}$ are the distances between the parallel axis that pass through the center of mass of segment III and segment II respectively along the three main directions. The final inertial values, relative to the centers of mass, are presented in Table 3.15.

Table 3.15 - Segments Inertias.

	Inertias		
	x (kg/m²)	y (kg/m²)	z (kg/m²)
Segment I (I_I)	0.0001	0.0001	0.0002
Segment II (I_{II})	0.0006	0.0007	0.00073
Segment III (I_{III})	0.00035	0.00104	0.00099
Segment IV (I_{IV})	0.0477	0.0048	0.0484

These inertias were rotated using the Mohr's circle to convert them into the referential used in this work. The foot inertias converted to the new referential are shown in Table 3.16.

Table 3.16 - Segments inertias converted into the new referential (after using the Mohr's circle).

	Inertias		
	x (kg/m^2)	y (kg/m^2)	z (kg/m^2)
Segment I (I_I)	0.0001	0.0001	0.0002
Segment II (I_{II})	0.0006	0.00065	0.00073
Segment III (I_{III})	0.0004	0.001	0.001

Off diagonal inertias were discarded, due to the increase of computational effort and due to their small value (Anderson & Pandy, 1999). Using the following formula (De Leva, 1996):

$$I_i = M_b \cdot m_i\% \cdot \left(L_i \cdot r_i\% \right)^2 \qquad (3.5)$$

where I_i is the segment inertia about a principal axis, M_b the mass of the considered subject, $m_i\%$ the segment mass percentage, L_i the segment length and $r_i\%$ the mean relative radius of gyration of the segment about the considered axis. The mean relative radiuses of gyration are shown in Table 3.17.

Table 3.17 - Segments mean relative radius of gyration about the principal axes.

	Radius of Gyration		
	x	y	z
Segment I ($r_I\%$)	30.29	30.29	42.84
Segment II ($r_{II}\%$)	39.81	41.18	43.70
Segment III ($r_{III}\%$)	21.94	34.21	34.28
Segment IV ($r_{IV}\%$)	27.11	25.31	8.60

Summarizing this chapter, an anthropometric complete summary is presented in Table 3.18. This table takes into account the generalized info previously presented: Table 3.10, Table 3.11, Table 3.12, Table 3.13 and Table 3.17; and reports the segments lengths, masses, inertias and the positions of the centers of mass in relation to the adjacent joint as a function of a general foot length (L_f), body height (H_b) and body mass (M_b).

Table 3.18 – Anthropometric summary of the model. The parameters (Lengths, Masses, Inertias and CM positions in relation to the adjacent joint) are presented as a function of a general foot length (L_f), body height (H_b) and body mass (M_b).

Anthropometric Table

Segment	Length	Adjacent Joint	CM position in relation to the adjacent joint			Mass	Inertia		
			x	y	z		x	y	z
I - Toes	$L_I =$ 27%·L_f	J1	$r_{1x}=$ 9.96%·L_f	$r_{1y}=$ 0.00%·L_f	$r_{1z}=$ 6.85%·L_f	$m_I =$ 0.289%·M_b	$I_{Ix} = m_I$ × 30.29%·L_I	$I_{Iy} = m_I$ × 30.29%·L_I	$I_{Iz} = m_I$ × 42.84%·L_I
II – Mid/Fore-foot	$L_{II} =$ 33%·L_f	J2	$r_{2x}=$ 14.85%·L_f	$r_{2y}=$ 0.00%·L_f	$r_{2z}=$ −7.04%·L_f	$m_{II} =$ 0.676%·M_b	$I_{IIx} = m_{II}$ × 39.81%·LI_I	$I_{IIy} = m_{II}$ × 41.18%·L_{II}	$II_{Iz} = m_{II}$ × 43.70%·L_{II}
III – Rear-foot	$L_{III} =$ 40%·L_f	J3	$r_{3x}=$ 1.20%·L_f	$r_{3y}=$ 0.00%·L_f	$r_{3z}=$ −14.31%·L_f	$m_{III} =$ 1.014%·M_b	$I_{IIIx} = m_{III}$ × 21.94%·L_{III}	$I_{IIIy} = m_{III}$ × 34.21%·L_{III}	$I_{IIIz} = m_{III}$ × 34.28%·L_{III}
IV - Leg	$L_{IV} =$ 24%·H_b	J4	$r_{4x}=$ 0.00%·H_b	$r_{4y}=$ 0.00%·H_b	$r_{4z}=$ −10.52%·H_b	$m_{IV} =$ 4.943%·M_b	$I_{IVx} = m_{IV}$ × 27.11%·L_{IV}	$I_{IVy} = m_{IV}$ × 25.31%·L_{IV}	$I_{IVz} = m_{IV}$ × 8.60%·L_{IV}

Chapter IV

Multibody Formulation

Important and relevant results arising from complex mechanical systems that undergo large displacements and rotations have been the target of many studies and analysis by the scientific community. The evolution of computational power, acquisition instruments and mathematical tools allowed the use of multibody approaches, which facilitate the systematic formulation and solution of complex and non-linear equations of motion (Silva, 2003). A Multibody system is defined as an assembly of two or more bodies that are joined together by kinematic pairs (joints), having the possibility of relative movement between them due to the application of external forces, Figure 4.1 (De Jalón & Bayo, 1994; Silva, 2003).

There are two main types of analyses that can be performed in these systems: Kinematic analysis and Dynamics analysis, the last one is divided in Forward dynamic analysis and Inverse dynamic analysis. In order to describe the position and orientation of each element of the multibody system a set of coordinates must be specified, although there are many types of coordinates capable of doing so, in the present work Fully Cartesian coordinates (Natural coordinates) (De Jalón & Bayo, 1994) were chosen. During the next sections a brief introduction to the multibody formulation used in the software Apollo is presented.

4.1. Fully Cartesian Coordinates

The position and orientation of a rigid body in a three dimensional space are described using the Cartesian coordinates of a set of points and unit vectors. Generally points are located in important positions of the mechanical system, such as extremities and joints, on the other hand, vectors are used to define rotational and direction axes of the joints. The use of natural coordinates to describe

rigid bodies avoids the introduction of any kind of angular variables to describe the orientation and rotation of each element. Another advantage of this formulation is the possibility of two adjacent rigid bodies to share points and vectors, reducing the number of coordinates necessary to describe the system as well as the number of algebraic equations needed to define kinematic pairs. Sometimes this can come as a weakness of the formulation if the objective is to calculate the internal reaction forces developed in the joints.

In order to perform kinematic or dynamic analysis of a mechanical system, the Cartesian coordinates of every point and vector are described in a column vector q , the vector of generalized coordinates. It is organized as follows:

$$q = \{x_{P1} \quad y_{P1} \quad z_{P1} \quad \cdots \quad x_{PN} \quad y_{PN} \quad z_{PN} \quad x_{V1} \quad y_{V1} \quad z_{V1} \quad \cdots \quad x_{VM} \quad y_{VM} \quad z_{VM}\}^{T}$$ (4.1)

where P stands for points, V for vectors, n and m are respectively the number of points and vectors. The total number of generalized coordinates is given by $nc = 3(n + m)$. The coordinates can be independent if they vary independently or dependent if they are related by algebraic expressions. Multibody formulations with fully Cartesian coordinates imply that the generalized coordinates describing the system are dependent, so algebraic relations need to be described in order to relate them, at every instant of time. These equations are called kinematic constraint equations and are mathematically described in the column vector Φ .

$$\Phi(q,t) = \left\{ \begin{array}{c} \Phi_1(q) \\ \vdots \\ \Phi_{ns}(q) \\ \Phi_{ns+1}(q,t) \\ \vdots \\ \Phi_{ns+nr}(q,t) \end{array} \right\} = 0$$ (4.2)

Φ_i represent the ith kinematic constraint equations, ns the total number of scleronomic constraints and nr the number of rheonomic constraints. The scleronomic constraints are the ones which do not have the explicit time variables, they are used to describe rigid body properties and kinematic pairs; on the other hand rheonomic constraints are the ones which have explicit time variables, they are associated with driver actuators. The sum of these variables gives the total number of holonomic constraints ($nh = ns + nr$).
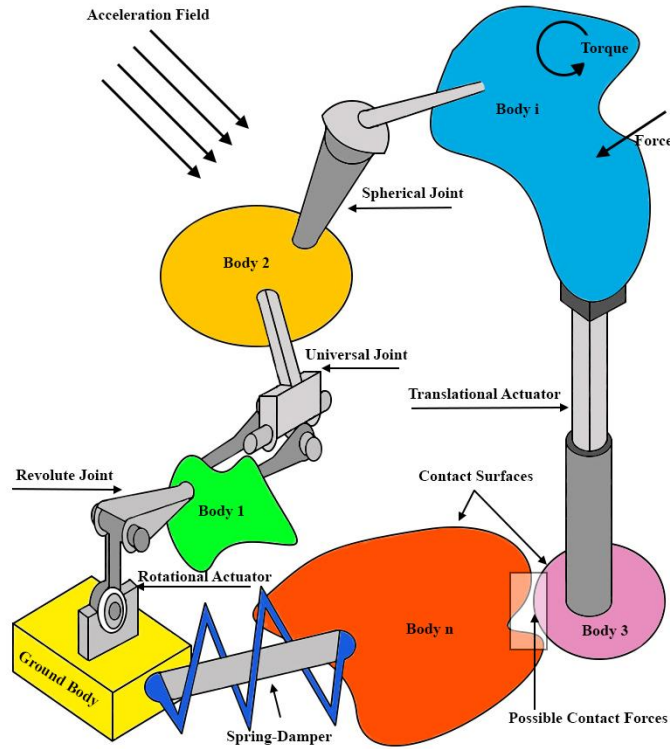
Figure 4.1 - General mechanical system modeled using a multibody approach.

4.2. Kinematic Analysis

In kinematic analysis the motion of the system is studied, and the position, velocity and acceleration of every element are analyzed independently of the external forces that produced it. To calculate the positions that satisfy the equation of kinematic constraints, the kinematic consistent positions, it would be necessary to solve the Equation (4.2). However, their non-linear behavior requires the use of numerical methods, such as the Newton-Raphson method to calculate the consistent position of the system during the period of analysis. Briefly, this is an iterative method that achieves quadratic convergence near the solution; the error in each iteration is proportional to the square of the error in the previous iteration. The Newton-Raphson method is based on the linearization of Equation (4.2), which results from its replacement by the first two terms of its expansion in a Taylor series, evaluated with an initial approximation vector q_i. So, for a given time t, Equation (4.2) comes as the following linear equations:

$$\Phi(\boldsymbol{q},t) \cong \Phi(\boldsymbol{q_i},t) + \Phi_{\boldsymbol{q}}(\boldsymbol{q_i})(\boldsymbol{q} - \boldsymbol{q_i}) = 0 \tag{4.3}$$

$\Phi_q(\boldsymbol{q_i})$ is the Jacobian matrix of the constraints, evaluated at the approximate solution q_i, composed by the partial derivatives of each kinematic constraint with respect to the generalized coordinates vector. Mathematically this matrix is expressed as:

43

$$\Phi_q(\boldsymbol{q}) = \frac{\partial \Phi_m}{\partial q_n} = \begin{bmatrix} \dfrac{\partial \Phi_1}{\partial q_1} & \dfrac{\partial \Phi_1}{\partial q_2} & \cdots & \dfrac{\partial \Phi_1}{\partial q_{nc}} \\ \dfrac{\partial \Phi_2}{\partial q_1} & \ddots & & \vdots \\ \vdots & & \ddots & \vdots \\ \dfrac{\partial \Phi_{nh}}{\partial q_1} & \cdots & \cdots & \dfrac{\partial \Phi_{nh}}{\partial q_{nc}} \end{bmatrix} \tag{4.4}$$

Where nh is the number of constraint equations and nc the number of dependent coordinates. Being an iterative procedure, $\boldsymbol{q} = \boldsymbol{q}_{i+1}$ represents an approximate solution of Equation (4.2) and it stops when the norm of residual $\Delta \boldsymbol{q}_i = \boldsymbol{q}_{i+1} - \boldsymbol{q}_i$ is less than a specified tolerance. So, Equation (4.3) can be expressed as:

$$\Phi_q(\boldsymbol{q}_i)\Delta \boldsymbol{q}_i = -\Phi(\boldsymbol{q}_i) \tag{4.5}$$

The velocity is calculated differentiating Equation (4.2) in order to time.

$$\dot{\Phi}(\boldsymbol{q},\dot{\boldsymbol{q}},t) = \frac{d\Phi(\boldsymbol{q},t)}{dt} = \frac{\partial \Phi(\boldsymbol{q},t)}{\partial t} + \frac{\partial \Phi(\boldsymbol{q},t)}{\partial \boldsymbol{q}}\frac{d\boldsymbol{q}}{dt} = 0 \tag{4.6}$$

Where $\partial \Phi(\boldsymbol{q},t) / \partial t$ is the partial derivatives vector in respect to time, $\partial \Phi(\boldsymbol{q},t) / \partial \boldsymbol{q}$ is the Jacobian matrix and $d\boldsymbol{q} / dt$ is the vector of generalized velocities $\dot{\boldsymbol{q}}$. The right-hand-side of the velocity equation can be defined as the vector $\boldsymbol{\nu}(t)$ and comes as:

$$\Phi_q \dot{\boldsymbol{q}} = \boldsymbol{\nu}(t) = -\frac{\partial \Phi(\boldsymbol{q},t)}{\partial t} \tag{4.7}$$

The steps presented to calculate the velocity vector can be repeated to calculate the acceleration vector, but instead of differentiating the kinematic constraints Equation (4.2) it's necessary to differentiate the velocity constraint Equation (4.7) in respect to time.

$$\ddot{\Phi}(\boldsymbol{q},\dot{\boldsymbol{q}},\ddot{\boldsymbol{q}},t) = \frac{d\dot{\Phi}(\boldsymbol{q},\dot{\boldsymbol{q}},t)}{dt} = \Phi_q \ddot{\boldsymbol{q}} + (\Phi_q \dot{\boldsymbol{q}})_q \dot{\boldsymbol{q}} + \boldsymbol{\nu}_t = 0 \tag{4.8}$$

$\boldsymbol{\nu}_t$ is the vector that contains the partial derivatives of vector $\boldsymbol{\nu}$ with respect to time. The right-hand-side of the acceleration equation can be defined as the vector $\boldsymbol{\gamma}(\boldsymbol{q},\dot{\boldsymbol{q}},t)$ and comes as:

$$\Phi_q \ddot{\boldsymbol{q}} = \boldsymbol{\gamma}(\boldsymbol{q},\dot{\boldsymbol{q}},t) = \boldsymbol{\nu}_t - (\Phi_q \dot{\boldsymbol{q}})_q \dot{\boldsymbol{q}} \tag{4.9}$$

It's important to refer the problem arising from the existence of redundant constraints in the vector $\Phi(\boldsymbol{q},t)$. These redundant constraints contribute with linear dependent lines in the Jacobian matrix, making it rank-deficient, causing Equation (4.5) to fail calculating the generalized coordinate vector, ending prematurely the kinematic analysis. Many approaches were developed to overcome this problem; one of them is the least-squares formulation (used in the code of the Apollo software), it is defined as:

$$\mathbf{\Phi}_q^T(\mathbf{q_i})\mathbf{\Phi}_q(\mathbf{q_i})\Delta\mathbf{q_i} = -\mathbf{\Phi}_q^T(\mathbf{q_i})\mathbf{\Phi}_q(\mathbf{q_i}) \tag{4.10}$$

4.3. Constraint Equations

When using Natural coordinates to analyze mechanical systems, there are three types of kinematic constraints to take into account:

- Rigid body constraints – Responsible for maintaining the rigid body characteristics of each element in the system;
- Joint constraints – Used in the definition of kinematic pairs and topology of the system;
- Driver constraints – Prescribe the motion of the system's driving elements.

Rigid body constraint and rotational driver constraints are identically formulated from the mathematical point of view, so they are presented together in the next section.

4.3.1. Rigid Body and Rotational Driver Constraints

Rigid body constraints are structural constraints; they are introduced in the analysis to preserve rigid body properties. When describing a rigid body with Natural coordinates, using a set of points and unit vectors, the rigid body properties are responsible for the maintenance of constant distance between any two points of the element and for the preservation of constant angles between any two vectors. In order to define the number of rigid body constraints of a given body, it is necessary to subtract the number of degrees of freedom to the number of Cartesian coordinates. The mathematical description of the constraints approached in this section (rigid body and rotational driver) can be defined with the same algebraic expression, the scalar product between two vectors, $\mathbf{u}$ and $\mathbf{v}$, given by:
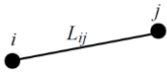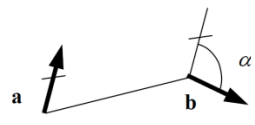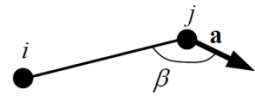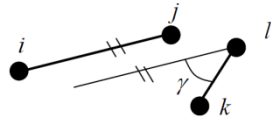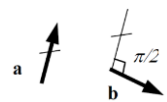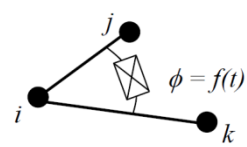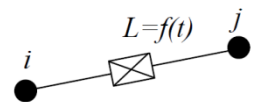
$$\mathbf{\Phi}^{SP}(\mathbf{q},t) = \mathbf{v}^t\mathbf{u} - L_v L_u \cos(\langle\mathbf{v},\mathbf{u}\rangle(t)) = 0 \tag{4.11}$$

where L_v and L_u are the lengths of vectors $\mathbf{u}$ and $\mathbf{v}$ and $\langle\mathbf{v},\mathbf{u}\rangle(t)$ is the angle defined between them. In Table 4.1 a detailed description of the possible applications of the scalar product constraint is presented.

The scalar product constraint presents a quadratic dependency on the generalized coordinates; therefore its contribution to the Jacobian matrix is linear and it's given by:

$$\Phi_q^{SP} = \frac{\partial(\mathbf{v}^T\mathbf{u})}{\partial\mathbf{q}} = \mathbf{u}^T\frac{\partial\mathbf{v}}{\partial\mathbf{q}} + \mathbf{v}^T\frac{\partial\mathbf{u}}{\partial\mathbf{q}} = \begin{bmatrix} \mathbf{0}^T & \cdots & \mathbf{u}^T & \cdots & \mathbf{0}^T & \cdots & \mathbf{v}^T & \cdots & \mathbf{0}^T \end{bmatrix} \tag{4.12}$$

Table 4.1 - The most common applications of the scalar product constraint and their respective physical meaning. Vectors r_i, r_j, r_k and r_l are the Cartesian coordinates of points i, j, k and l and unit vectors a and b, used in the definition of rigid bodies (Silva, 2003).

Constraint Description	v	u	L_v	L_u	$\langle v,u \rangle$	Graphical representation
Constant distance between points i and j	$(r_j - r_i)$	$(r_j - r_i)$	L_{ij}	L_{ij}	0	
Unit vector	a	a	1	1	0	
Constant angle between unit vectors a and b	a	b	1	1	α	
Constant angle between segment r_{ij} and unit vector a	$(r_j - r_i)$	a	L_{ij}	1	β	
Constant angle between segments r_{ij} and r_{kl}	$(r_j - r_i)$	$(r_l - r_k)$	L_{ij}	L_{kl}	γ	
Orthogonal unit vectors	a	b	1	1	$\pi / 2$	
Rotational driver about a revolute joint located in point i, using segments r_{ij} and r_{kl}	$(r_j - r_i)$	$(r_k - r_i)$	L_{ij}	L_{ik}	$\phi = f(t)$	
Translational driver defined between point i and point j belonging to different rigid bodies	$(r_j - r_i)$	$(r_j - r_i)$	$L = f(t)$	$L = f(t)$	0	

The resultant right-hand sides of the velocity and acceleration constraint equations are respectively given by:

$$\boldsymbol{\nu}^{SP}(t) = -L_v L_u \sin(\langle \boldsymbol{v}, \boldsymbol{u} \rangle(t)) \frac{\partial \langle \boldsymbol{v}, \boldsymbol{u} \rangle(t)}{\partial t} \tag{4.13}$$

and

$$\boldsymbol{\gamma}^{SP}(\dot{\boldsymbol{q}}, t) = \boldsymbol{\nu}_t^{SP}(t) - 2(\dot{\boldsymbol{v}}^T \dot{\boldsymbol{u}}) \tag{4.14}$$

where

$$\boldsymbol{\nu}_t^{SP}(t) = -L_v L_u \cos(\langle \boldsymbol{v}, \boldsymbol{u} \rangle(t)) \left(\frac{\partial \langle \boldsymbol{v}, \boldsymbol{u} \rangle(t)}{\partial t} \right)^2 + \sin(\langle \boldsymbol{v}, \boldsymbol{u} \rangle(t)) \frac{\partial^2 \langle \boldsymbol{v}, \boldsymbol{u} \rangle(t)}{\partial t^2} \tag{4.15}$$

A great number of mechanical systems can be described using the procedure described in the previous section. However when rigid bodies have a more complex structure other approaches have to be applied, for example the Linear Combination constraint (Silva, 2003). In the present work these formulations will not be addressed.

4.3.2. Kinematic Joint Constraints

Joint kinematic constraints are used to describe the relative motion between the different elements of a mechanical system restricted by a kinematic pair. The algebraic equations that describe the kinematic constraint relate the natural coordinates of two rigid bodies, constraining their movement and consequently reducing the number of degrees of freedom. Only the joints used in the present work will be detailed in the next sections.

4.3.2.1. Spherical Joint

The spherical joint represents a ball and socket type of joint that restricts the movement to the rotations around the three axes (3 DOF's); it restrains the motion between the two rigid bodies (the three translations), as depicted in Figure 4.2. In a formulation with natural coordinates there are two ways to model this joint: 1) sharing a point between the two rigid bodies, with no need to introduce any joint constraints equations; 2) introducing a proper joint constraint. In this last case there are two different points belonging to the two rigid bodies that share the same position in space. So this relation comes as:

$$\boldsymbol{\Phi}^{SPH}(\boldsymbol{q}) = \boldsymbol{r}_n - \boldsymbol{r}_m = 0 \tag{4.16}$$

Where $\boldsymbol{r}_n$ and $\boldsymbol{r}_m$ represent the position of points n and m in the global reference frame.
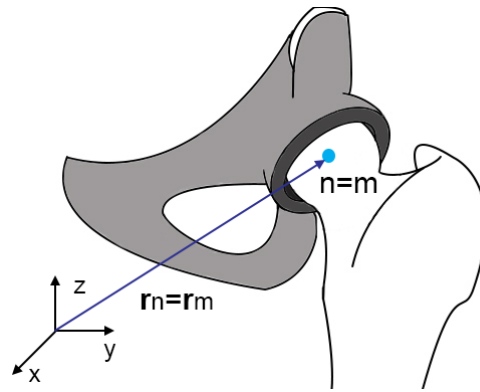
Figure 4.2 - Representation of a spherical joint.

4.3.2.2. Revolute Joint

The revolute joint represents a hinge joint that restricts the movement to the rotation of the rigid bodies around the unit vector used to describe the joint axis (1 DOF), Figure 4.3; it restraints the motion between the two bodies (the three translations) and two rotations. Once again, there are two ways to model this joint: 1) sharing a point between the two rigid bodies, with no need to introduce any joint constraints equations; 2) introducing proper joint constraints. Regarding the last case, the first joint constraint that has to be applied is the same as the one described by Equation (4.16), two different points in space share the same position in space. The second joint constraint arises from the consideration of vector u and its replacement by two different unit vectors a and b that belong to different rigid bodies and that have the same components in space. The mathematical relation is expressed by:

$$\mathbf{\Phi}^{REV}(\boldsymbol{q}) = \boldsymbol{b} - \boldsymbol{a} = 0 \tag{4.17}$$

Revolute joints can also be used to describe axial rotation between elements. This procedure is described by the use of two points that are shared between two different rigid bodies, or, if needed using proper joint constraint equations. In this last case, the joint constraint equation results from applying Equation (4.16).
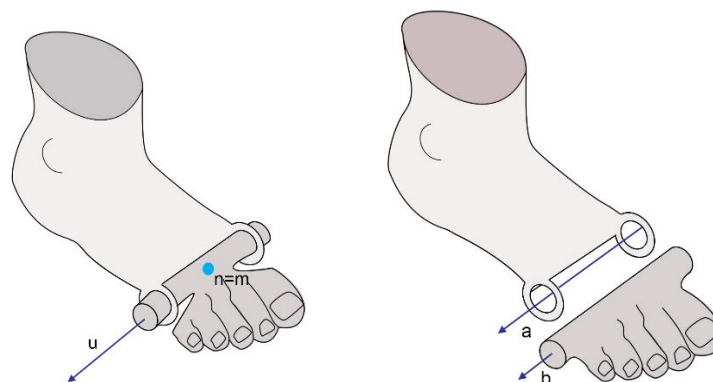
Figure 4.3 - Representation of a revolute joint.

4.3.2.3. Universal Joint

The universal joint represents two hinge joints that restrict the movement to the rotation of the rigid bodies around two axes (2 DOF's), Figure 4.4; it restraints the motion between the two bodies (the three translations) and one rotation. There are two ways to define this joint model: implicitly sharing a point between the two rigid bodies, and in this case, it is necessary to generate an expression that guarantees the constant angle between the vectors (vide Table 4.1). If the joint is defined explicitly, an additional constraint equation must be considered, in order to ensure that the two points that define the kinematic pair share the same spatial position as in Equation (4.16).
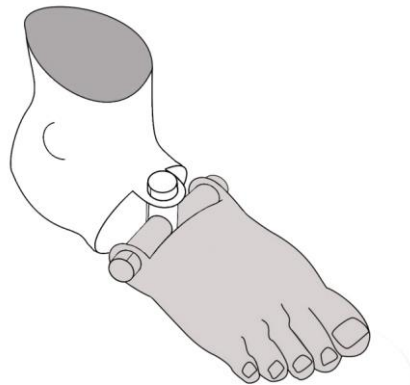
Figure 4.4 - Representation of a universal joint.

4.4. Dynamic Analysis

The study of the relation between the motion and its causes – forces and moments of force - it's called Dynamics. The premise behind a dynamic problem is to understand the action of these forces and torques in the dynamic response multibody system, considering also its inertial characteristics – mass, inertia and center of mass position. In the present work only the two maind dynamic problems will be presented – forward dynamic analysis and inverse dynamic analysis (De Jalón & Bayo, 1994).

4.4.1. Forward Dynamics

The forward dynamics problem permits simulating the motion of a multibody system, when a set of known forces and moments is applied. Such problems are used to simulate the evolution of a system over a given time interval (De Jalón & Bayo, 1994).

4.4.1.1. The principle of virtual power

The motion equations of a constrained multibody system can be obtained using several procedures. In the present work the Principle of Virtual Power is reflected due to the fact that it is the one used by the Apollo software. The principle establishes that the sum of the virtual power produced by the inertial and external forces acting in a mechanical system must be zero in any instant in time. Mathematically the principle is expressed as:

$$P^* = \sum_{i=1}^{nc} \boldsymbol{f}_i \dot{\boldsymbol{q}}_i^* \equiv \dot{\boldsymbol{q}}^{*T} \boldsymbol{f} = 0 \tag{4.18}$$

where $\dot{q}^*$ is a virtual velocity vector that represents a set of imaginary velocities, it belongs to the null space of the Jacobian matrix:

$$\boldsymbol{\Phi}_q^T \dot{\boldsymbol{q}}^* = 0 \tag{4.19}$$

vector $\boldsymbol{f}$ represents all the generalized forces that produce virtual power and it is defined as:

$$\boldsymbol{f} = \boldsymbol{M}\ddot{\boldsymbol{q}} - \boldsymbol{g} \tag{4.20}$$

The term $\boldsymbol{M}\ddot{\boldsymbol{q}}$ stands for the inertial forces, with $\boldsymbol{M}$ defined as the global mass matrix and $\ddot{\boldsymbol{q}}$ the vector of generalized accelerations. The term $\boldsymbol{g}$ represents the generalized external applied forces including the velocity-dependent inertial forces, in which the centrifugal and Coriolis forces are part. Regarding the force vector $\boldsymbol{f}$ it must be noted that the internal forces, the ones associated with the kinematic constraints, are not included in the previous equation because they do not produce virtual power, because they are associated in action/reaction pairs. Nevertheless, these forces can be calculated using the Lagrange multiplier method (Silva, 2003):

$$\boldsymbol{g}^\Phi = \boldsymbol{\Phi}_q^T \boldsymbol{\lambda} \tag{4.21}$$

where $\boldsymbol{g}^\Phi$ is a generalized force vector containing the internal constraint forces, and $\boldsymbol{\lambda}$ is the Lagrange multipliers vector. Physically, the rows of the Jacobian matrix represent the direction of the constraint forces and the vector of Lagrange multipliers their magnitude. Taking into account Equations (4.18) ,(4.20) and (4.21), and knowing that the product $\dot{\boldsymbol{q}}^T \boldsymbol{\Phi}_q^T \boldsymbol{\lambda}$ belongs to the null space of the Jacobian matrix, then the principle of virtual power can be expressed as:

$$P^* = \dot{\boldsymbol{q}}^{*T}(\boldsymbol{M}\ddot{\boldsymbol{q}} - \boldsymbol{g} + \boldsymbol{\Phi}_q^T \boldsymbol{\lambda}) = 0 \tag{4.22}$$

4.4.1.2. Equations of Motion

In a multibody system with nc generalized coordinates and nh holonomic constraints, it is always possible to find $nc - nh$ arbitrary virtual accelerations and nh Lagrange multipliers that make, in Equation (4.22), the term $\boldsymbol{M}\ddot{\boldsymbol{q}} - \boldsymbol{g} + \boldsymbol{\Phi}_q^T \boldsymbol{\lambda}$ to be null. This term represents the equations of motion, and it is rewritten as:

$$\boldsymbol{M}\ddot{\boldsymbol{q}} + \boldsymbol{\Phi}_q^T \boldsymbol{\lambda} = \boldsymbol{g} \tag{4.23}$$

This expression stands for a second order ordinary differential equation (ODE) with nc equations and $nc + nh$ unknowns, which correspond to the generalized acceleration vector $\ddot{\boldsymbol{q}}$ and to the vector of the Lagrange multipliers $\boldsymbol{\lambda}$. To calculate the solution of Equation (4.23), nh additional equation are needed, to ensure that the equations of motion and the kinematic restrictions are fulfilled, the additional equations should be provided by Equation (4.2). Despite being more adequate, achieving a

solution would be much more complicated; instead the procedure presented in Equation (4.9) is applied. So the rearrangement is presented as:

$$\begin{bmatrix} \boldsymbol{M} & \boldsymbol{\Phi}_q^T \\ \boldsymbol{\Phi}_q & 0 \end{bmatrix} \begin{Bmatrix} \ddot{\boldsymbol{q}} \\ \boldsymbol{\lambda} \end{Bmatrix} = \begin{Bmatrix} \boldsymbol{g} \\ \boldsymbol{\gamma} \end{Bmatrix} \qquad (4.24)$$

In order to transform Equation (4.24) in a system of second order ODE's, the Lagrange multipliers have to be eliminated from it. This result on an ODE system expressed in terms of generalized acceleration vector and can be integrated in time, given the initial conditions for the position and velocity vectors. These conditions need to be consistent with kinematics of the multibody system:

$$\boldsymbol{\Phi}(\boldsymbol{q}_0) = 0 \qquad (4.25)$$

$$\boldsymbol{\Phi}_q \dot{\boldsymbol{q}}_0 = \boldsymbol{\nu}(t_0) \qquad (4.26)$$

4.4.1.3. Lagrange Multipliers and Internal Forces

As discussed before, the internal forces represent the forces that the system generated internally in order to satisfy the kinematic constraints that define the system. There are two methods that provide explicit results for the reaction forces. The first is used when kinematic joints are modeled using shared points and unit vectors, meaning that the kinematic restrictions defining these joints are imposed implicitly, making the calculation described before unable to generate results regarding the internal forces. The procedure used to overcome this situation establishes for each reporting time step, the dynamic equilibrium equations of each rigid body, and obtains the reaction forces as the solution of these equations (De Jalón & Bayo, 1994). The second procedure, the one applied in the present model, consists in creating a mechanical system in which there are no shared points or vectors. In this expanded system, additional points and unit vectors are defined in order to allow all kinematic joints to be explicitly defined, using the method defined in the section *Kinematic Joint Constraints*. Both procedures have their disadvantages; the first requires a complex implementation and requires additional information of the topology of the system. The second is computationally less efficient and it increases the size of the system, it should only be used when the calculation of the reaction forces at the joints is necessary.

4.4.1.4. Baumgarte stabilization method

In the present work the method chosen to solve the equations of motion is the direct integration method, explained in the next section (De Jalón & Bayo, 1994). In order to assure the convergence of the method, a stabilization procedure is essential. The Baumgarte method converts unstable differential equations into stable ones (Baumgarte, 1972). From the instable acceleration differential equation:

$$\ddot{\boldsymbol{\Phi}} = 0 \Rightarrow \boldsymbol{\Phi}_q \ddot{\boldsymbol{q}} = \boldsymbol{\gamma} \qquad (4.27)$$

Applying the Baumgarte stabilization method:

$$\ddot{\boldsymbol{\Phi}} + 2\alpha\dot{\boldsymbol{\Phi}} + \beta^2\boldsymbol{\Phi} = 0 \tag{4.28}$$

Given the first and second derivatives of the constraints equations:

$$\begin{cases} \ddot{\boldsymbol{\Phi}} = \boldsymbol{\Phi}_q\ddot{\boldsymbol{q}} - \boldsymbol{\gamma} \\ \dot{\boldsymbol{\Phi}} = \boldsymbol{\Phi}_q\dot{\boldsymbol{q}} - \boldsymbol{\nu} \end{cases} \tag{4.29}$$

Using Equation (4.29) in Equation (4.28):

$$\boldsymbol{\gamma}^* = \boldsymbol{\gamma} - 2\alpha(\boldsymbol{\Phi}_q\dot{\boldsymbol{q}} - \boldsymbol{\nu}) - \beta^2\boldsymbol{\Phi} \tag{4.30}$$

Replacing γ by γ^* in Equation (4.24), results the stabilized system:

$$\begin{bmatrix} \boldsymbol{M} & \boldsymbol{\Phi}_q^T \\ \boldsymbol{\Phi}_q & 0 \end{bmatrix}\begin{bmatrix} \ddot{\boldsymbol{q}} \\ \boldsymbol{\lambda} \end{bmatrix} = \begin{Bmatrix} \boldsymbol{g} \\ \boldsymbol{\gamma} - 2\alpha(\boldsymbol{\Phi}_q\dot{\boldsymbol{q}} - \boldsymbol{\nu}) - \beta^2\boldsymbol{\Phi} \end{Bmatrix} \tag{4.31}$$

The constants α and β must be adjusted for every analysis between 10 and 50.

4.4.1.5. Integration of the Equations of Motion

The next step of the analysis is the integration of the equations of motion, this step is essential to advance the analysis in time. Analytical solutions are impractical to obtain, due to the high level of complexity of these equations, so numerical methods have to be applied. In particular, several efficient integration algorithms can be used to compute solutions for first order ODE's, giving specific initial conditions, this is called first-order initial-value problems.

To use this kind of algorithms, the second-order ODE's presented by Equation (4.31) has to be transformed into a first-order initial-value problem. This is achieved with a numerical process called direct integration. Two vectors have to be defined: the $\dot{\boldsymbol{y}}$ containing the generalized velocities and accelerations for the actual time step t and $\boldsymbol{y}$ which contains the generalized coordinates and velocities for the next time step $t + \Delta t$. Therefore:

$$\dot{\boldsymbol{y}}_t = \begin{bmatrix} \dot{q} \\ \ddot{q} \end{bmatrix}_t \text{ and } \boldsymbol{y}_{t+\Delta t} = \begin{bmatrix} q \\ \dot{q} \end{bmatrix}_{t+\Delta t} \tag{4.32}$$

In the present work an integrator based on the predictor-corrector Adams-Moulton-Bashforth methods is used to perform the integration of the first order initial-values problems. See Figure 4.5 for the flow-chart of the Initial Value Method adopted in the software.

52
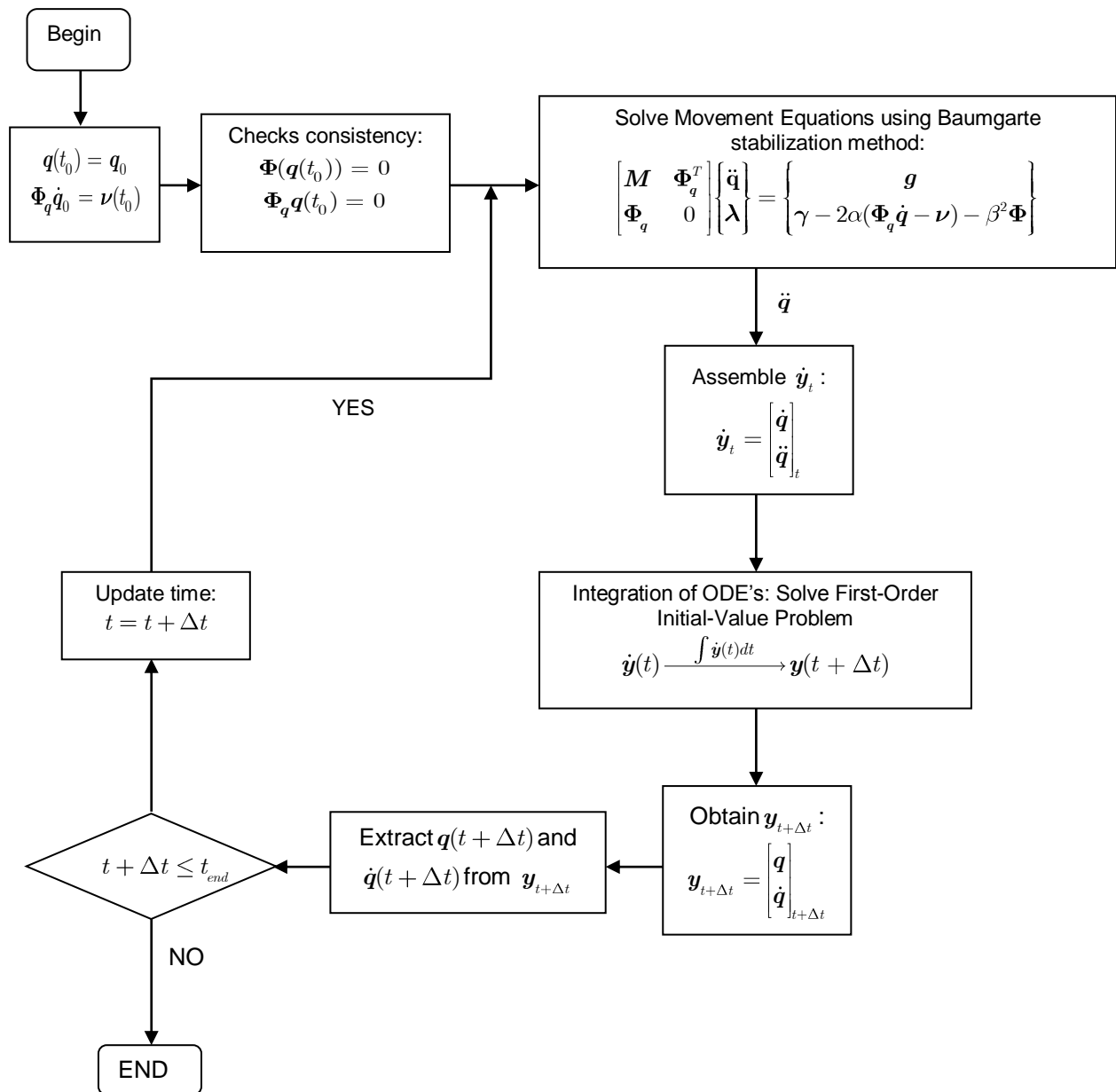
Figure 4.5 - Direct Integration Algorithm. Flow-chart of the process used to numerically integrate the equations of motion of mechanical systems.

4.4.1.6.   Mass Matrix for the Basic Rigid Body

So far the equations that were discussed could be applied by any type of generalized dependent coordinates. In this section the methodologies discussed are specific to Natural coordinates. When using this type of coordinates, the rigid bodies can be described by different kinematic structures, which depend on the topology of the system and on the type of kinematic joints to which they are attached. At a first look, one can think that to describe the mass and inertial properties of each different type of rigid body many different mass matrices are needed. In reality all of these matrices can be obtained from the mass matrix of a basic rigid body through a coordinate's transformation (De Jalón & Bayo, 1994; Silva, 2003). An important aspect is that each rigid body has a local reference frame rigidly attached and its origin does not need to be coincident with the body

53

center of mass and the direction of its reference axes does not need to be coincident with the body's center of mass, Figure 4.6.
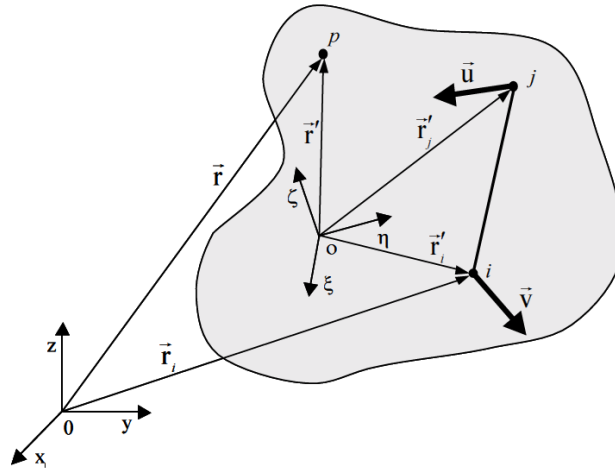
Figure 4.6 - Basic rigid body. The kinematic structure of the basic rigid body is made of two points (i and j) and two non-coplanar unit vectors (u and v). Point p represents a generic point belonging to this rigid body. A local reference frame (oξηζ) is rigidly attached to the body, having its origin in point o, which is not necessarily its center-of-mass. The reference frame (xyz) represents the inertial reference frame (Silva, 2003).

The virtual power generated within the rigid body by the inertial forces is expressed in its integral force by:

$$P^* = -\rho \int_\Omega \dot{\boldsymbol{r}}^{*T} \ddot{\boldsymbol{r}} d\Omega \tag{4.33}$$

Where ρ stands for the density of the rigid body and $\dot{\boldsymbol{r}}$ and $\ddot{\boldsymbol{r}}$ are respectively the virtual velocity and acceleration vectors of the generic point p, belonging to the rigid body. Applying an appropriate coordinate transformation, these vectors can be written in terms of the rigid body's generalized velocities and accelerations vectors. This transformation is achieved considering that vector $\boldsymbol{r}$ (vector defining the position of point p) can be described by the Cartesian coordinates of segment r_{ij} and unit vectors $\boldsymbol{u}$ and $\boldsymbol{v}$, as:

$$\boldsymbol{r} - \boldsymbol{r}_i = c_1(\boldsymbol{r}_j - \boldsymbol{r}_i) + c_2\boldsymbol{u} + c_3\boldsymbol{v} \tag{4.34}$$

c_1, c_2 and c_3 are the coordinates of segment r_{ip} in the 3D base formed by vectors r_{ij}, $\boldsymbol{u}$ and $\boldsymbol{v}$. So the previous equation comes as:

$$\boldsymbol{r} = \begin{bmatrix} (1-c_1)\boldsymbol{I}_3 & c_1\boldsymbol{I}_3 & c_2\boldsymbol{I}_3 & c_3\boldsymbol{I}_3 \end{bmatrix} \begin{Bmatrix} \boldsymbol{r}_i \\ \boldsymbol{r}_j \\ \boldsymbol{u} \\ \boldsymbol{v} \end{Bmatrix} \tag{4.35}$$

In a compact form:

$$\boldsymbol{r} = \boldsymbol{C}\boldsymbol{q}_e \tag{4.36}$$

54

where I_3 stands for a three by three identity matrix, C is the transformation matrix (constant in time), and q_e represents the vector of generalized coordinates describing the basic body. Equation (4.36) can be differentiated twice yielding:

$$\dot{r} = C\dot{q}_e \tag{4.37}$$

$$\ddot{r} = C\ddot{q}_e \tag{4.38}$$

where $\dot{q}_e$ and $\ddot{q}_e$ are the generalized velocity and acceleration vectors of the basic rigid body. The numerical values of c_1, c_2 and c_3 can be obtained by rewriting Equation (4.34) in the local coordinate system of the rigid body:

$$r' - r_i' = c_1(r_j' - r_i') + c_2 u' + c_3 v' \tag{4.39}$$

In a matrix form:

$$(r' - r_i') = \begin{bmatrix} r_{ij} & u' & v \end{bmatrix} \begin{Bmatrix} c_1 \\ c_2 \\ c_3 \end{Bmatrix} = X'c \tag{4.40}$$

Where X' contains the local coordinates of segment r_{ij} and vectors u and v in the reference frame of the rigid body, so it can be inverted. Solving the equation for vector c:

$$c = X'^{-1}(r' - r_j') \tag{4.41}$$

Using the virtual power of the inertial forces expression again, Equation (4.33), and replacing the Equations (4.37) and (4.38), results in:

$$P^* = -\rho \int_\Omega \dot{q}_e^{*T} C^T C \ddot{q}_e d\Omega \tag{4.42}$$

$\dot{q}_e^*$ and $\dot{q}_e$ are independent of the body volume Ω and can be isolated from the integral, resulting in the mass matrix expression for a basic rigid body:

$$M = \rho \int_\Omega C^T C d\Omega \tag{4.43}$$

Expanding the matrices:

$$M = \int_\Omega \rho \begin{bmatrix} 1 - 2c_1 + c_1^2 I_3 & c_1 - c_1^2 I_3 & c_2 - c_1 c_2 I_3 & c_3 - c_1 c_3 I_3 \\ c_1 - c_1^2 I_3 & c_1^2 I_3 & c_1 c_2 I_3 & c_1 c_3 I_3 \\ c_2 - c_1 c_2 I_3 & c_1 c_2 I_3 & c_2^2 I_3 & c_2 c_3 I_3 \\ c_3 - c_1 c_3 I_3 & c_1 c_3 I_3 & c_2 c_3 I_3 & c_3^2 I_3 \end{bmatrix} d\Omega \tag{4.44}$$

Through integration (De Jalón & Bayo, 1994), Equation (4.44) becomes:

$$\boldsymbol{M} = \begin{bmatrix} (m - 2ma_1 + z_{11})\boldsymbol{I}_3 & (ma_1 - z_{11})\boldsymbol{I}_3 & (ma_2 - z_{12})\boldsymbol{I}_3 & (ma_3 - z_{13})\boldsymbol{I}_3 \\ (ma_1 - z_{11})\boldsymbol{I}_3 & z_{11}\boldsymbol{I}_3 & z_{12}\boldsymbol{I}_3 & z_{13}\boldsymbol{I}_3 \\ (ma_2 - z_{21})\boldsymbol{I}_3 & z_{21}\boldsymbol{I}_3 & z_{22}\boldsymbol{I}_3 & z_{23}\boldsymbol{I}_3 \\ (ma_3 - z_{31})\boldsymbol{I}_3 & z_{31}\boldsymbol{I}_3 & z_{32}\boldsymbol{I}_3 & z_{33}\boldsymbol{I}_3 \end{bmatrix} \tag{4.45}$$

where m is the total mass of the rigid body, a_i, is the first area moments of the rigid body and z_{ij} the second area moments of the rigid body. This mass matrix is constant in time, so it is only evaluated in the beginning of the analysis. It depends of a set of ten different values: total mass of the rigid body, the coordinates of the center of mass in the local reference frame and the six different elements of the inertia tensor, also calculated with respect to the local reference frame. This section presents the mass matrix of an element with two basic points and two non-collinear unit vectors. Sometimes it is not possible to identify this collection of points and vectors, so other simple kinematic structures are used instead, however no further explanation will be given regarding the topic. The detailed explanation of this other structures can be found in De Jalón & Bayo (1994) and Silva (2003).

4.4.1.7.   External applied Forces and Moments

Dynamic analysis of mechanical systems involves the application of external forces an moments to the rigid bodies. The use of natural coordinates requires the transformation of these external forces or moments into generalized forces that can be assembled into the generalized force vector. The required steps for these transformations are detailed in the work of De Jalón & Bayo (1994) and Silva (2003), further explanation on this topic exceeds the purpose of the present work.

4.4.2. Inverse Dynamics

The inverse dynamic problem allows calculating the forces and torques that produce a specific movement. The problem requires the position, velocity and acceleration of the systems and all the external forces applied (De Jalón & Bayo, 1994). The equations of motion used to describe this type of analysis are the same as the one utilized in forward dynamics. However, the objectives of the analysis are different and so the unknown terms to calculate in those equations.

In order to perform an inverse dynamic analysis, it is required that the motion corresponding to the task under study is already known and it is consistent with the kinematic restrictions describing the system. This means that the Cartesian coordinates of a set of points and unit vectors need to be obtained in a previous stage and that they have to fulfill the kinematic constraints Equations (4.2).

The generalized velocity and acceleration vectors can be calculated from the generalized coordinates, using two different procedures:

1) Application of the generalized coordinates to the kinematic equations describing the velocities and accelerations of the system. Equations (4.7) and (4.9).
2) Interpolation of the trajectories of each generalized coordinate using cubic splines and then obtaining their velocity and acceleration using spline differentiation techniques.

The following stage involves the construction of the mass matrices and generalized force vectors of all vectors describing the mechanical system and their respective assembly in the system's

equation of motion. The stabilization solution and integration methods are no longer needed since the motion of the system is fully known.

To solve the inverse dynamics problem and to obtain its internal and external forces, there are several methods that can be applied. However in this work only two of them are considered: the Lagrange multipliers method and the Newton method.

4.4.2.1. Lagrange Multipliers Method

The Lagrange multipliers method considers that each external force is paired with a kinematic constraint that can be any of the types referred previously, including driver actuators. Drivers are used to guide specific degrees of freedom, according to an initially prescribed kinematics or according to a known guiding function. So, additional (in a number equal to the degrees of freedom of the system) constraint equations are introduced in the Jacobian matrix of the constraints. The equations of motion, given by Equation (4.23), are assembled and solved in an inverse dynamics perspective according to the Lagrange multipliers vector, as follows:

$$\Phi_q^T \lambda = g - M\ddot{q} \tag{4.46}$$

The Lagrange multipliers associated with the driving constraints are used to calculate the external forces associated with each degree of freedom. The rest of the Lagrange multipliers are used to calculate the internal forces developed in the kinematic pairs and rigid bodies.

4.4.2.2. Newton Method

The Newton method considers that with each degree of freedom is associated an external actuator that produces an unknown external force required for the system to reproduce the observed motion. To accomplish this, the generalized force vector g from the equation of motion is divided in two parts:

$$g = g_e - g_d \tag{4.47}$$

g_e is the term containing all the known external forces and g_d is the term associated with the unknown external forces produced by external actuators. The negative signal is a matter of convenience of the calculations. The vector related to the unknown external forces is expressed by the product of the matrix containing the geometrical information regarding the direction of the external forces produced by the actuator (Γ) with the vector containing the unknown magnitudes of these external forces (f_d).

$$g_d = \Gamma^T f_d \tag{4.48}$$

Replacing Equations (4.47) and (4.48) in the motion equation, results in:

$$\begin{bmatrix} \Phi_q^T & \Gamma^T \end{bmatrix} \begin{Bmatrix} \lambda \\ f_d \end{Bmatrix} = \{ g_e \quad -M\ddot{q} \} \tag{4.49}$$

In a compact form:

$$\bar{\boldsymbol{\Phi}}_q^T \bar{\boldsymbol{\lambda}} = \boldsymbol{g} - \boldsymbol{M}\ddot{\boldsymbol{q}} \tag{4.50}$$

As one can notice Equation (4.50) is very similar to Equation (4.46), proving that both methods are very similar. The main difference is that the Newton method leads directly to the determination of the magnitude of the external driving forces (Silva, 2003).

If a system is over-constrained there are more unknowns than equations of motion, meaning that an infinite set of solutions can be obtained from Equation (4.46) and (4.50). In order to obtain an unique solution, the minimum norm condition is used (De Jalón & Bayo, 1994).

4.5.   Leg and Foot Model Implementation

One of the main goals of this thesis is the implementation of the leg and foot model in the academic software *Apollo,* a multibody dynamics software, coded in Fortran, that has been developed along the years at Instituto Superior Técnico (Silva, 2003).This software makes use of Fully Cartesian coordinates, described in the previous sections. Typically, for a better definition of the multibody system, the points that define it are located strategically in joints and extremities of the rigid bodies and unit vectors are used to define rotational and direction axes of joints, avoiding the introduction of angular variables, since these are implicit in the model (De Jalón & Bayo, 1994).

The first step to implement the model in the *Apollo* software consist in the creation of a *.mdl file (Modeling file). This file requires the mass and inertias of each segment (presented in Chapter III), the local coordinates of the points of each segment and the local vectors that define the joints. The calculations regarding the local coordinates of the points are described in Table 4.2 and Table 4.3 followed by a detailed description of them. A complete visual description is presented in Figure 4.7.
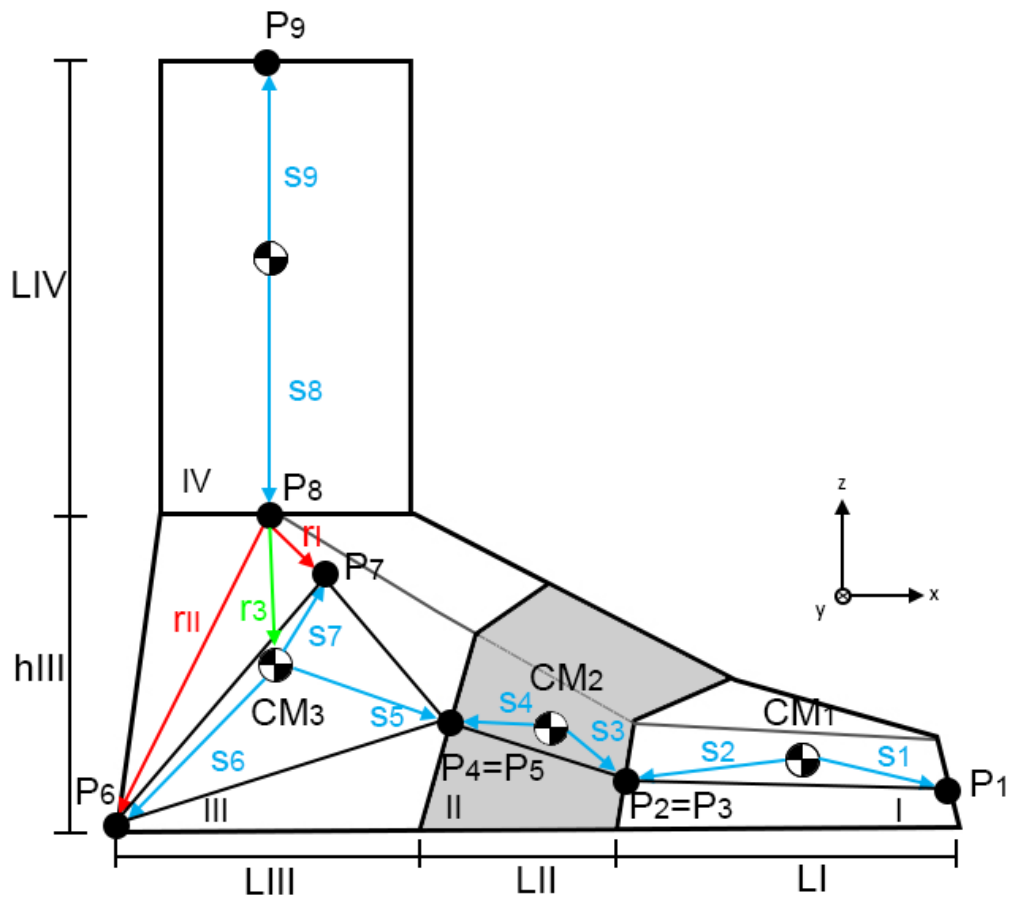
Figure 4.7 - Model scheme for the implementation in Apollo. Representation of the four segments, the corresponding centers of mass and important modeling vectors (Table 4.2 –and Table 4.3) – Right Foot.

As referred before the points defining the model are located strategically in joints and extremities of the rigid bodies, so the points (depicted in Figure 4.7) correspond to:

P_1 – Extremity of the toes;

P_2 and P_3 – Metatarsophalangeal joint;

P_4 and P_5 – Midtarsal joint;

P_6 - Extremity of the calcaneus;

P_7 – Talocalcaneal joint;

P_8 – Talocrural joint;

P_9 – Knee joint.

The information regarding the local vectors connecting the points is detailed in the following tables (Table 4.2 and Table 4.3). These vectors are once again presented with the formulation described in Section 3.2.1.

Table 4.2 – Foot vectors description - Coordinates relative to the local reference frame of the segments which is attached.

	Initial Point	Final Point	$\dfrac{x_i}{L_f}\times 100$	$\dfrac{y_i}{L_f}\times 100$	$\dfrac{z_i}{L_f}\times 100$
Vectors (Foot)					
$\mathbf{s}_1$	CM_1	P_1	17.04	0.00	-6.85
$\mathbf{s}_2$	CM_1	$P_2 = P_3$	-9.96	0.00	-6.85
$\mathbf{s}_3$	CM_2	$P_2 = P_3$	18.15	0.00	-7.04
$\mathbf{s}_4 = -\mathbf{r}_2$	CM_2	$P_5 = P_4$	-14.85	0.00	7.04
$\mathbf{s}_5$	CM_3	$P_5 = P_4$	15.40	0.00	-4.69
$\mathbf{r}_{II}$	P_8	P_6	-23.41	0.00	-28.00
$\mathbf{s}_6$	CM_3	P_6	-24.60	0.00	-13.69
$\mathbf{s}_7$	CM_3	P_7	$r_{Ix} - 1.20$	r_{Iy}	$r_{Iz} + 14.31$
$\mathbf{r}_I$	P_8	P_7	r_{Ix}	r_{Iy}	r_{Iz}
$\mathbf{r}_3$	P_8	CM_3	1.20	0.00	-14.31

Table 4.3 - Leg vectors description - Coordinates relative to the local reference frame of the segments which is attached.

	Initial Point	Final Point	$\dfrac{x_i}{h_b}\times 100$	$\dfrac{y_i}{h_b}\times 100$	$\dfrac{z_i}{h_b}\times 100$
Vectors (Leg)					
$\mathbf{s}_8$	$CM4$	P_8	0.00	0.00	-13.77
$\mathbf{s}_9$	$CM4$	P_9	0.00	0.00	10.52

The results presented in the previous tables are based on the anthropometric information reported in Table 3.10, Table 3.12 and Table 3.13.The detailed explanation of the computation of each individual model vector is described as follows:

- $\mathbf{s}_1$ – Vector obtained from the sum of the length of segment I described in Chapter III with vector s_2. Component Y was considered to be null;
- $\mathbf{s}_2$ – Vector equal to symmetric r_3 (Table 3.12);
- $\mathbf{s}_3$ – X component of the vector obtained from the sum of the length of segment II (Table 3.10) with the X component of vector $\mathbf{s}_4$. Y and Z were considered to be the symmetric components of vector $\mathbf{s}_4$, in order for the center of mass to be coincident with the segment;
- $\mathbf{s}_4$ – Vector equal to symmetric $\mathbf{r}_2$ (Table 3.12);
- $\mathbf{s}_5$ – Vector equal to $\mathbf{r}_{3J2}$ (Table 3.12);
- $\mathbf{r}_{II}$ – X component of the vector obtained from the difference between the X component of vector $\mathbf{r}_{J32}$ (Table 3.12) and the length of segment III; Y component assumed to be null; Z component is equal to the height of segment III (hIII);
- $\mathbf{s}_6$ – Vector obtained from the difference of $\mathbf{r}_{II}$ with $\mathbf{r}_3$ (Table 3.12);
- $\mathbf{s}_7$ – Vector obtained from the difference of $\mathbf{r}_I$ with $\mathbf{r}_3$ (Table 3.12);

- $\mathbf{r}_l$ – Experimental vector obtained by connecting the medium point of the talocrural axis with the medium point of the talocalcaneal axis (Dul & Johnson, 1985). This vector represents the massless link;
- $\mathbf{r}_3$ – Vector $\mathbf{r}_3$ (Table 3.12);
- $\mathbf{s}_8$ – Vector $\mathbf{r}_{4J3}$ (Table 3.13);
- $\mathbf{s}_9$ – Vector equal to symmetric $\mathbf{r}_4$ (Table 3.13).

It is crucial to understand that having this information (Table 4.2 and Table 4.3) together with the information presented in Chapter III (Table 3.18), the model is easily formulated for each individual, only requiring the knowledge of the individual height, foot size and weight. In order to build the kinematic model, a complete description of the kinematic joints is needed (De Jalón & Bayo, 1994; Silva, 2003). As stated previously, the study of the internal forces generated in the joints is achieved through the consideration of explicit joints. The detailed explanation of the four explicit joints, considered in the foot model, is as follows:

- Metatarsophalangeal Joint – Revolute Joint defined by two different points, P_2 and P_3 belonging to the two rigid bodies (Body 1 and Body 2, Figure 4.8) that share the same position in space, and by two different unit vectors, $\mathbf{v}_1$ and $\mathbf{v}_2$, that belong to different rigid bodies (Body 1 and Body 2, Figure 4.8) and that have the same components in space;
- Midtarsal Joint – Universal Joint defined by two different points, P_4 and P_5 belonging to the two rigid bodies (Body 3 and Body 4, Figure 4.8) that share the same position in space, and two different unit vectors, $\mathbf{v}_3$ (vertical axis) and $\mathbf{v}_4$ (horizontal axis), that belong to different rigid bodies (Body 3 and Body 4, Figure 4.8) and that maintain a right-angle between them;
- Talocalcaneal Joint – Revolute Joint defined by P_7 and by $\mathbf{v}_5$;
- Talocrural Joint – Revolute Joint defined by P_8 and by $\mathbf{v}_6$.

The theoretical value of these joints vectors is presented in Table 4.4 and the final scheme of the model is depicted in Figure 4.8.

Table 4.4 - Theoretical joint vectors description based on Anderson & Pandy (1999).

	Joint Vectors			
	Description	x	y	z
$\mathbf{v}_1$	Metatarsophalangeal joint axis	$-\mathrm{Sin}(18°)$	$-\mathrm{Cos}(18°)$	0.00
$\mathbf{v}_2$	Metatarsophalangeal joint axis	$-\mathrm{Sin}(18\,°)$	$-\mathrm{Cos}(18°)$	0.00
$\mathbf{v}_3$	Midtarsal joint (vertical axis)	0.00	0.00	1.00
$\mathbf{v}_4$	Midtarsal joint (horizontal axis)	0.00	-1.00	0.00
$\mathbf{v}_5$	Talocalcaneal joint axis	$\mathrm{Cos}(35.3°)\mathrm{Cos}(19.8°)$	$\mathrm{Cos}(35.3°)\mathrm{Sin}(19.8°)$	$\mathrm{Sin}(35.3°)$
$\mathbf{v}_6$	Talocrural joint axis	$-\mathrm{Sin}(6°)\mathrm{Cos}(8°)$	$-\mathrm{Cos}(6°)\mathrm{Cos}(8°)$	$-\mathrm{Sin}(8°)$
$\mathbf{v}_7$	Knee joint	1.00	0.00	0.00
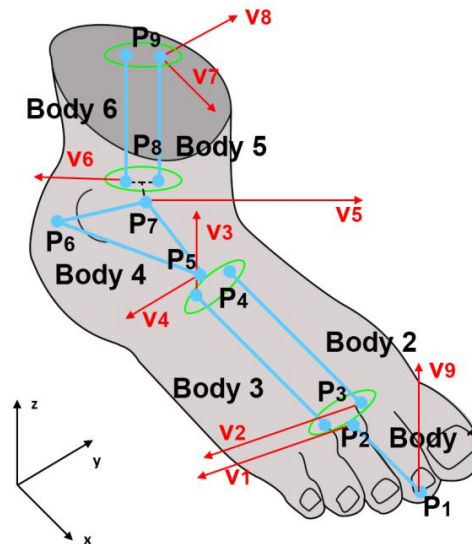
Figure 4.8 - Apollo Modelling scheme. (Red) Vectors; (Blue) Bodies; (Green) Highlight of the points that limit the coincident segments; (Doted lines) Massless Link.

An essential detail of this model is that the non-intersecting axis of the Talocalcaneal Joint and the Talocrural Joint. This is achieved by considering a massless link that maintains a constant distance between the axis, depicted by the segment between P7 and P8 in Figure 4.8. Despite being spatially separated these joints together work as a Universal Joint. This behavior is explained through the constraints detailed further. Another important detail is the consideration of segment II (mid-foot and fore-foot), as well as segment IV (leg), as two coincident segments (connecting the same points) with half the mass of the entire segment. This formulation is useful to calculate the internal rotation angles and moments of these segments and to avoid the use of spherical joints, which introduce some difficulties in the inverse dynamic analysis.

To compute the parameters that define the model, such as the explicit joints and the massless link, it is necessary to build kinematic constraints, as seen in Section 4.3.2. The constraints can be divided into two types: Inner Product Constraints and Superposition Constraints. The first assures a constant inner product formulation between vectors and segments. The second assures the superposition of points or vectors. So, the model requires three superposition constraints:

1. Between P_3 and P_2;
2. Between P_4 and P_5;
3. Between v_1 and v_2;

And five inner product constraints:

1. That assure a 90º angle between $\mathbf{v}_3$ and $\mathbf{v}_4$;
2. That assure a constant length between P_7 and P_8;
3. That assure a constant angle between $\mathbf{v}_5$ and $\mathbf{v}_6$;
4. That assure a constant angle between the segment defined by P_7 and P_8, and $\mathbf{v}_5$;
5. That assure a constant angle between the segment defined by P_7 and P_8, and $\mathbf{v}_6$

The first and third superposition constraints are used to define the revolute joint between Body 1 and Body 2, the metatarsophalangeal joint. The second superposition constraint along with the first inner

product constraint defines the universal joint between Body 3 and Body 4, the midtarsal joint. The last four inner product constraints are used to define the massless link between Body 4 and Body 5; imposing a constant length and constant angles necessary to define the universal joint behavior to $\mathbf{v}_5$ and $\mathbf{v}_6$. This behavior represents the talocrural and talocalcaneal joint.

Chapter V

Acquisition and Data Treatment

In this chapter, a detailed explanation of the methods used to analyze the reliability of the model during gait is presented. Two approaches were used for this purpose: the first, a kinematic evaluation, based on the angles produced at the joints; the second, a kinetic evaluation, based on the inverse dynamics formulation, were the internal reaction forces and the moments were studied, taking into account the ground reaction forces.

5.1. Acquisition Protocol

The first stage comprehends the kinematic data acquisition using a markers protocol. The data was acquired in LBL – Lisbon Biomechanics Laboratory at Instituto Superior Técnico. The trials made use of the fourteen infrared reflective cameras existent in the laboratory – Qualisys ProReflex and two video cameras. The software applied for the acquisition was the Qualisys Track Manager (QTM). In order to acquire the data from external forces, three AMTI-OR6-7 force platforms (508mm x 464mm) were used. The software used to treat the data was the Qualisys Track Manager (QTM) version 2.8 (Qualisys AB, 2013). The sampling frequency was 100Hz for the cameras and 1000Hz for the force plates.

The model proposed in this work is innovative regarding the segments that it considers, so the markers protocol to apply to the model had to be developed. The basis of this procedure is the *Milwaukee Foot Model* (MFM) (Abuzzahab *et al.*, 1993), Figure 1.3, with some variations. The developed protocol uses thirteen reflective markers for each foot/leg complex, in which two of them are only use for static acquisitions, as depicted in Figure 5.1 and Table 5.1. The reflective markers

used in the trials are spherical with flat bases, passive and they have 19mm of diameter, except for the ones used only in static acquisitions that have 11mm of diameter.

Table 5.1 – Markers set protocol description. (s) Markers that were used only in static acquisitions.

Marker	Anatomical Location
M1	Medial aspect of the Hallux
M2	Top head of the Phalange II
M3	Medial aspect of the head of Metatarsal I
M4	Lateral aspect of the head of Metatarsal V
M5	Medial apex of the tuberosity of the navicular
M6	Lateral apex of the tuberosity of the cuboid
M7	Apex of the medial Malleolus
M8	Apex of the lateral Malleolus
M9	Posterior aspect of the Calcaneus
M10(s)	Super-medial aspect of the talus (approximally on top of the synovial sheath of the extensor hallucis longus)
M11(s)	Postero-lateral "corner" of the heel
M12	Medial apex of the head of the tibia
M13	Lateral apex of the head of the fibula
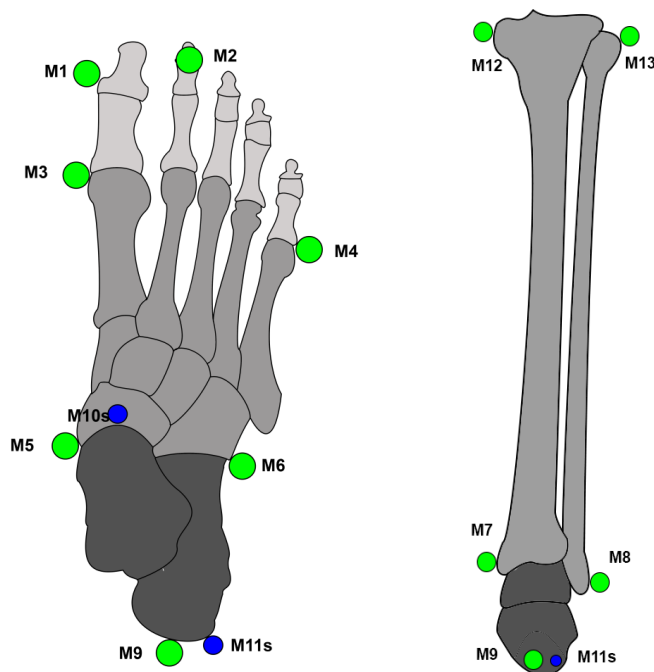
Figure 5.1 – Markers set protocol. (Left) Foot top view; (Right) Leg and rear-foot back view. Blue markers used only in static acquisitions.

5.2. Data Treatment Protocol

5.2.1. Data Treatment using QTM

In order to perform a kinematic and kinetic analysis, it is crucial to previously treat the data. The markers trajectory acquisition and treatment is performed using the QTM software. An Automatic Identification of Markers (AIM) model with 22 reflective markers (26 in static acquisitions) was defined for an efficient assignment of the trajectories. The acquisitions were divided by gait cycles, using the initial contact (IC) of the foot with a force plate, as the first event. It is important to notice that one should consider at least 10 frames before the IC of the foot being analyzed and at least 10 frames after the second IC of the same foot. This consideration is essential to perform a correct filtering in the Apollo software. The treated data was then exported to a *.tsv file (table-separated value) to be treated in Matlab software.

5.2.2. Evaluation of the kinematic data

The kinematic markers position data was exported from the QTM software as a *.tsv file, and directly analyzed by a routine developed in Matlab. The first step of the evaluation comprehended the use of a third order low pass digital Butterworth filter with 6Hz as frequency of cut. The filtered data correspondent to each marker was then assigned to a three column matrix, where each column represented respectively the x, y and z coordinates, and each line represented the frame. Using this information it was possible to define vectors that were used to calculate the angles between the model segments. Taking into account Figure 5.1, a description of the vectors used is presented in Table 5.2.

Table 5.2 - Vectors used in Matlab to calculate the kinematic angles. M_i represent the coordinates of the respective marker. All the vectors were normalized.

Description	Vector	Formula
Knee Joint	$\boldsymbol{v}_{Knee}$	$M_{13} - M_{12}$
Talocrural Joint	$\boldsymbol{v}_{Talocrural}$	$M_8 - M_7$
Midtarsal Joint	$\boldsymbol{v}_{Midtarsal}$	$M_6 - M_5$
Metatarsophalangeal Joint	$\boldsymbol{v}_{Metatarsophalangeal}$	$M_4 - M_3$
Leg z Axis	$\boldsymbol{z}_{Leg}$	$\dfrac{M_{12} + M_{13}}{2} - \dfrac{M_7 + M_8}{2}$
Leg x Axis	$\boldsymbol{x}_{Leg}$	$(\boldsymbol{z}_{Leg} \times \boldsymbol{v}_{Knee})$
Leg y Axis	$\boldsymbol{y}_{Leg}$	$(\boldsymbol{z}_{Leg} \times \boldsymbol{x}_{Leg})$
Rear-foot x axis	$\boldsymbol{x}_{RF}$	$\dfrac{M_5 + M_6}{2} - M_9$
Rear-foot z axis	$\boldsymbol{z}_{RF}$	$(\boldsymbol{v}_{Midtarsal} \times \boldsymbol{x}_{RF})$
Rear-foot y axis	$\boldsymbol{y}_{RF}$	$(\boldsymbol{z}_{RF} \times \boldsymbol{x}_{RF})$
Mid-foot & Fore-foot x Axis 1	$\boldsymbol{x}_{MFFF1}$	$\dfrac{M_3 + M_4}{2} - \dfrac{M_5 + M_6}{2}$
Mid-foot & Fore-foot z Axis 1	$\boldsymbol{z}_{MFFF1}$	$(\boldsymbol{v}_{Metatarsophalangeal} \times \boldsymbol{x}_{MFFF1})$
Mid-foot & Fore-foot y Axis 1	$\boldsymbol{y}_{MFFF1}$	$(\boldsymbol{z}_{MFFF1} \times \boldsymbol{x}_{MFFF1})$
Mid-foot & Fore-foot x Axis 2	$\boldsymbol{x}_{MFFF2}$	$\dfrac{M_3 + M_4}{2} - \dfrac{M_5 + M_6}{2}$
Mid-foot & Fore-foot z Axis 2	$\boldsymbol{z}_{MFFF2}$	$(\boldsymbol{v}_{Midtarsal} \times \boldsymbol{x}_{MFFF2})$
Mid-foot & Fore-foot y Axis 2	$\boldsymbol{y}_{MFFF2}$	$(\boldsymbol{z}_{MFFF2} \times \boldsymbol{x}_{MFFF2})$
Toes x axis	$\boldsymbol{x}_{Toes}$	$M_2^* - \dfrac{M_3 + M_4}{2}$
Toes z axis	$\boldsymbol{z}_{Toes}$	$(\boldsymbol{v}_{Metatarsophalangeal} \times \boldsymbol{x}_{Toes})$
Toes y axis	$\boldsymbol{y}_{Toes}$	$(\boldsymbol{z}_{Toes} \times \boldsymbol{x}_{Toes})$
Massless Link	$\boldsymbol{v}_{Massless}$	$\dfrac{M_{10s} + M_{11s}}{2} - \dfrac{M_7 + M_8}{2}$
Talocalcaneal Joint	$\boldsymbol{v}_{Talocalcaneal}$	$M_{10s} - M_{11s}$
Rear-foot Top	$\boldsymbol{v}_{RFT}$	$\dfrac{M_5 + M_6}{2} - \dfrac{M_{10s} + M_{11s}}{2}$

Note: M_2^* has the x, y coordinates of M_2 and the z coordinate of M_1. The use of two different Cartesian Axes for the Mid-foot & Fore-foot segment is related with the calculation of the angles and moments for the internal rotation, explained further.

Using the four-quadrant inverse tangent Matlab function (atan2, receiving as arguments, the cross product between the vectors of interest and the dot product of the same vectors) it was possible to evaluate the progression of the angles along the time of the aquisition. The formulation is presented in Table 5.3 and Figure 5.3.

Table 5.3 - Kinematic Angles formulation.

Description	Angle	Formula
Dorsiflexion and Plantarflexion Metatarsophalangeal Joint	ϕ_1	$\left(a\tan 2((-\boldsymbol{x}_{MFFF1} \times \boldsymbol{z}_{Toes}), (-\boldsymbol{x}_{MFFF1} \cdot \boldsymbol{z}_{Toes})) - \dfrac{\pi}{2} \right) \cdot (-1)$
Dorsiflexion and Plantarflexion Midtarsal Joint	ϕ_2	$\left(a\tan 2((\boldsymbol{z}_{RF} \times \boldsymbol{x}_{MFFF1}), (\boldsymbol{z}_{RF} \cdot \boldsymbol{x}_{MFFF1})) - \dfrac{\pi}{2} \right) \cdot (-1)$
Abduction and Adduction Midtarsal Joint	ϕ_3	$\left(a\tan 2((\boldsymbol{y}_{RF} \times \boldsymbol{x}_{MFFF1}), (\boldsymbol{y}_{RF} \cdot \boldsymbol{x}_{MFFF1})) - \dfrac{\pi}{2} \right)$
Dorsiflexion and Plantarflexion Talocrural Joint	ϕ_4	$\left(a\tan 2((\boldsymbol{x}_{RF} \times \boldsymbol{z}_{Leg}), (\boldsymbol{x}_{RF} \cdot \boldsymbol{z}_{Leg}) - \dfrac{\pi}{2} \right) \cdot (-1)$
Inversion and Eversion Talocalcaneal Joint	ϕ_5	$\left(a\tan 2((\boldsymbol{y}_{RF} \times \boldsymbol{z}_{Leg}), (\boldsymbol{y}_{RF} \cdot \boldsymbol{z}_{Leg}) - \dfrac{\pi}{2} \right) \cdot (-1)$
Internal Rotation Mid-foot & Fore-foot	ϕ_6	$\left(a\tan 2((\boldsymbol{z}_{MFFF2} \times \boldsymbol{v}_{Metatarsophalangeal}), (\boldsymbol{z}_{MFFF2} \cdot \boldsymbol{v}_{Metatarsophalangeal})) - \dfrac{\pi}{2} \right)$
Internal Rotation Leg	ϕ_7	$\left(a\tan 2((\boldsymbol{x}_{Leg} \times \boldsymbol{v}_{Talocrural}), (\boldsymbol{x}_{Leg} \cdot \boldsymbol{v}_{Talocrural})) - \dfrac{\pi}{2} \right)$

The subtraction of $\dfrac{\pi}{2}$ is related with the fact that the angle being calculated with the four-quadrant inverse tangent does not represent directly the angle of the respective joint motion, as depicted in Figure 5.2. As one can see from Table 5.3 and Figure 5.3 the vectors used to calculate the movements are deviated from $[0 \pm n\pi], n \in \mathbb{N}$ angles. This happens because the outcome of this function always defaults to angles ranging from $[-\pi, \pi]$. So in order to represent the real kinematic motion angle, the subtraction is needed. The product by the scale factor (-1) defines the signal associated with each movement. For the Dorsiflexion and Plantarflexion, the convention used was: positive and negative respectively. For the Abduction and Adduction the principle used was: positive and negative respectively. Regarding Inversion and Eversion, the used convention was: positive and

negative respectively. Finally regarding the internal rotation, the principle used was: positive for the movement from the inside (medial) to the outside (lateral) and negative otherwise.
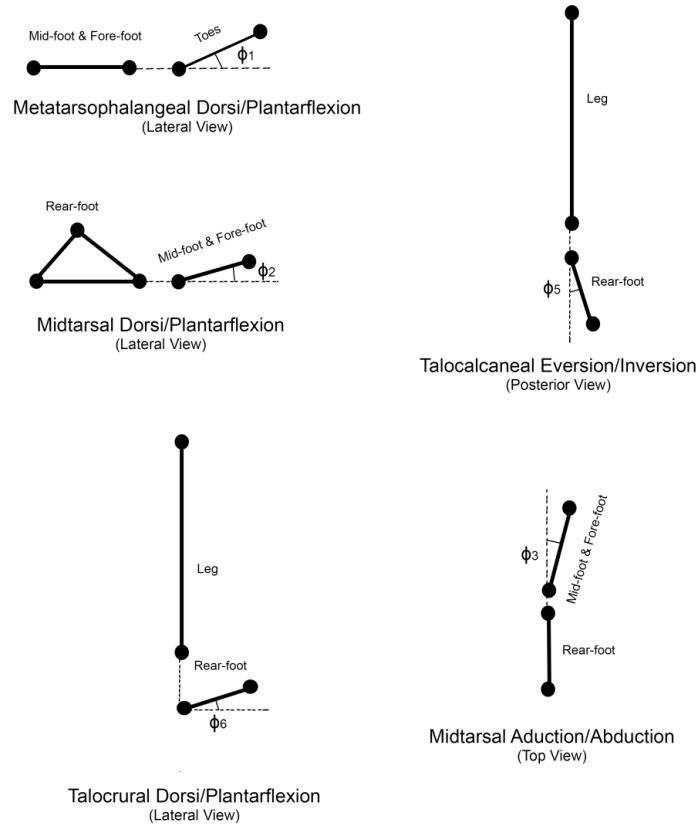
Figure 5.2 - Kinematic angles representation.
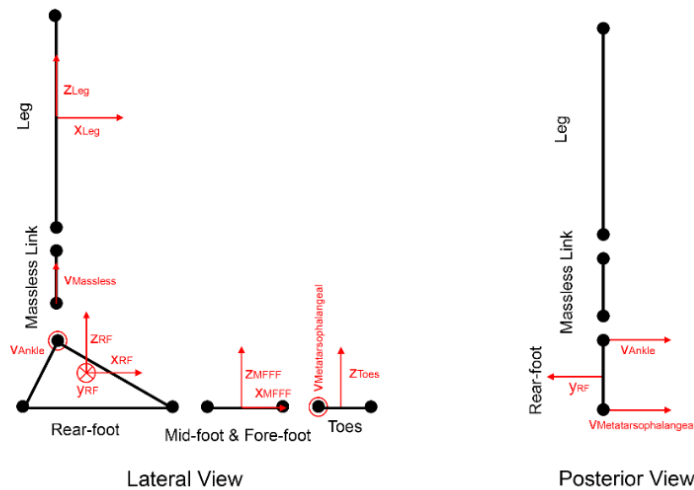
Figure 5.3 - Kinematic vectors used for the calculation of the kinematic angles.

5.2.3. Data preparation to be used in Apollo

To perform an inverse dynamic analysis using the Apollo software, four types of files are needed: *.mdl (modelling files), *.sml (simulation files), *.frc (forces file) and *.dat (data files). Each analysis requires one modelling file and one simulation file. The first, as briefly approached in Section

4.5, comprehends the information regarding the model: masses, inertias, local coordinates of the points and vectors defining each segment, parameters that define the drivers that guide each degree of freedom and the parameters regarding the joints that connect the segments. The modelling file can receive more information but that won't be addressed in the present work. The second covers the information regarding the initial position of each segment center of mass, the initial Euler angles, and angular velocities in the global reference frame. The simulation file also requires the time parameters regarding the analysis and the gravity field vector. The data files are used to guide each degree of freedom of the system (DOF) and therefore they comprehend the information regarding the system drivers, existing one for each DOF. For each analysis the software also requires one force file that comprehends the ground reaction forces and their application points. After the simulation is completed, the software generates a *.out file that contains: global coordinates of the model points and vectors, velocities, accelerations, center of mass global positions, moments and internal reaction forces.

5.2.3.1. Conversion of the kinematic data to the model (Simulation and Modeling Files)

The model implemented in the modelling and simulation files was already detailed in Section 4.5. This section is intended to explain the process used to merge the multibody model with the acquired experimental data. Taking into account the information presented in Table 4.2, Table 4.3, Figure 4.8 and Table 5.2, and knowing that the kinematic vectors are presented in a global reference frame and that the model vectors are the conversion of those vectors into the correspondent body local referential, a resume table (Table 5.4) is presented. A remark has to be made to the distinct axis between $MFFF_1$ and $MFFF_2$. The axis of $MFFF_1$ correspond to the axis of Body 2 and the axis of $MFFF_2$ correspond to the axis of Body 3 (Figure 4.8). Defining two different axis on the same segment allows the calculation of the internal rotation of the rigid bodies.

Table 5.4 - Description of the conversion between the kinematic vectors and the theoretical vectors.

Description	Kinematic Vectors (Global RF) Table 5.2	Theoretical Vectors (Local RF) Table 4.2, Table 4.3, Table 4.4 and Figure 4.8	Body Figure 4.8
Metatarsophalangeal Joint	$\boldsymbol{v}_{Metatarsophalangeal}$	$\boldsymbol{v}_1$	1
Toes z axis	$\boldsymbol{z}_{Toes}$	$\boldsymbol{v}_9$	1
Metatarsophalangeal Joint	$\boldsymbol{v}_{Metatarsophalangeal}$	$\boldsymbol{v}_2$	2
Mid-foot & Fore-foot z Axis 2	$\boldsymbol{z}_{MFFF2}$	$\boldsymbol{v}_3$	3
Rear-foot y axis	$\boldsymbol{y}_{RF}$	$\boldsymbol{v}_4$	4
Talocalcaneal Joint	$\boldsymbol{v}_{Talocalcaneal}$	$\boldsymbol{v}_5$	4
Talocrural Joint	$\boldsymbol{v}_{Talocrural}$	$\boldsymbol{v}_6$	6
Leg x Axis	$\boldsymbol{x}_{Leg}$	$\boldsymbol{v}_7$	5
Leg y Axis	$\boldsymbol{y}_{Leg}$	$\boldsymbol{v}_8$	5
Toes x axis	$\boldsymbol{x}_{Toes}$	$\dfrac{\overrightarrow{P_2 P_1}}{\left|\overrightarrow{P_2 P_1}\right|}$	1
Mid-foot & Fore-foot x Axis 1	$\boldsymbol{x}_{MFFF1}$	$\dfrac{\overrightarrow{P_4 P_3}}{\left|\overrightarrow{P_4 P_3}\right|}$	2
Mid-foot & Fore-foot x Axis 2	$\boldsymbol{x}_{MFFF2}$	$\dfrac{\overrightarrow{P_4 P_3}}{\left|\overrightarrow{P_4 P_3}\right|}$	3
Rear-foot x axis	$\boldsymbol{x}_{RF}$	$\dfrac{\overrightarrow{P_6 P_5}}{\left|\overrightarrow{P_6 P_5}\right|}$	4
Rear-foot Top	$\boldsymbol{v}_{RFT}$	$\dfrac{\overrightarrow{P_7 P_5}}{\left|\overrightarrow{P_7 P_5}\right|}$	4
Massless Link	$\boldsymbol{v}_{Massless}$	$\overrightarrow{P_8 P_7}$	-
Leg z Axis	$\boldsymbol{z}_{Leg}$	$\dfrac{\overrightarrow{P_9 P_8}}{\left|\overrightarrow{P_9 P_8}\right|}$	5/6

5.2.3.2. Data files preparation

The preparation of the data files containing the information about the system drivers was carried out using the Matlab software. Each data file can contain one of five different types of information:

1) Angles between one unit vector and one segment (vector defined by two points);
2) Angles between two unit vectors;
3) Angles between two segments (vectors defined by two points);
4) Global coordinates of one point (x,y,z);
5) Global coordinates of a vector (x,y,z);.

Further explanation on the construction of data files is presented in Appendix A. To guide the degrees of freedom of the system ten drivers were used, whose calculation is further explained in Table 5.5. The reason why the formulation used to calculate the driving angles vary from the one used to calculate the kinematic angles (Table 5.3) is related with the simplicity of the model. In order to build an efficient computational model some vectors were not formulated in the Apollo modelling file, so the driving files are only providing angles between explicit segments or vectors (Table 5.4).

Table 5.5 - Drivers description and formulation.

Description	Driver Type	Formula (Using the kinematic vectors)
Dorsiflexion and Plantarflexion (Metatarsophalangeal Joint)	1	$a\tan2((-\boldsymbol{x}_{MFFF1} \times \boldsymbol{z}_{Toes}),(-\boldsymbol{x}_{MFFF1} \cdot \boldsymbol{z}_{Toes}))$
Dorsiflexion and Plantarflexion (Midtarsal Joint)	1	$a\tan2((\boldsymbol{z}_{MFFF2} \times -\boldsymbol{x}_{RF}),(\boldsymbol{z}_{MFFF2} \cdot -\boldsymbol{x}_{RF}))$
Abduction and Adduction (Midtarsal Joint)	1	$a\tan2((\boldsymbol{x}_{MFFF2} \times \boldsymbol{y}_{RF}),(\boldsymbol{x}_{MFFF2} \cdot \boldsymbol{y}_{RF}))$
Dorsiflexion and Plantarflexion (Talocrural Joint)	3	$a\tan2((\boldsymbol{z}_{Leg} \times \boldsymbol{v}_{RFT}),(\boldsymbol{z}_{Leg} \cdot \boldsymbol{v}_{RFT}))$ (P)
Inversion and Eversion (Talocalcaneal Joint)	1	$a\tan2((\boldsymbol{z}_{Leg} \times \boldsymbol{y}_{RF}),(\boldsymbol{z}_{Leg} \cdot \boldsymbol{y}_{RF}))$
Internal Rotation (Mid-foot & Fore-foot)	2	$a\tan2((\boldsymbol{z}_{MFFF2} \times \boldsymbol{v}_{Metatarsophalangeal}),(\boldsymbol{z}_{MFFF2} \cdot \boldsymbol{v}_{Metatarsophalangeal}))$
Internal Rotation Leg	2	$a\tan2((\boldsymbol{z}_{Leg} \times \boldsymbol{v}_{Talocrural}),(\boldsymbol{z}_{Leg} \cdot \boldsymbol{v}_{Talocrural}))$
Knee Point Coordinates	4	$(M_{12} + M_{13})/2$
Knee Vector 1 Coordinates	5	$\boldsymbol{x}_{Leg}$
Knee Vector 2 Coordinates	5	$\boldsymbol{y}_{Leg}$

(P) means that both vectors $\boldsymbol{z}_{Leg}$ and $\boldsymbol{v}_{RFT}$ were projected on the plane normal to vector $\boldsymbol{v}_{Ankle}$.

As one can deduce, the number of drivers prescribed to the system is higher than the number of DOF's of the system (Driver type 4 and 5 count as one driver per axis, so three each). So, sixteen

drivers are being prescribed for only thirteen DOF's which mean that some are redundant due to the model and software convenience. The routine developed exports this information automatically into different *.dat files.

5.2.3.3. Force file preparation

The information regarding the Ground Reaction Forces (GRFs) from the three force platform and the center of pressure curve (COP) at each time step was exported from the QTM software as three *.tsv files, one for each platform, and processed by a Matlab routine. The first step of the evaluation comprehended the use of a third order low pass digital Butterworth filter with 16Hz as frequency of cut. The filtered data correspondent to each platform was then assigned to a six column matrix, where the first three columns represented respectively the x, y and z coordinates of GRFs and the following three the x, y and z coordinates of the COP, and each line represented the frame. Another important parameter is also calculated by the routine, a vector containing information that allows the Apollo software to know in which segment of the model is the force being applied. In the end of the routine the information is exported automatically into a *.frc file. Further explanation on the construction of force files is presented in Appendix A.

5.2.4. Data Treatment Summary

This section is intended to present a summary of how all the data, reported in this document, is gathered to produce the results. The first step is the introduction of the subject specific parameters (height, weight and foot length), obtained in the laboratory, in the anthropometric tables (Table 3.10, Table 3.11, Table 3.12, Table 3.13, Table 3.17 and their summary, Table 3.18) and in the model formulation tables (Table 4.2 and Table 4.3). This allows the formulation of great part of the modulation file. The following step comprehends the application of the markers set protocol and the laboratory acquisitions. The third step implies the data treatment in the QTM software followed by the application of the Matlab routines. These routines generate: the rest of the information needed to complete the modulation file (through static acquisitions), the data required to build a simulation file (through dynamic acquisitions), the data and force files and the kinematic results. Having the four files required by the Apollo to perform an inverse dynamics analysis, the out file is created. This file contains the dynamic results, as a matter of visualization, this data is treated again using Matlab to generate the kinetic plots. A flow-chart with this information is presented in Figure 5.4.
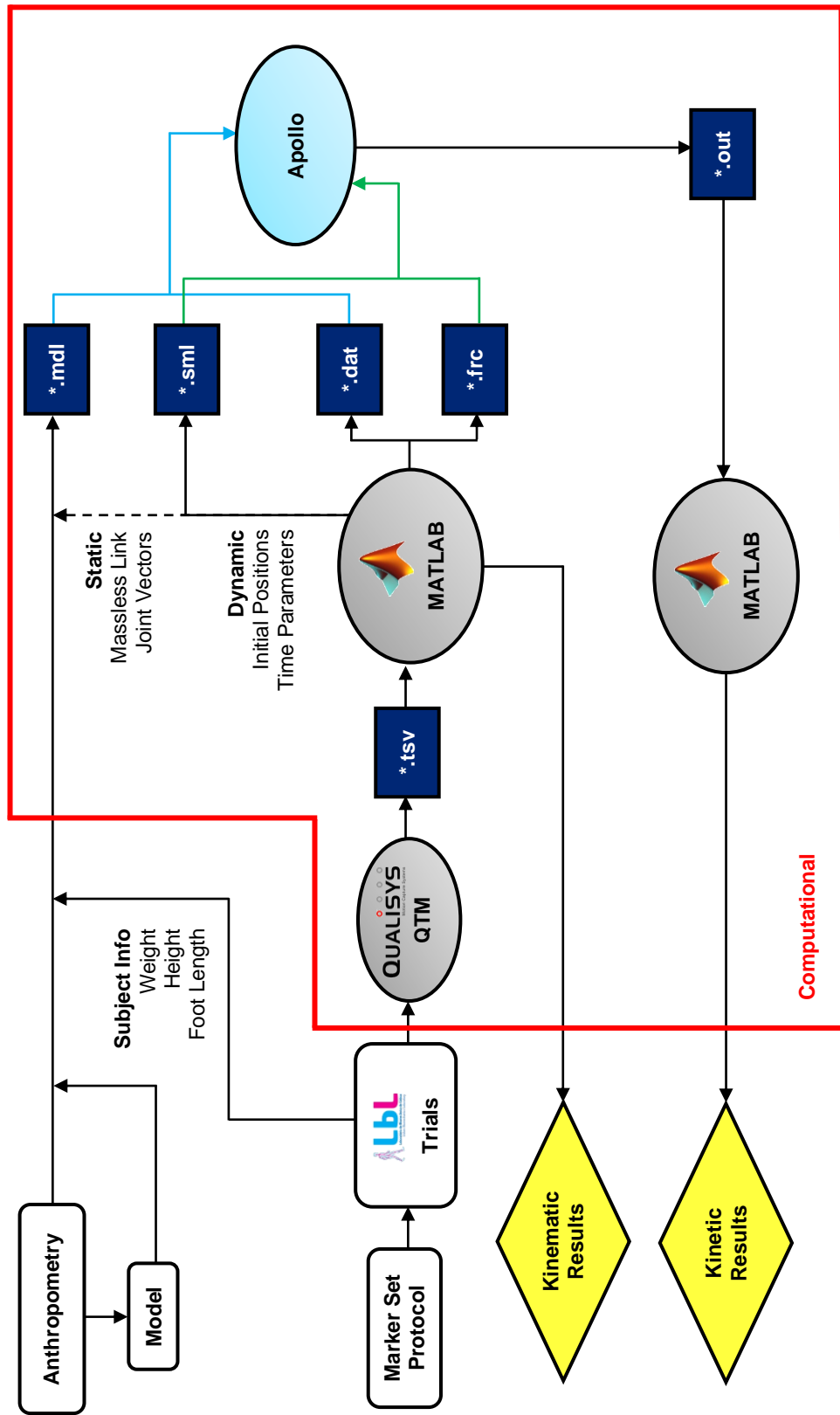
Figure 5.4 - Flow-chart summarizing the data treatment protocol.

Chapter VI

Results and Discussion

In order to test the proposed foot model, two sets of trials were performed. These acquisitions had as subjects a healthy man (23 years old, 87kg, 1,87m and with a foot size of 27cm) and a healthy woman (23 years old, 52kg, 1,53m with a foot size of 21cm), both with no history of gait disorders. The subjects were asked to walk through a walkway equipped with the force plates, without them being influenced by their existence. The markers set protocol used and the laboratory configuration existent at the time of the acquisitions were already described in Chapter V. From all the trials performed, five trials from each subject were chosen to report the results. These trials, as referred previously, represent an entire gait cycle, using the Initial Contact (IC) of the right foot with the second force plate, as the first event. So all the results analyzed derive from the right foot. The graphical outcome from both subjects will be presented simultaneously in the plots, using solid lines to represent the mean of the five trials and light areas to characterize the mean more (upper limit) or less (lower limit) the standard deviation (calculated at each time step). Subject 1 corresponds to the healthy man and subject 2 to the healthy woman, Figure 6.1.
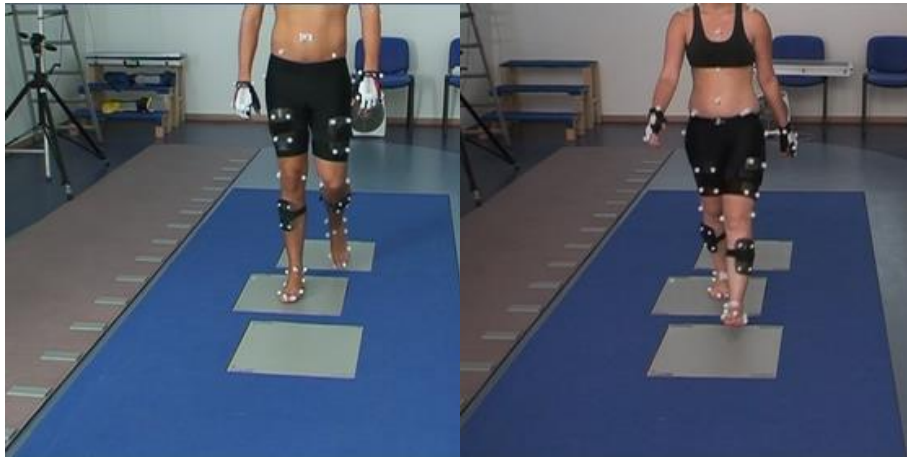
Figure 6.1 - Subject 1 (Right); Subject 2 (Left).

6.1. Kinematic Results

6.1.1. Joint Angles

Joint angular displacement has been widely used to detect gait disorders. This evaluation is performed by detecting deviations from typical patterns. In this work, typical patters will be used to assess the validity of the results produced by the model. The variety of foot joint angles results existent in the bibliography is limited, usually the authors stay limited to the angle produced at the talocrural joint, and therefore the first result to be presented is the referred one, Figure 6.2.
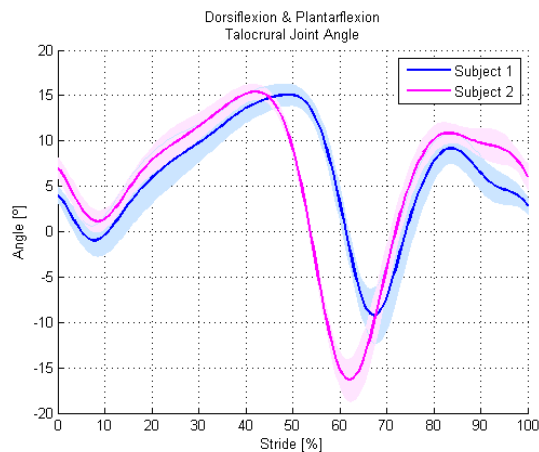

Figure 6.2 - Talocrural Joint Angle, Dorsiflexion (+) and Plantarflexion (-).

The pattern presented in Figure 6.2 is a well-known pattern for a normal talocrural angle variation during gait (Abuzzahab, Harris, Kidder, & Johnson, 1994; Bruening *et al.*, 2012a; Gonçalves, 2010; Kidder *et al.*, 1996; Leardini *et al.*, 2007; Lundgren *et al.*, 2008; MacWilliams *et al.*, 2003; Winter, 1991). Two peaks (maximum and minimum) stand out in this pattern. The maximum relates with the terminal stance phase [30-50%], were the foot reaches its maximal dorsiflexion angle. The minimum is related to the maximum plantarflexion angle, which occurs during the initial swing [60-70%]. The evaluation of the offsets is similar to the one reported by Bruening *et al.* (2012a) that uses a similar marker set protocol.

Proceeding to the analysis of the angle produced at the metatarsophalangeal joint, Figure 6.3.
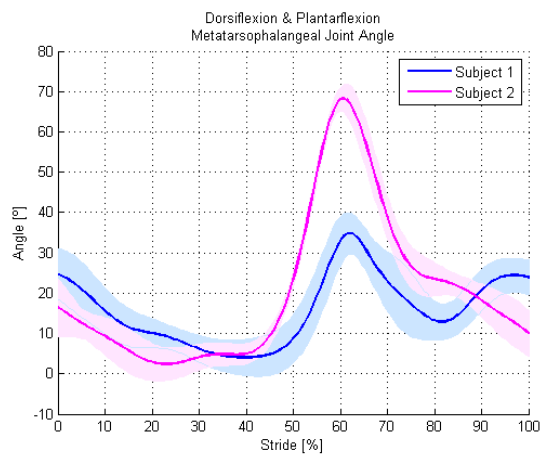

Figure 6.3 - Metatarsophalangeal Joint Angle, Dorsiflexion (+) and Plantarflexion (-).

The result presented in Figure 6.3 is similar to the one presented by Bruening *et al.* (2012a) and Kidder *et al.* (1996), an immediate deduction can be taken from it; the angle values barely reach negative values. This means that pronounced plantarflexion at the metatarsophalangeal joint during gait is an uncommon event. One can notice that the angle values reach 0º during [20-40%] of the stride, corresponding to the midstance, when the foot is flatten on the ground. After this phase the angle values increase rapidly, this happens during the terminal stance, when the foot is touching the ground only with the toes. This increase is more pronounced in subject 2 but still within the range of healthy values.

Figure 6.4 represents the angle produced due to plantarflexion and dorsiflexion at the midtarsal joint.
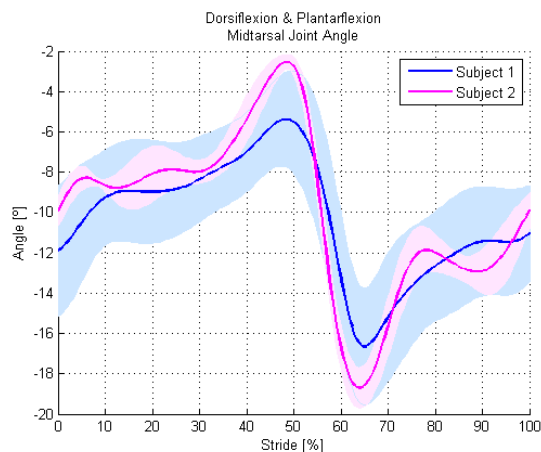
Figure 6.4 – Midtarsal Joint Angle, Dorsiflexion (+) and Plantarflexion (-).

It is interesting to notice in Figure 6.4 that this joint during a gait cycle is always at plantar flexion, this is due to the arches of the foot. During the loading response and midstance phases, the weight of the whole body is being applied on the foot in contact with the ground. This event leads to the compliance of the arch, and so the plantarflexion is attenuated (the angle becomes less negative), the angle increases, between [0-50%] of the stride. The instant the foot leaves the ground is clearly represented

by an abrupt decrease in the angle value, becoming more negative, accentuating the plantarflexion. This pattern is once again supported by Bruening *et al.* (2012a) and Kidder *et al.* (1996).

Figure 6.5 represents the outcome regarding the adduction and abduction at the midtarsal joint.
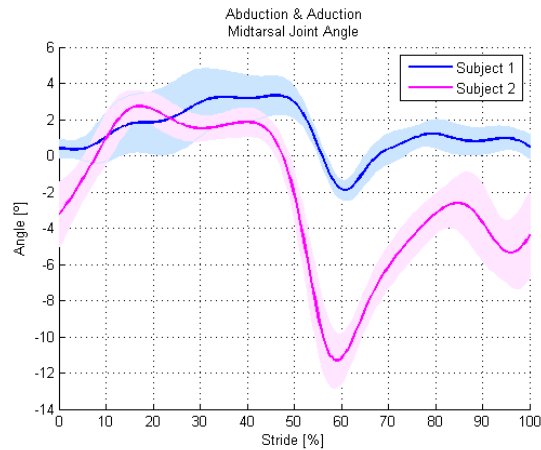

Figure 6.5 – Midtarsal Joint Angle, Abduction (+) and Adduction (-).

The signal notation used to evaluate this angle is the same as the one used by Kidder *et al.* (1996) and inverse to the one used by Bruening *et al.* (2012a). This results in an inverted graphic comparing to the second reference. However the pattern is similar to both of them, barely presenting angle changes until [50-70%] of the stride when the foot is adducted at the pre-swing and initial swing phase. The difference between subjects is due to the possible misplacement of the Calcaneus marker in subject 1. It was seen that a small deviation from the intended position in this marker generates erroneous results and due to the size of the markers it is sometimes difficult to have the perception of the right position. As one can see in Table 5.3, the adduction/abduction angle is calculates using y_{RF}, this vector calculation is based on the position of this marker, so a misplacement originated in its location can explain the difference in the angles results.

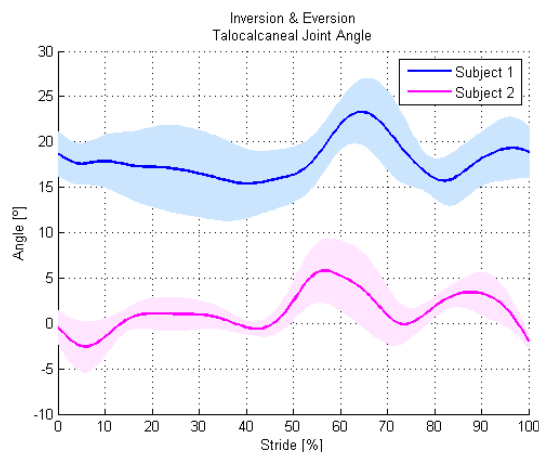Proceeding to the analysis of the inversion/eversion angle at the talocalcaneal joint, Figure 6.6.

Figure 6.6 - Talocalcaneal Joint Angle, Inversion (+) and Eversion (-).

The pattern presented in Figure 6.6 is identical to the one presented by Bruening *et al.* (2012a) and Kidder *et al.* (1996), however the signal notation used to evaluate this angle is the same as the one used in the first reference and inverted regarding the second. Both subjects present foot inversion during the majority of the gait cycle, and small angle variations. The offset presented in subject 1 is probably due the misplacement of the calcaneus marker.

Figure 6.7 presents the results for the internal rotation angle of the mid-foot and fore-foot segment.
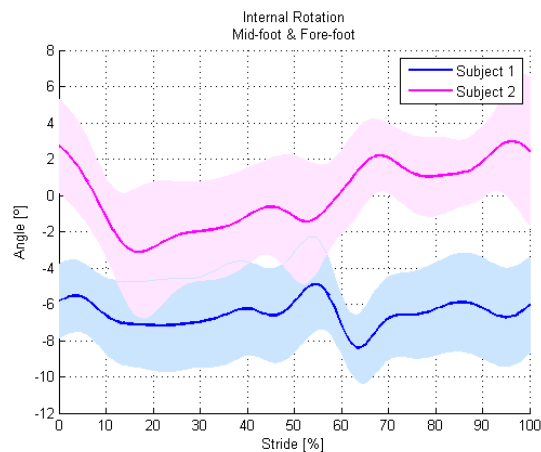

Figure 6.7 – Mid-foot and Fore-foot Internal Rotation. From Medial to Lateral (+).

This result is not discussed in the bibliography, and as one can see from the graphic, the reason is the small variation presented and the proximity to 0º. The small angle values also justify the apparently high standard deviation. This means that this segment barely rotates over itself. Figure 6.8 stands for the angle variation that characterizes the leg internal rotation.
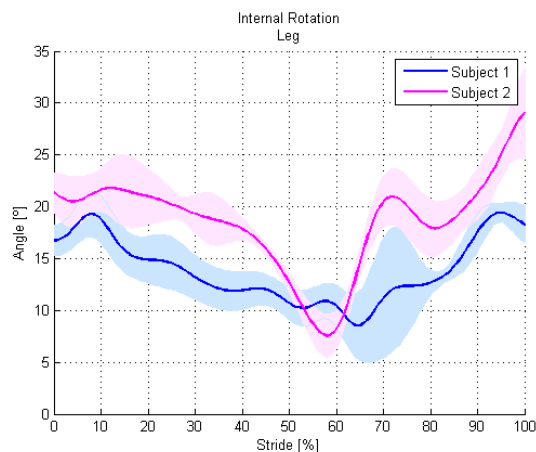
Figure 6.8 - Leg Internal Rotation. From Medial to Lateral (+).

Once again, this result is rarely presented in the bibliography; however it provides a valid understanding of the leg rotation. As one can see from Figure 6.8, both participants present a positive angle during the entire gait cycle; meaning that the leg points toward the lateral side. However during the stance phase [0-60%], a slight rotation of the leg to the medial side is verified in both subjects. During the swing phase [60-100%] the opposite happens, the rotation to the lateral side is accentuated.

6.2. Kinetic Results

6.2.1. Ground Reaction Forces

The GRF results, Figure 6.9, were normalized in respect to the subject body mass. Evaluating this results, one can perceive that they represent characteristic patterns (Gonçalves, 2010; Silva, 2003; Winter, 1991) The standard deviations are very small, proving that the ground reaction forces provide a well-defined and conserved curve. This curve is of extreme importance because it allows a good measure of comparison between healthy and pathological subjects. Notice that the reaction forces in Y are very small comparing to the others, leading to a higher standard deviation. Another interesting aspect of these results is the first peak in the ground reaction force in the transversal component (Z plot); it represents the body weight acceptance (normalized).
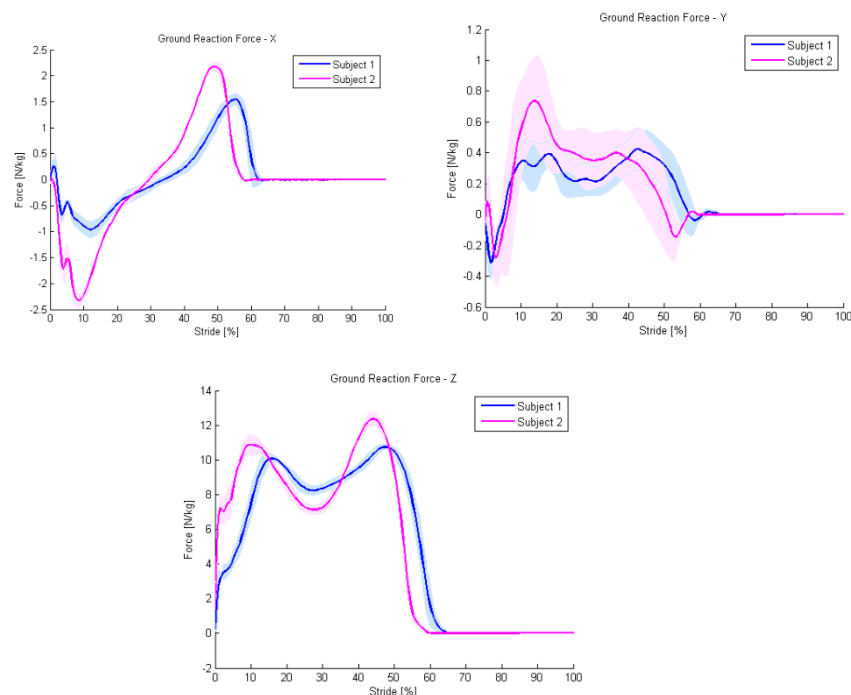
Figure 6.9 - Ground Reaction Forces. (Top)(Left) Reaction Force in X, (Right) Reaction Force in Y; (Bottom) Reaction Force in Z.

6.2.2. Joints Moments of Forces

Moments of force, result from the combined action of the muscular, ligament and friction forces acting to cause body rotation about a specific axis. In normal gait, the joint angles do not reach their extreme limits and the friction forces are minimal. So, the moment can be interpreted as due to muscle forces only (Winter, 1991). The inverse dynamic analysis, allows the calculation of the internal forces in kinematic pairs (Lagrange multipliers methods). Adding a driving actuator (constraint equation) for each DOF of the model, the simulation enables the calculation of the Lagrange multipliers associated to each joint torque (Silva, 2003).

The present model has sixteen drivers' actuators, producing the correspondent forces and joint moments of force. It should be noted that except for the drivers correspondent to points and vectors trajectories, that do not produce joint moments of force but instead they generate driving forces. From the initial sixteen, only seven will be approached, the ones regarding the kinematic angle drivers presented previously, all of them were normalized in respect to the subject body mass. The signals convention adopted was the one used by Winter (1991) and Silva (2003). This formulation considers the extensor moment as positive, due to the attempt of pushing the body away from the ground (Winter, 1991) and the flexor moment as negative for the opposite reason. Basically, the ground reaction forces produce a physiological moment that has to be opposed by the body (Gonçalves, 2010). The moment generated by this opposition is the one that will be presented. The first result to be analyzed is the moment generated at the talocrural joint, Figure 6.10.
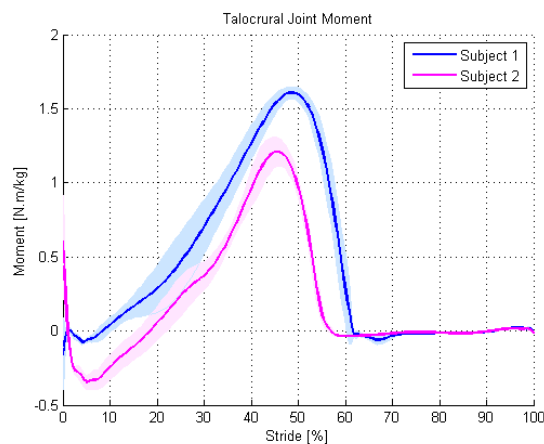
Figure 6.10 – Talocrural Joint Moment. Plantarflexion (+) and Dorsiflexion (-).

The pattern presented in Figure 6.10 is a well-known result (Bruening *et al.*, 2012b; Gonçalves, 2010; Silva, 2003; Winter, 1991). Evaluating the graphic one can see that it shows a plantarflexion moment almost during the entire stance phase [10-60%]. So the ground reaction forces are generating a physiologic dorsiflexion moment and the body has to respond producing a contrary plantarflexion moment. During the swing phase the moment is kept null, there are no ground reaction forces acting.

Proceeding to the analysis of the moment generated at the metatarsophalangeal joint, Figure 6.11 .

Figure 6.11 – Metatarsophalangeal Joint Moment. Plantarflexion (+) and Dorsiflexion (-).

The previous graphic shows a similar result as the one obtain by Bruening *et al.* (2012b), moment values rounding zero. However during the initial contact [0-10%] the results show a dosrflexion torque, this is the body response to the physiologic plantarflexion generated by the ground reaction forces. Again the moments are kept null during the swing phase.

The evaluation of Figure 6.12 is similar to the one applied to Figure 6.10, the result shows plantarflexion moments during the stance phase [10-60%], except for the initial contact. The ground reaction forces are generating a physiologic dorsiflexion moment and the body has to respond producing a contrary plantarflexion moment. During the swing phase the moment is kept null, there are no ground reaction forces acting.
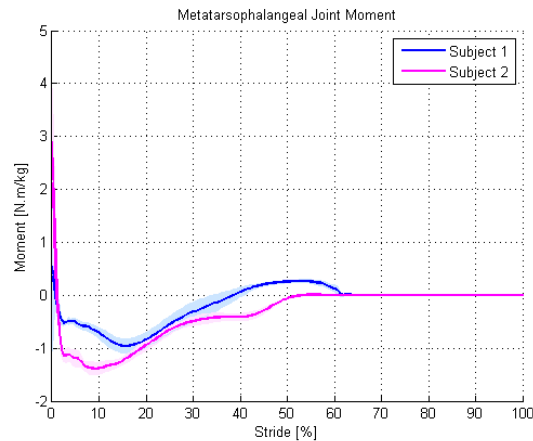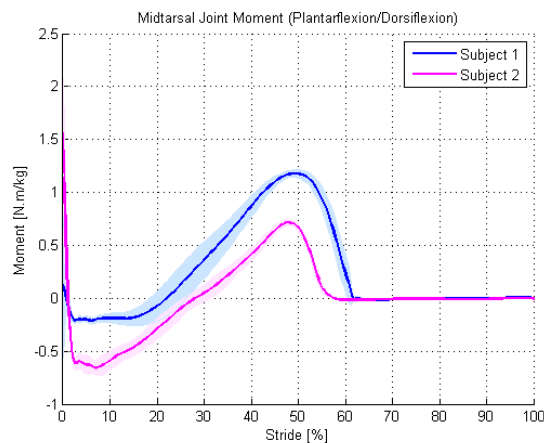

Figure 6.12 – Midtarsal Joint Moments. Plantarflexion (+) and Dorsiflexion (-).

Figure 6.13 presents the abduction and adduction moments generated during a gait cycle. A first look to this result may lead to some erroneous conclusions. The first thing that as to be approached are the small values of the torque, this is due to the small value of the ground reaction force at Y (Figure 6.9), responsible for generating the physiological moment that will be opposed by the body. So if the physiological moment is small, the opposing body torque response will also be small. Comparing to the result presented by Bruening *et al.* (2012b), the result from subject 2 is identical, abduction moment during the majority of the stance phase. Subject 1 results are again due to the misplacement of the Calcaneus marker, already discussed.
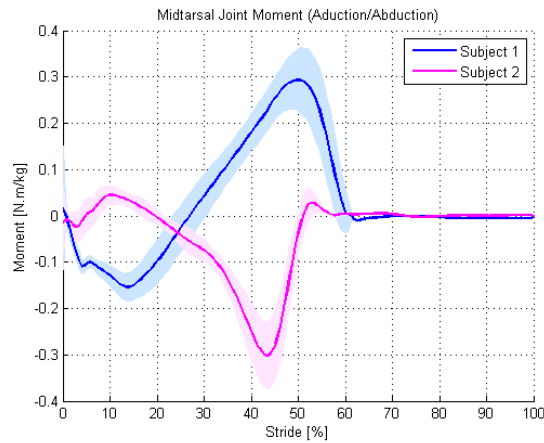
Figure 6.13 - Midtarsal Joint Moments. Adduction (+) and Abduction (-).

Proceeding to the analysis of the moment generated at the talocalcaneal joint, Figure 6.14. The outcome of subject 2 is identical to the one presented by Bruening *et al.* (2012b), showing eversion moment during the majority of the stance phase. The erroneous result of subject 1 is the result of the misplacement of the Calcaneus reflective marker as stated before, so it will not be addressed.
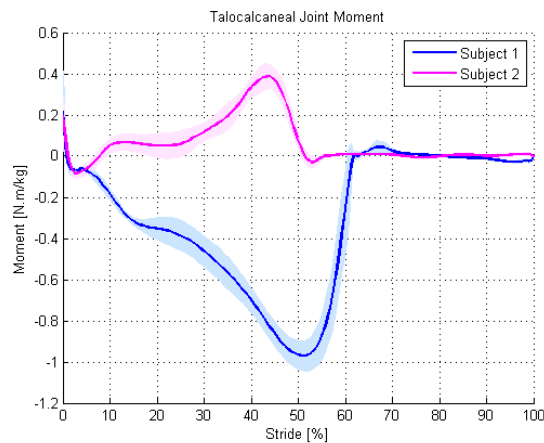
Figure 6.14 - Talocalcaneal Joint Moments. Eversion (+) and Inversion (-).

The analysis of Figure 6.15 shows different results between the subjects. Due to the small amount of subjects and to the lack of references, an expected result is missing, so both can be evaluated. The results show that for subject 2 the ground reaction forces are generating a physiologic internal rotation moment from the medial side to the lateral side and the body has to respond producing a contrary moment (from lateral to medial). The contrary happens to subject 1; the torque is being generated from the medial side to the lateral side.
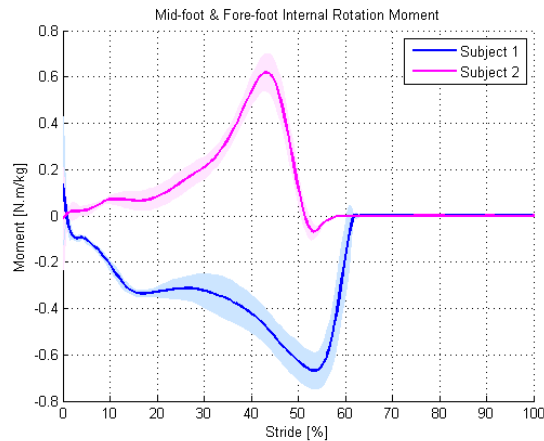
Figure 6.15 – Mid-foot and Fore-foot Internal Rotation Moment. From Lateral to Medial (+).

The result presented in Figure 6.16, show that the moment generated due to the leg internal rotation is very small. This is due to the small ground reaction forces in the Y direction. If the physiological moment generated by the ground reaction forces is small, the body response will be a small opposing moment as well. Once again, no reference results can be used to compare this pattern.
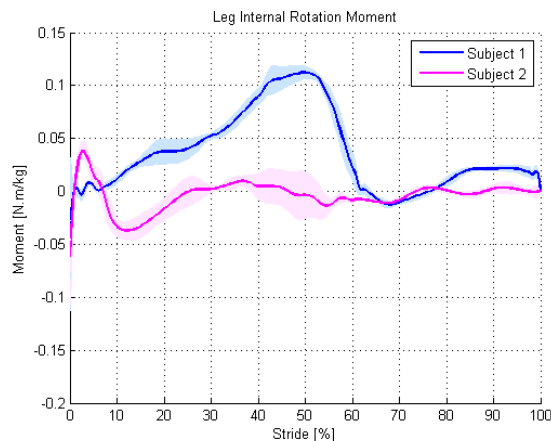
Figure 6.16 - Leg Internal Rotation Moment. From Lateral to Medial (+).

6.2.3. Joints Internal Reaction Forces

This section is intended to demonstrate the robustness and reliability of the Apollo software with the calculation of the joints internal reaction forces, a relevant information from the biomechanical point of view, and that many times is discarded. The joint internal reaction forces have to agree with Newton's third law, the joints have to act as the reaction force pair for the ground. So the results have to be symmetric to the ones presented in Section 6.2.1, as Figure 6.17 demonstrates.

86
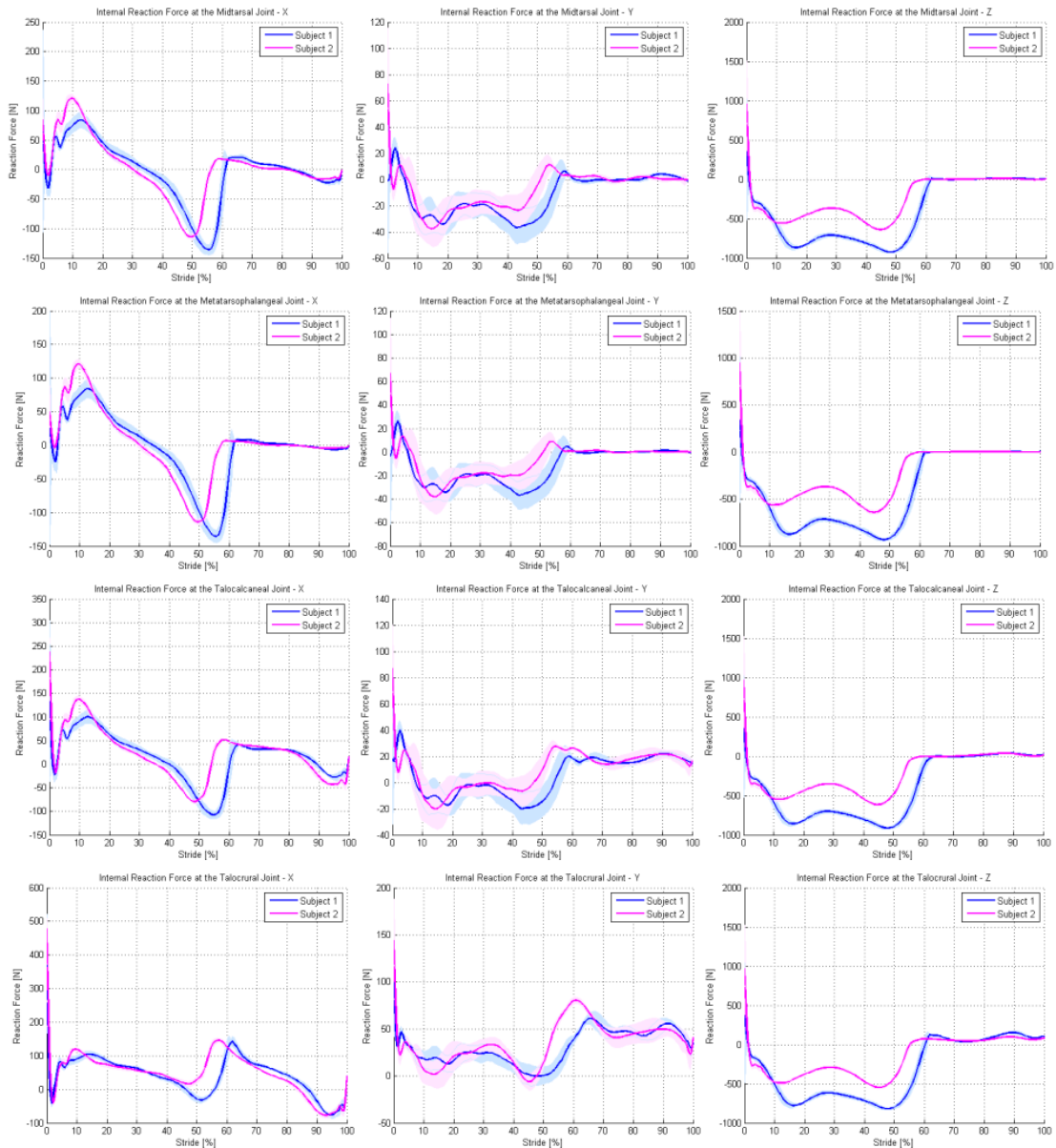
Figure 6.17 – Internal Reaction Forces: (1st Row) Midtarsal Joint; (2nd Row) Metatarsophalangel Joint; (3rd Row) Talocalcaneal Joint; (4th Row) Talocrural Joint. (1st Column) X IRF's; (2nd Column) Y IRF's; (3rd Column) Z IRF's.

6.2.4. Graphic Visualization of the model

In order to visualize the results given by the *.out a Matlab routine was adapted from Veiga (2012), animApollo.fig. This routine enables the user to visualize the entire simulation, choosing the preview velocity, camera angle, zoom and the camera distance to the model. It also allows the user to choose whether he wants the joint vectors and segments centers of mass to be displayed or not, Figure 6.18 and Figure 6.19.
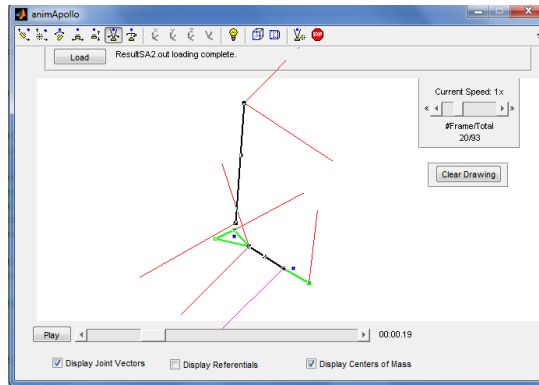
Figure 6.18 – Model display with the joint vectors and segments center of mass using the Matlab routine animApollo.fig
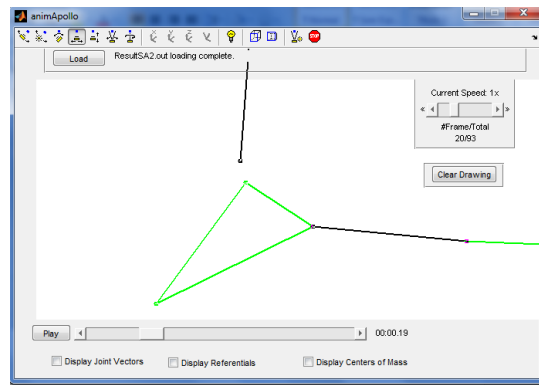
Figure 6.19 - Massless link detail of the model displayed using the Matlab routine animApollo.fig.

As an example of the routine capacities, Figure 6.20 and Figure 6.21 depict iterations of a gait cycle; stance and swing phase respectively.
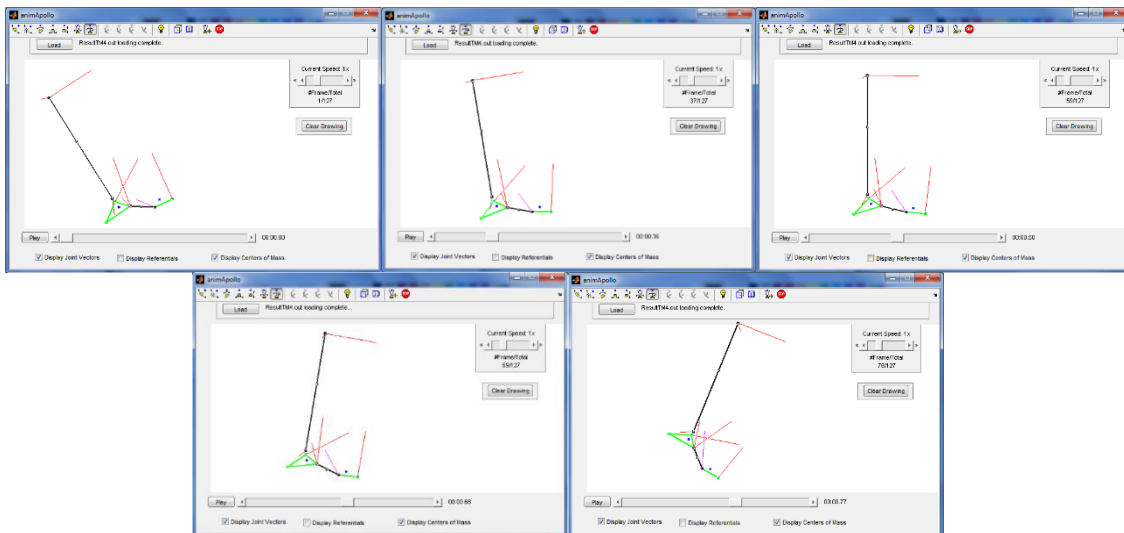
Figure 6.20 – Stance phase of the gait cycle depicted using the Matlab routine animApollo.fig. (Top)(Left) IC, (Center) LR, (Right) MS; (Bottom)(Left) TS, (Right) PS.
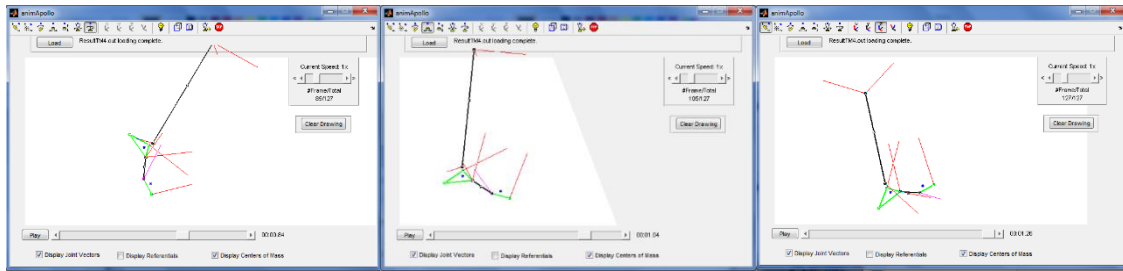
Figure 6.21 - Swing phase of the gait cycle depicted using the Matlab routine animApollo.fig. (Left) IS, (Center) MiS, (Right) TSw.

Chapter VII

Conclusions and Future Work

This thesis arises from a necessity, specifically from the need of a more realistic and reliable foot model that would provide new degrees of freedom that the existent models do not present. So the propose model is divided into four segments: (1) Leg (tibia and fibula), (2) Rear-foot (calcaneus), (3) Mid-foot and Fore-foot (navicular, cuboid, cuneiforms and metatarsals) and (4) Toes (Phalanges). This choice emerged from the authors' laboratory experience. Where a set of movements that were easily detected, were not being quantify, especially movements happening at the midtarsal and tarsometatarsal joint.

For the present work the author was aiming to achieve three main objectives. The first comprehended the development of an anthropometric table of a four segment leg and foot complex. This table would be able to calculate the lengths, masses, inertias and centers of mass positions of the bodies that the model requires from three single inputs – weight, height and foot size. The second objective regarded the formulation of a three-dimensional multibody leg and foot model, using a multibody formulation with natural coordinates, for its implementation in the academic software Apollo (Silva, 2003) through a modeling file. The third objective comprehended the application of the model in a gait cycle, to study the kinematics and kinetics of the model. This required the formulation of a markers set protocol that had the necessary information to represent the proposed model and that enabled data processing to generate the remaining files to be used by the academic software Apollo (Silva, 2003).

In order to fulfill these objectives, several topics had to be addressed to support the author's decisions. Chapter I make an exhaustive literature review, especially regarding kinematic and kinetic models, in order to specify the scientific base that surrounds this problematic. Chapter II describes the

osteology and arthrology of the system being modeled, giving an inside of the anatomical, physiological and biomechanics aspects that the model had to reproduce. Chapter III approaches two complete bibliographic references about the foot that sustain the anthropometric measures used in the formulation of the model. Chapter IV presents a brief multibody formulation description that governs the way that the author modeled the leg and foot system.

Regarding the anthropometric table proposed, it was achieved using the work by Anderson & Pandy (1999) and Parham *et al.* (1989). This table was divided in five modules: lengths (Table 3.10), masses (Table 3.11), radius of rotation (Table 3.17), and anthropometric vectors (Table 3.12 and Table 3.13); summarized in Table 3.18. Starting from these tables, the model, the second goal, was promptly generated. In Section 4.5, however some subroutines had to be developed in the software, using Fortran, in order to facilitate its implementation. These functions did not influence the core of the software, they were mainly implemented to make explicit some subroutines that the user did not have any control.

One of the principal modelling challenges was to separate the Talocrural and the Talocalcaneal by a massless link and making this joint to function as a universal joint with a non-right angle. The purpose of this idea was to avoid the problem pointed out by Anderson & Pandy (1999) that the addition of the talus, due to its small mass, would increase the integration time for the model considerably. The implementation of this massless link segment, which works as a universal joint, was achieved through the implementation of four inner product constraints (Section 4.5). These constraints increase the Jacobian Constraints matrix size but do not influence the coordinate's vector size because the massless link definition uses known points and vector, so the complexity of the model is not increased. Another important modelling objective was the implementation of the midtarsal joint, which was accomplished due to its formulation as a universal joint with a right angle. The last modeling objective was the possibility to study the internal leg rotations and the same for the mid-foot and fore-foot segment. This was achieved through the separation of both of these segments into two rigid bodies.

The third objective was achieved through the development of the markers set protocol described in Table 5.1 and Figure 5.1. This protocol is easily applied in clinical context; it does not need a considerable amount of time to implement as it uses a medium number of marker in its definition. The data from de QTM software was analyzed with some routines implemented using the Matlab software. These routines allowed the construction of key files that were needed for the Apollo inverse dynamics simulation, and for the visualization of the results. The results were evaluated using two different approaches; on one hand the comparison between the model results and typical patterns for the same data, and on the other hand the evaluation of these results along the gait cycle and analyzing their viability. This evaluation was performed along Chapter VI, presenting good and promising results for the model. The kinematic angles analysis were in the majority of cases consistent with known patterns, the ones that were deviated from the expected values are justified by a misapplication of the marker set protocol. The ground reaction forces also fulfilled typical measures.

Regarding the kinetic moment analysis, once again the model results are in general consistent with the bibliography; the ones that deviate from the expected have the same explanation as the ones for the kinematic analysis, misapplication of the marker set protocol. So, one can conclude that the

massless link formulation assured the typical kinematic and kinetic patterns regarding the talocalcaneal joint and the talocrural. The midtarsal joint brought some interesting results regarding the compliance of the arch of the foot during a gait cycle, and proved that this degree of freedom should not be overlooked. Other results such as the mid-foot and fore-foot internal rotation and the abduction/adduction at the midtarsal joint demonstrated that these movements are almost residuals in healthy subjects. In conclusion, the model is reliable, presenting the expected patterns for known bibliography results, like: the talocrural dorsiflexion/planterflexion angle, the metatarsophalangeal dorsiflexion/planterflexion angle and the talocalcaneal inversion/eversion angle. It is also more realistic than the common models, presenting innovative results, like the midtarsal plantarflexion/dorsiflexion angle, the internal leg rotation, the internal mid-foot and fore-foot rotation angle and the midtarsal adduction/abduction angle, despite presenting small values for the last two.

A brief remark has to be made to the Apollo software. It was proved that this software is as reliable and robust software to use in multibody simulations using natural coordinates. It presented compelling and trustworthy results that enabled the model validation. This work also contributed to the further development of this academic software, essentially giving more freedom to the user to implement multibody models. However, the software requires some learning time due to the lack of a complete user's manual. Appendix A is an attempt to bridge part of this gap.

7.1. Future Work

In this section a brief look into the possibilities that this model provides and into the work that has to be done, is presented. For a better division of ideas, a topic structure is presented.

- The first step to improve the reliability of the model comprehends the performance of more trials, using a larger range of subjects;
- The model can be applied to a hole body model in order to test its influence among the rest of the body;
- The application of a contact detection method to the foot model could provide innovative results regarding the foot-ground interaction;
- The simulation of human movement in forward dynamics using the proposed foot model;
- The model provided good perspectives to be applied in pathological gait analysis, having a larger number of degrees of freedom can enable the evaluation of different gait disorders;
- The further study around these understudied degrees of freedom can provide some valid information to be applied in humanoid robots, in order to make their gait more identical to the human gait.

References

Abboud, R. J. (2002). Relevant foot biomechanics. *Current Orthopaedics*, *16*, 165–179.

Abuzzahab, F. S., Harris, G. F. ., Kidder, S. M., & Johnson, J. E. (1994). A Kinetic, Biomechanical Model of the Foot and Ankle.

Abuzzahab, F. S., Harris, G. F., Kidder, S. M., & Johnson, J. E. (1993). A clinical system for foot and ankle motion analysis. *15th Annual International Conference of the IEEE Engineering in Medicine and Biology Society* (pp. 1067–1068). San Diego, CA, USA.

Alkjaer, T., Simonsen, E. B., & Dyhre-Poulsen, P. (2001). Comparison of inverse dynamics calculated by two- and three-dimensional models during walking. *Gait & Posture*, *13*(2), 73–7.

Anderson, F. C., & Pandy, M. G. (1999). A Dynamic Optimization Solution for Vertical Jumping in Three Dimensions. *Computer Methods in Biomechanics and Biomedical Engineering*, *2*(3), 201–231.

Anderson, F. C., & Pandy, M. G. (2001). Static and dynamic optimization solutions for gait are practically equivalent. *Journal of Biomechanics*, *34*, 153–161.

Bahr, R., & Krosshaug, T. (2005). Understanding injury mechanisms: a key component of preventing injuries in sport. *British Journal of Sports Medicine*, *39*(6), 324–9.

Barnett, C. H., & Napier, J. R. (1952). The axis of rotation at the ankle joint in man. Its influence upon the form of the talus and the mobility of the fibula. *Journal of Anatomy*, *86*(1), 1–9.

Baumgarte, J. (1972). Stabilization of Constraints and Integrals of Motion in Dynamical Systems. *Computer Methods in Applied Mechanics and Engineering, Vol.1* (pp. 1–16).

Blajer, W., Dziewiecki, K., & Mazur, Z. (2007). Multibody modeling of human body for the inverse dynamics analysis of sagittal plane movements. *Multibody System Dynamics*, *18*(2), 217–232.

Bruening, D. A., Cooney, K. M., & Buczek, F. L. (2012a). Analysis of a kinetic multi-segment foot model part I: Model repeatability and kinematic validity. *Gait & Posture*, *35*(4), 529–34.

Bruening, D. A., Cooney, K. M., & Buczek, F. L. (2012b). Analysis of a kinetic multi-segment foot model part II: kinetics and clinical implications. *Gait & Posture*, *35*(4), 535–40.

Canseco, K., Long, J., Marks, R., Khazzam, M., & Harris, G. (2008). Quantitative characterization of gait kinematics in patients with hallux rigidus using the Milwaukee foot model. *Journal of Orthopaedic Research*, *26*(4), 419–27.

Canseco, K., Long, J., Marks, R., Khazzam, M., & Harris, G. (2009). Quantitative motion analysis in patients with hallux rigidus before and after cheilectomy. *Journal of Orthopaedic Research*, *27*(1), 128–34.

Carson, M. C., Harrington, M. E., Thompson, N., O'Connor, J. J., & Theologis, T. N. (2001). Kinematic analysis of a multi-segment foot model for research and clinical applications: a repeatability analysis. *Journal of Biomechanics*, *34*(10), 1299–307.

Chandler, R. F., Clauser, C. E., Mcconville, J. T., & Young, J. W. (1975). *Investigation of Inertial Properties of the Human Body*. Wright-Patterson Air Force Base, OH, USA.

Clauser, C. E., Mcconville, J. T., & Young, J. W. (1969). *Weight, Volume, and Center of Mass of Segments of the Human Body*. Wright-Patterson Air Force Base, OH, USA.

Contini, R. (1972). Body Segment Parameters Part II. *Artificial Limbs*, *16*(1), 1–19.

Dabnichki, P. (1998). Biomechanical testing and sport equipment design. *Sports Engineering*, *1*(2), 93–105.

De Jalón, J. G., & Bayo, E. (1994). *Kinematic and Dynamic Simulation of Multibody Systems - The Real-Time Challenge*. New York, NY, USA: Springer-Verlag.

De Leva, P. (1996). Adjustments to Zatsiorsky-Seluyanov's Segment Inertia Parameters. *Journal of Biomechanics*, *29*(9), 1223–1230.

Delp, S. L. (1990). *Surgery Simulation: A computer graphics system to analyze and design musculoskeletal Reconstructions of the lower limb*. PhD Thesis, Stanford University.

Delp, S. L., Loan, J. P., Hoy, M. G., & Zajac, F. E. (1990). An interactive Graphics-Based Model of the Lower Extremity to Study Orthopaedic Surgical Procedures. *IEEE Transactions on Biomedical Engineering*, *37*(8), 757 – 767.

Deschamps, K., Staes, F., Roosen, P., Nobels, F., Desloovere, K., Bruyninckx, H., & Matricali, G. a. (2011). Body of evidence supporting the clinical use of 3D multisegment foot models: a systematic review. *Gait & Posture*, *33*(3), 338–49.

DiDomenico, L. A., & Cross, D. (2012). Tarsometatarsal/Lisfranc joint. *Clinics in podiatric medicine and surgery*, *29*(2), 221–42, vii–viii.

Dopico, D., & Luaces, A. (2011). Dealing with multiple contacts in a human-in-the-loop application. *Multibody System*, *25*(2), 167–183.

Drillis, R., & Contini, R. (1966). Body Segment Parameters. New York, NY, USA.

Drillis, R., Contini, R., & Bluestein, M. (1964). Body Segment Parameters - A Survey of Measurement Techniques. *Artificial Limbs*, *25*, 44–66.

Dul, J., & Johnson, G. E. (1985). A kinematic model of the human ankle. *Journal of Biomedical Engineering*, *7*(2), 137–143.

Esperança Pina, J. A. (1999). *Anatomia Humana da Locomoção* (3rd ed.). Lidel - Edições Técnicas, Lda.

Gonçalves, S. (2010). *Advanced Computer Methods for Pathological and Non-Pathological Human Movement Analysis*. Masters Thesis, Instituto Superior Técnico - Universidade de Lisboa.

Gray, H. (1989). *Gray's Anatomy*. (L. H. Williams, L. Peter; Warwick, Roger; Dyson, Mary; Bannister, Ed.) (37th ed.). London, England, United Kingdom: Guanabara Koogan (Portuguese Translation).

Hall, S. J. (2011). *Basic Biomechanics* (6th ed.). McGraw-Hill.

Hanavan, E. P. (1964). *A Mathematical Model of the Human Body*. Wright-Patterson Air Force Base, OH, USA.

Hatze, H. (1980). A mathematical model for the computational determination of parameter values of anthropomorphic segments. *Journal of Biomechanics*, *13*(10), 833–43.

Henning, C. E., Lynch, M. A., & Glick, K. R. (1985). An in vivo strain gage study of the anterior cruciate ligament elongation of the anterior cruciate ligament. *The America Journal of Sports Medicine*, *13*(1), 22–26.

Herzog, W., Archambault, J. M., Leonard, T. R., & Nguyen, H. K. (1996). Evaluation of the Implatable Force Tranducer for Chronic Tendon-Force Recordings. *Journal of Biomechanics*, *29*(1), 103–109.

Hicks, J. H. (1953). The Mechanics of the Foot I-The Joints. *Journal of Anatomy*, *87*(4), 345–357.

Hyon, S., & Cheng, G. (2007). Disturbance Rejection for Biped Humanoids. *IEEE International Conference on Robotics and Automation* (pp. 2668 – 2675).

Isman, R. E., & Inman, V. T. (1969). Anthropometric studies of the human foot and ankle. *Bulletin of Prosthetics Research*.

Jensen, R. K. (1975). Estimation of the Biomechanical Properties of Three Body Types Using a Photogrammetric Method. *Journal of Biomechanics*, *11*, 349–358.

Khazzam, M., Long, J. T., Marks, R. M., & Harris, G. F. (2006). Preoperative gait characterization of patients with ankle arthrosis. *Gait & Posture*, *24*(1), 85–93.

Khazzam, M., Long, J. T., Marks, R. M., & Harris, G. F. (2007). Kinematic Changes of the Foot and Ankle in Patients with Systemic Rheumatoid Arthritis and Forefoot Deformity. *Journal of Orthopaedic Research*, *25*(3), 319–329.

Kidder, S. M., Abuzzahab, F. S., Harris, G. F., & Johnson, J. E. (1996). A System for the Analysis of Foot and Ankle Kinematics During Gait. *IEEE Transactions on Rehabilitation Engineering*, *4*(1), 25–32.

Koopman, B., Grootenboer, H. J., & De Jongh, H. J. (1995). An inverse dynamics model for the analysis, reconstruction and prediction of bipedal walking. *Journal of Biomechanics*, *28*(11), 1369–76.

Lakany, H. (2008). Extracting a diagnostic gait signature. *Pattern Recognition*, *41*(5), 1627–1637.

Leardini, A., Benedetti, M. G., Berti, L., Bettinelli, D., Nativo, R., & Giannini, S. (2007). Rear-foot, mid-foot and fore-foot motion during the stance phase of gait. *Gait & Posture*, *25*(3), 453–62.

Leardini, A., Benedetti, M. G., Catani, F., Simoncini, L., & Giannini, S. (1999). An anatomically based protocol for the description of foot segment kinematics during gait. *Clinical Biomechanics*, *14*(8), 528–536.

Lees, A., Barton, G., & Robinson, M. (2010). The influence of Cardan rotation sequence on angular orientation data for the lower limb in the soccer kick. *Journal of Sports Sciences*, *28*(4), 445–50.

Livesay, G. a, Fujie, H., Kashiwaguchi, S., Morrow, D. a, Fu, F. H., & Woo, S. L. (1995). Determination of the In Situ Forces and Force Distribution within the Human Anterior Cruciate Ligament. *Annals of Biomedical Engineering*, *23*(4), 467–74.

Long, J. T., Eastwood, D. C., Graf, A. R., Smith, P. a, & Harris, G. F. (2010). Repeatability and sources of variability in multi-center assessment of segmental foot kinematics in normal adults. *Gait & Posture*, *31*(1), 32–6.

Lundgren, P., Nester, C., Liu, A., Arndt, A., Jones, R., Stacoff, A., Wolf, P., et al. (2008). Invasive in vivo measurement of rear- , mid- and forefoot motion during walking. *Gait & Posture*, *28*(1), 93–100.

MacWilliams, B. A., Cowley, M., & Nicholson, D. E. (2003). Foot kinematics and kinetics during adolescent gait. *Gait & Posture*, *17*(3), 214–24.

Manter, J. T. (1941). Movements of the Subtalar and Transverse Tarsal Joints. *The Anatomical Record*, *80*(4), 397–410.

Marks, R. M., Long, J. T., Ness, M. E., Khazzam, M., & Harris, G. F. (2009). Surgical reconstruction of posterior tibial tendon dysfunction: prospective comparison of flexor digitorum longus substitution combined with lateral column lengthening or medial displacement calcaneal osteotomy. *Gait & Posture*, *29*(1), 17–22.

Martin, R. B. (1999). A Genealogy of Biomechanics. *23rd Annual Conference of the American Society of Biomechanics*. Pittsburgh, PA, USA.

Mcconville, J. T., & Churchill, T. (1981). *Anthropometric Relationships of body and body segment moments of inertia*. Wright-Patterson Air Force Base, OH, USA: Air Force Aerospace Medical Research Laboratory, Aerospace Medical Division, Air Force Systems Command.

McConville, J. T., Clauser, C. E., Churchill, T. D., Cuzzi, J., & Kaleps, I. (1980). *Anthropometric relationships of body and body segment moments of inertia*.

Meglan, D. A. (1991). *Enhaced Analysis of human locomotion*. Ohio State.

Moreira, P. F. (2009). *Development of a three dimensional contact model for foot groun interaction in gait simulations*. Masters Thesis, Universidade do Minho.

Myers, K. A., Wang, M., Marks, R. M., & Harris, G. F. (2001). Validation of a multi-segment foot and ankle kinematic model for pediatric gate. Milwaukee, WI, USA.

Neptune, R. R., Wright, I. C., & Van Den Bogert, A. J. (2000). A method for numerical simulation of single limb ground contact events: Application to Heel-Toe Running. *Computer Methods in Biomechanics and Biomedical Engineering*, *3*(4), 321–334.

Ness, M. E., Long, J., Marks, R., & Harris, G. (2008). Foot and ankle kinematics in patients with posterior tibial tendon dysfunction. *Gait & posture*, *27*(2), 331–9.

Pandy, M. G., & Berme, N. (1988). Synthesis of human walking: a planar model for single support. *Journal of Biomechanics*, *21*(12), 1053–60.

Pandy, Marcus G. (2001). Computer Modeling and Simulation of Human Movement. *Annual Review of Biomedical Engineering*, *3*, 245–73.

Parham, K. R., Gordon, C. C., & Bensel, C. K. (1989). *Anthropometry of the Foot and Lower Leg of U.S. Army Soldiers: Fort Jackson, SC -- 1985.* Natick, MA, USA.

Procter, P., & Paul, J. P. (1982). Ankle joint biomechanics. *Journal of Biomechanics*, *15*(9), 627–634.

Qualisys AB. (2013). Qualisys Track Manager User Manual.

Silva, Miguel T. (2003). *Human Motion Analysis using Multibody Dynamics and Optimization Tools.* PhD Thesis, Instituto Superior Técnico - Universidade de Lisboa.

Silva, Miguel Tavares, & Ambrósio, J. A. C. (2002). Kinematic Data Consistency in the Inverse Dynamic Analysis of Biomechanical Systems. *Multibody System Dynamics*, *8*, 219–239.

Silva, P. C., Silva, M. T., & Martins, J. M. (2010). Evaluation of the contact forces developed in the lower limb/orthosis interface for comfort design. *Multibody System Dynamics*, *24*(3), 367–388.

Simon, J., Doederlein, L., McIntosh, a S., Metaxiotis, D., Bock, H. G., & Wolf, S. I. (2006). The Heidelberg foot measurement method: development, description and assessment. *Gait & posture*, *23*(4), 411–24.

Theologis, T. N., Harrington, M. E., Thompson, N., & Benson, M. K. D. (2003). Dynamic foot movement in children treated for congenital talipes equinovarus. *The Journal of Bone & Joint Surgery*, *85-B*(4), 572–7.

Tortora, G. J., & Derrickson, B. (2007). *Introduction to the Human Body, The essentials of anatomy and physiology* (7th ed.). John Wile & Sons, Inc.

Turner, D. E., Helliwell, P. S., Emery, P., & Woodburn, J. (2006). The impact of rheumatoid arthritis on foot function in the early stages of disease : a clinical case series. *BMC Musculoskeletal Disorders*, *7*(102), 1–8.

Turner, D. E., & Woodburn, J. (2008). Characterising the clinical and biomechanical features of severely deformed feet in rheumatoid arthritis. *Gait*, *28*, 574–580.

Vasconcelos, C. (2010). *Active Orthosis for Ankle Articulation Pathologies.* Masters Thesis, Instituto Superior Técnico - Universidade de Lisboa.

Veiga, J. (2012). *Matching of a Hierarchical Muscle Fatigue Model with Subject-specific Endurance Times.* Masters Thesis, Instituto Superior Técnico - Universidade de Lisboa.

Vilà, R. P. (2012). *Application of Multibody Dynamics Techniquesto the Analysis of Human Gait.* PhD Thesis, Universitat Politècnica de Catalunya.

Winter, D. A. (1990). *Biomechanics and Motor Control of Human Movement.* Waterloo, Ontario, Canada: John Wile & Sons, Inc.

Winter, D. A. (1991). *Biomechanics and Motor Control of Human Gait: Normal, Elderly and Pathological* (2nd ed.). Waterloo, Ontario, Canada: University of Waterloo Press.

Woodburn, J., Nelson, K. M., Siegel, K. L., Kepple, T. M., & Gerber, L. H. (2004). Multisegment Foot Motion During Gait : Proof of Concept in Rheumatoid Arthritis. *The Journal of Rheumatology*, *31*(10), 1918–27.

Appendix A

A. Apollo User Guide

This Appendix is intended to give an overview on how to create the necessary files to run an inverse dynamic simulation in the Apollo software. This summary will only approach the data used in the files used to analyze the model described in the present work.

A.1. Creation of modulation files (*.mdl)

In this section a brief description on how to build a modulation Apollo file for inverse dynamics is given.

Note: Each tag appears only once.

Header

Tag: *HEADER

Input: The header input is not important, it serves to introduce the file, and it is basically a small description of the modulation.

Example:

```
*HEADER
Model for Right Lower Extremity (Leg and Foot)
```

Main Parameters

Tag: *MAIN PARAMETERS

Input: The main parameters are represented by a single line of input. This line has 25 entries listed below. When the parameter is not at use, the entry is 0, otherwise is as the description mentions.

Table A.1 - Apollo modulation file main parameters description.

Position	Description	Reference
1	Number of points	NPOINT
2	Number of vectors	NUVEC
3	Number of rigid bodies	NRIGIDBOD
4	Number of superposition constraints	NSUPERPOS
5	Number of inner product constraints	NINNERPROD
6	Number of cylindrical joints	NCYLIND
7	Number of prismatic joints	NPRISM
8	Number of revolution drivers	NKDRV
9	Number of translational drivers	NTDRV
10	Number of Spring-Damper-Actuator	NSDA
11	Number of Force/Torque	NFT
12	Number of wheels	NWHL
13	Number of car directions	NSTEER
14	Number of biomechanics models	NBMDL
15	Number of FEM Links	NFEMLINK
16	Number of Bushing elements	NBE
17	Number of Sphere Plane contact elements	NSPC
18	Number of Ligaments	NLIG
19	Number of Muscles	NMUSCLE
20	Number of Foot Model	NFM
21	Number of Hill type muscles	NMHILL
22	Number of controllers	NCTRL
23	Number of sensors	NSNSR
24	Number of actuators	NACT_CTRL

Example:
```
*MAIN PARAMETERS
9 9 6 3 6 0 0 10 0 0 0 0 0 0 0 0 0 0 0 0 0 0 0 0 0
```

Ground Body

Tag: *GROUND BODY

Input: The first line of input has the number of points that will be defined as ground points and their respective indexes. The second line of input has the number of vectors that will be defined as ground vectors and their respective indexes. The following lines are the coordinates (x y z) of the points and vectors mentioned in the first two lines according to the global referential. The coordinates have to be ordered according to their appearance in the first two lines. Notice that this parameter was kept null for the analysis presented in this thesis (no ground body was used). However, the tag must be there with one 0 in the second line.

Example:

```
*GROUND BODY
1 9
0
-0.269327+000 0.291123+000  0.302556E+000
```

Rigid Bodies

Tag: *RIGID BODIES

Sub-Tag: BODY=…

Input: The first line of input has the body mass and the inertia (Ix Iy Iz). The second line of input has the number of points that define the body and their respective indexes. The third line of input has the number of unitary vectors that belong to that body and their respective indexes. The following lines are the coordinates (x y z) of the points mentioned in previous lines according to the local referential followed by the coordinates (x y z) of the unitary vectors. The coordinates have to be ordered according to their appearance in the previous lines.

Example:

```
*RIGID BODIES
BODY=Toes
0.2051 0.0001 0.0001 0.0002
2 1 2
2 1 9
0.046000 0.000000 -0.018500
-0.02690 0.005100 -0.018500
-0.19340 -0.98110 0.00000
0.000000 0.000000 1.000000
```

Superposition Constraint

Tag: *SUPERPOSITION CONSTRAINT

Sub-Tag: SP=…

Input: Two types of input can be defined: the first one is applied when a shared point is defined and the second is applied when overlapping vectors are needed. To distinguish both situations the fifth entry works as a flag, it has to be 0 in the first situation and 1 in the second.

Table A.2 - Superposition Constraint types description.

Type 1	Body 1 Index	Body 2 Index	Shared Point in Body 1	Shared Point in Body 2	Flag =0
Type 2	Body 1 Index	Body 2 Index	Shared Vector in Body 1	Shared Vector in Body 2	Flag=1

Example:

```
*SUPERPOSITION CONSTRAINT

SP=Toes_Meta_pnt
1 2 2 3 0
```

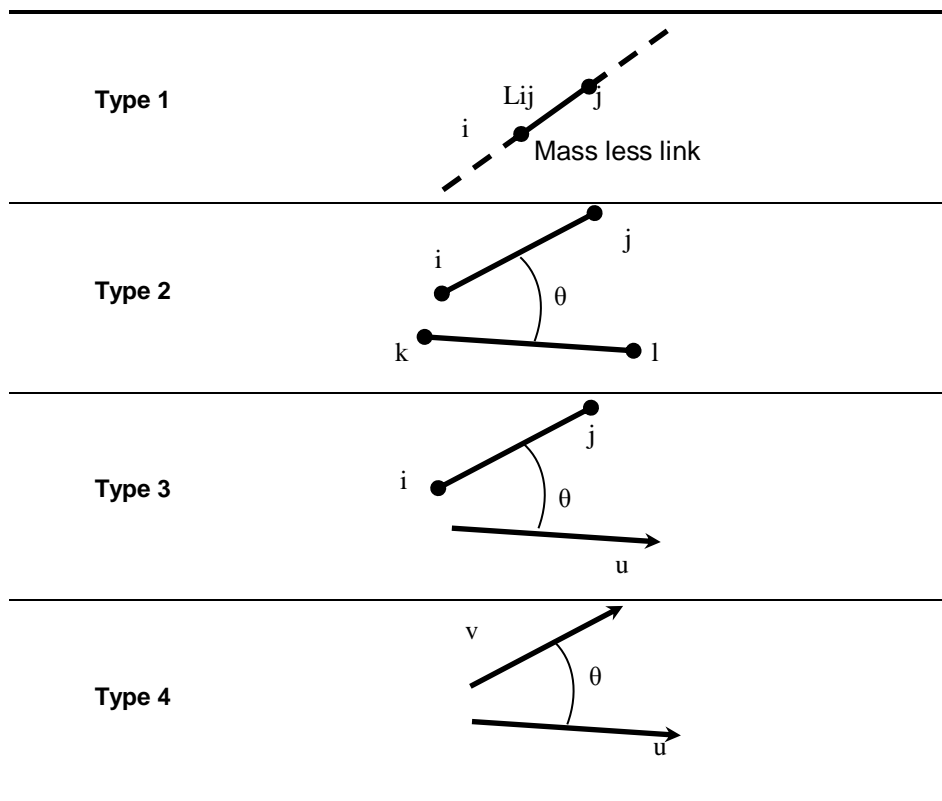**Inner Product Constraint**

Tag: *INNER PRODUCT CONSTRAINT

Sub-Tag: IP=…

Input: Four types of input can be defined: the first one is applied when a mass less link connection is required, it implies a constant length between two points (Flag =0); the second type is used when a constant angle between two segments defined by two points each is needed (Flag =1); the third type is applied when a constant angle between a two point segment and a unit vector is required (Flag =2); the fourth type is used when we a constant angle between two unit vectors is defined (Flag =3). The details of the input are explained in Table A.3 and Table A.4.

Table A.3 - Inner Product Constraint types description.

Type	Body 1 Index	Body 2 Index	Flag	Ii Point body 1	Ij Point body 1	Length mass less link Lij		Length body 1 Lij	Length body 2 Lkl	Angle θ
Type 1	Body 1 Index	Body 2 Index	Flag = 0	Ii Point body 1	Ij Point body 2	Length mass less link Lij				
Type 2	Body 1 Index	Body 2 Index	Flag = 1	Ii Point body 1	Ij Point body 1	Ik Point body 2	Il Point body 2	Length body 1 Lij	Length body 2 Lkl	Angle θ
Type 3	Body 1 Index	Body 2 Index	Flag = 2	Ii Point body 1	Ij Point body 2	Iu Vector index	Length body 1 Lij	Angle θ		
Type 4	Body 1 Index	Body 2 Index	Flag = 3	Iu Vector index	Iv Vector index	Angle θ				

Table A.4 - Inner Product Constraint types visualization**.**

Example:

```
*INNER PRODUCT CONSTRAINT

IP=Meta_Rear
3 4 3 3 4 90
```

Revolution Drivers

Tag: *KINEMATIC DRIVERS

Sub-Tag: DRIVER=n, where n is the number of the *.dat correspondent to this driver. The data files must be named as: 'Driver_n'.

Input: Six types of input can be defined: the first one is used when a trajectory driver is applied to a point (Flag =1); the second type is used when a trajectory driver is applied to a vector (Flag =2); the third type is applied when the distance between two point needs to be guided (Flag =3); the fourth type is used when the angle between two segments (vectors defined by two points) needs to be guided (Flag =4); the fifth type is used when the angle between two unit vectors needs to be guided (Flag =5); the sixth type is used when the angle between one segment and one unit vector needs to be guided (Flag =6). This input is divided in two lines. The first comprehends the flag, the second the information about the bodies, segments and vectors, detailed in Table A.5.

Table A.5 - Driver types description.

Type	Body 1	Point			
1	Index	body 1			
Type	Body 1	Vector			
2	Index	body 1			
Type	Body 1	Body 2	Point	Point	
3	Index	Index	body 1	body 2	
Type	Body 1	Body 2	Point 1	Point 2	Point 1	Point 2
4	Index	Index	body 1	body 1	body 2	body 2
Type	Body 1	Body 2	Vector	Vector	
5	Index	Index	body 1	body 2	
Type	Body 1	Body 2	Point 1	Point 2	Vector
6	Index	Index	body 1	body 1	body 2

Example:

```
*KINEMATIC DRIVERS

DRIVER=1
6
2 1 3 4 9
```

A.2. Creation of simulation files (*.sml)

In this section a brief description on how to build a simulation Apollo file for inverse dynamics is given.

Note: Each tag appears only once.

Header

Tag: *HEADER

Input: The header input is not important, it serves to introduce the file, and it is basically a small description of the simulation.

Example:

```
*HEADER
simulation file for footlegmodel
```

Analysis Type

Tag: *ANALYSIS TYPE

Input: Two types of input can be introduced: FORWARD or INVERSE depending on the type of analysis pretended.

Example:

```
*ANALYSIS TYPE
INVERSE
```

Initial Information

Tag: *INITIAL INFORMATION

Sub-Tag: BODY=…

Input: The initial information contains the information regarding the first step of analysis about each body. This information comprehends the center of mass position (x, y, z) initial Euler angles, and initial acceleration.

Example:

```
*INITIAL INFORMATION

BODY=Toes
-0.108527 0.262523 -0.012044 0.000000 0.000000 0.000000
0.0 0.0 0.0 0.0 0.0 0.0
```

Gravity Information

Tag: *GRAVITY FIELD VECTOR

Input: The gravity field vector contains the coordinates (x,y,z) that the user wants to attribute to the gravity field.

Example:

```
*GRAVITY FIELD VECTOR
0.00 0.00 -9.81
```

Animation

Tag: *DO ANIMATION

Description: This input is the tag itself, in case of absence the software does not perform the analysis animation.

Example:

```
*DO ANIMATION
```

Centers of Mass Report

Tag:*REPORT CENTERS OF MASS

Description: This input is the tag itself, in case of absence the software will not export the position, velocity, and acceleration of the centers of mass in each step to the *.out file.

Example:

```
*REPORT CENTERS OF MASS
```

Read the Forces and Moments file

Tag: *DISCRETE FORCES AND MOMENTS

Input: The input is divided in two lines: the first contains the name of the *.frc file; the second contains the number of frames under analysis.

Example:

```
*DISCRETE FORCES AND MOMENTS
3ªPassadaDir.frc
124
```

Time information

Tag: *START/STOP/STEP

Input: The input is a vector with the information regarding the start time of the analysis, the final time, and the step.

Example:

```
*START/STOP/STEP
0.0 1.23 0.01
```

A.3.   Creation of data files (*.dat)

There are two types of data files. The first type comprehends the drivers that guide angles (type 4, 5 and 6) the second type comprehends the drivers that guide trajectories (type 1 and 2). Regarding the first type, its formulation is very simple, the first line presents the analysis number of frames and the rest of the lines are divided in two columns. The first column is the time step; the

second is the angle correspondent to that time step. Notice that Apollo is not robust enough to deal with angles near the interval $[0 \pm n\pi], n \in \mathbb{N}$.

Example:

```
121
0.000 60.001783
0.010 60.388428
0.020 60.929443
0.030 61.631623
0.040 62.488628
0.050 63.481672
0.060 64.582815
0.070 65.758548
```

The second type is formulated like the first, but instead of two columns from the first line it has four. The first is again the time step; the second, third and fourth comprehend respectively the x, y and z coordinates of the point or vector, depending on the type of driver.

Example:

```
121
0.000 -0.000635 0.225964 0.493165
0.010 0.008770 0.226365 0.492737
0.020 0.018209 0.226656 0.492636
0.030 0.027661 0.226821 0.492872
0.040 0.037104 0.226841 0.493426
0.050 0.046517 0.226696 0.494246
0.060 0.055865 0.226370 0.495256
0.070 0.065098 0.225856 0.496362
```

A.4. Creation of force and moments files (*.frc)

The force file is a complex file; it takes into account a large quantity of information. The file begins with two lines of guiding information; the software does not read it but they have to be there. The third line details the number of force and moments respectively that will be analyzed. The fourth line comprehends the information about the bodies that will undergo the influence of the force/moment; it details the rigid bodies' numbers. From the fifth line until the end, the document is divided in columns: the first is the frame number; the second is a column containing the rigid body number that is under the influence of the force/moment at that frame; the third is the time step; from the fourth to the sixth is the value of the force in x, y and z respectively; from the seventh to the ninth is the global coordinates (x, y and z) of the Center of Pressure (COP); from the tenth to the twelfth is the value of the moments in x, y and z respectively (if they are being applied).

Example:

```
FRAME   FL1     TIME  F1X     F1Y     F1Z           AP1X        AP1Y        AP1Z
                [S]   [N]     [N]     [N]           [m]         [m]         [m]
1       0
1       2     4
1       4     0.000   2.258   -6.564  32.635  0.117362004  0.236696912  0.000000000
2       4     0.010   29.070  -26.226 327.141 0.106141286  0.244583215  0.000000000
3       4     0.020   -6.279  -25.526 298.347 0.111896029  0.244414617  0.000000000
4       4     0.030   -42.626 -23.342 358.499 0.108840275  0.245570062  0.000000000
5       4     0.040   -76.410 -11.279 367.088 0.112412547  0.245066952  0.000000000
6       4     0.050   -54.950 -7.696  388.457 0.114059962  0.244643956  0.000000000
7       4     0.060   -38.362 -2.218  427.503 0.115964316  0.243725232  0.000000000
```